SISSA
Scuola
Internazionale
Superiore di
Studi Avanzati

Neuroscience Area – PhD course in

Functional and Structural Genomics

Foxg1 promotes *Grin1* translation in neocortical neurons

Candidate:

Osvaldo Basilio Artimagnella

Advisor:

Prof. Antonio Mallamaci

Academic Year 2019-20

“I don't know half of you half as well as I should like;
and I like less than half of you half as well as you deserve.”

— J.R.R. Tolkien, The Fellowship of the Ring

Abstract

Mainly known as a transcription factor patterning the rostral brain and governing its histogenesis, Foxg1 has been also detected outside the nucleus, however biological meaning of that has been only partially clarified. Here, moving from widespread Foxg1 expression in axons and dendrites of neocortical glutamatergic neurons, we investigated its implication in translational control. We documented an impact of Foxg1 on ribosomal recruitment of *Grin1*-mRNA, encoding for the main subunit of NMDA receptor. Next, we showed that Foxg1 increases Grin1 protein level by enhancing translation of its mRNA, while not increasing its stability. Such enhancement was associated to increased translational initiation and, possibly, polypeptide elongation. Molecular mechanisms underlying that included Foxg1 interaction with Eif4e, Eef1d and Pum1 as well as with *Grin1*-mRNA. Besides, we found that Grin1 *de novo* synthesis becomes particularly prominent in silent neurons and Foxg1 is needed for that. Finally, a dedicated TRAP-seq survey showed that functional Foxg1 implication in translation is a pervasive phenomenon, affecting hundreds of synaptic genes. All that points to Foxg1 as a key effector, crucial to prompt tuning of neocortical pyramid activity, namely an issue with profound physiological and neuropathological implications.

Contents

1. INTRODUCTION

1.1. Telencephalic development and neocortex histogenesis

The mammalian neocortex is the brain structure characterized by a complex neural network that processes, especially in human, higher order information, such as sensory perception, language, consciousness, emotion, and memory. The neocortex is composed by a myriad of neuronal subtypes in terms of morphology, function, and gene expression. Its development requires highly regulated mechanisms according to a precise spatio-temporal order, both to generate all neural cells and to properly assemble and integrate them in functional neural circuits.

In the developing embryo, at the end of gastrulation, the embryonic dorsal leaflet, named neuroectoderm, is involved in the neurulation phase, a morphogenetic developmental program that will lead to the formation of the Central Nervous System (CNS). The CNS is rostrally composed by three encephalic structures known as Forebrain (Prosencephalon), Midbrain (Mesencephalon) and Hindbrain (Rhombencephalon), and caudally by the spinal cord. The anterior-most part of the Forebrain is termed telencephalon, which is developed by three main sequential events: 1) rostro-caudal and dorso-ventral specification; 2) control of cellular proliferation and differentiation rate; 3) patterning and cerebral layering. These steps are regulated in a spatio-temporal manner by the interplay of several extrinsic factors, secreted from signaling centers, and intrinsic factors. Extrinsic factors, also named morphogens, include members of fibroblast growth factors (FGFs; mainly the FGF8), bone morphogenetic proteins (BMPs), and wingless/int proteins (WNTs) as well as sonic hedgehog (SHH) families, which form a concentration gradient from the center of secretion. More in details, SHH is produced ventrally from the prechordal plate (underlying the telencephalic territory), FGF8 is produced rostrally from the anterior neural ridge (ANR)[1] and a number of BMPs and WNTs proteins are produced caudo-medially from the dorsal roof (**Fig. 1.1.1**). The morphogen gradient is read from neuroepithelial cells, coordinating the spatially restricted expression of transcription factors, that – in turn – define specific regions inside the telencephalon [reviewed in Sur and Rubenstein, 2005].

[1] The ANR is a region in the neural plate which acts as a secondary organizer and secretes signaling molecules that generate the anterior-posterior patterning of the forebrain.

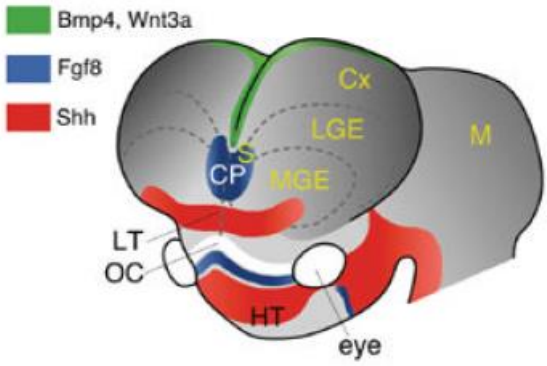

Fig. 1.1.1. Morphogens secreted from signaling centers generate positional information in the telencephalon. Cx: cortex, LGE: lateral ganglionic eminence, MGE: medial ganglionic eminence, CP: commissural plate or ANR. Adapted from Rakic, 2009.

Along the dorso-ventral axis, telencephalon is subdivided into sub-domains thanks to expression of specific transcription factor genes, such as *Nkx2.1*, *Gsx2*, *Pax6*, and *Emx2* [Wilson and Houart, 2004] (**Fig. 1.1.2, Left**). The dorsal telencephalon (the pallium, main source of excitatory glutamatergic neurons) will give rise to the archicortex (subiculum, hippocampus and dentate gyrus), the paleocortex (olfactory piriform cortex and enthorinal cortex) and the neocortex, the largest region of the telencephalon. The ventral telencephalon (the subpallium, main source of inhibitory GABAergic neurons) will mainly generate basal ganglia, which consist in lateral (caudatus, putamen) and medial (globus pallidus) ganglionic eminences, and a part of amigdala [Molyneaux et al., 2007] (**Fig. 1.1.2, Right**).

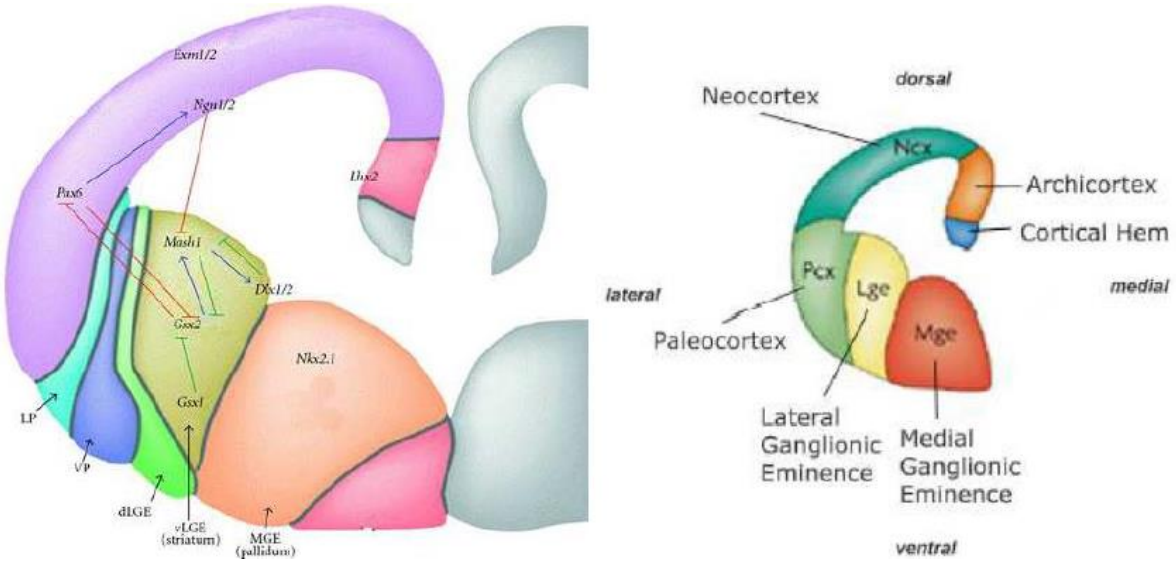

Fig. 1.1.2. Subdomains and specific molecular markers of developing telencephalon. (Left): the image was adapted from Wilson and Houart, 2004. **(Right)**: domains of the dorsal cortex and ventral basal ganglia. Modified from Molyneaux et al., 2007.

The mammalian neocortex is a highly organized six-layered structure that contains different neural cell types. They are generated according to three consecutive and partially overlapping waves: neurons are the first, followed by astrocytes, and then oligodendrocytes [Kriegstein and Alvarez-Buylla, 2009] (**Fig. 1.1.2, Top**). These cells do not origin all within the cortex itself but only projection glutamatergic neurons of layers II-VI, astrocytes, and post-natal oligodendrocytes [Gorski et al., 2002; Kessaris et al., 2006]. Conversely, glutamatergic Cajal-Retzius cells (CRs) of layer I, inhibitory GABAergic interneurons[2], and pre-natal oligodendrocytes are generated outside the pallium [Bielle et al., 2005; Hardy and Friedrich Jr, 1996; Wonders and Anderson, 2006], reaching the cerebral cortex via tangential migration across the telencephalon.

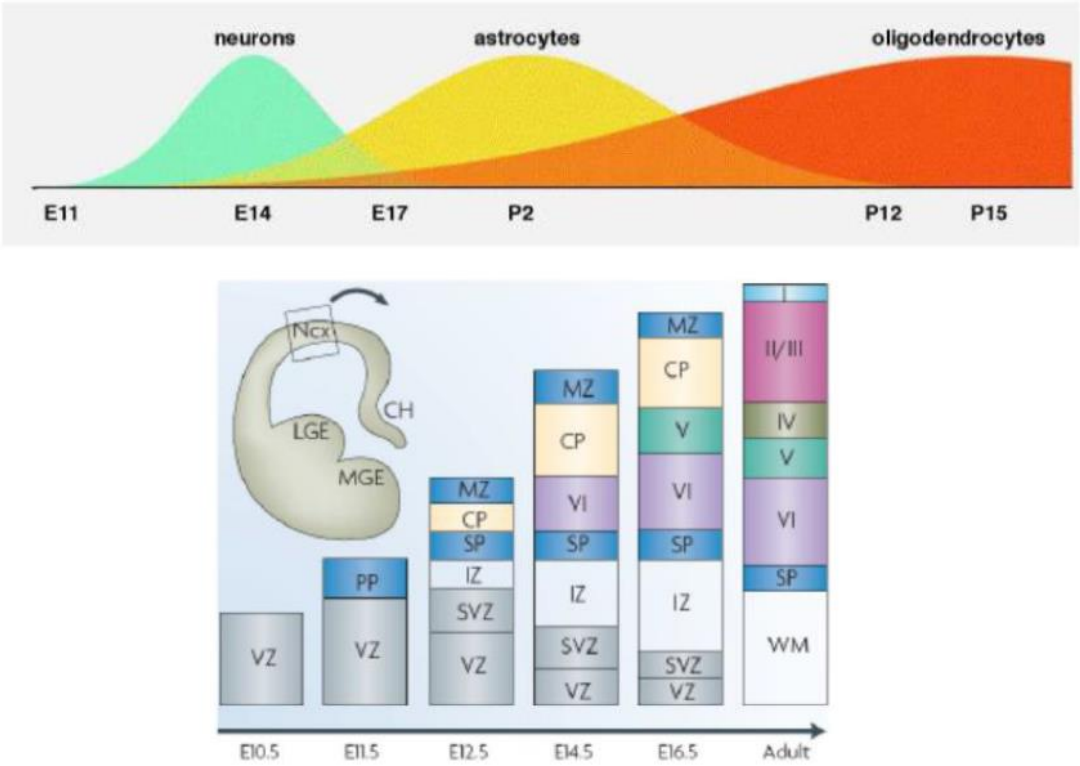

Fig. 1.1.2. Murine cortico-cerebral histogenesis. (Top): peaks of neuronogenic and astrocytogenic waves are at E14, and P2 respectively. Oligodendrocytes are continuously generated during post-natal life. Taken from Mallamaci, unpublished. **(Bottom)**: timing of cortical neurogenesis in mouse**.** Neocortical neurons are generated according to "inside-out" rule. Adapted from Molyneaux et al., 2007.

[2] In primates a subset of GABAergic interneurons is generated in VZ and SVZ of the pallium [Letinic et al., 2002; Zecevic et al., 2011].

During early development, cortical neural progenitors are generated from the so-called ventricular zone (VZ), a proliferative layer within the dorso-lateral telencephalic neuroepithelium. In mice, at embryonic day E9.5 apical progenitors of VZ start to proliferate by repeating symmetric cell division, expanding the VZ. At E10.5, neuroepithelial cells gives rise the so-called radial glial cells (RGCs), polarized cells with cell bodies within the VZ, and radial marginal protrusions reaching the pial surface. RGCs proliferate by asymmetric cell division, producing immature post-mitotic neurons and basal progenitors (or intermediate progenitors, IPCs), populating the subventricular zone (SVZ). From E11.5 to E17.5, corresponding to the neuronogenic window, RGCs and IPCs continue to proliferate, producing projection neurons of different neocortical layers in a tightly controlled spatio-temporal order. Neurons start to migrate outside the VZ and SVZ along radial processes of RGCs into the cortical plate (CP), and differentiate in mature neurons, reaching their final cortical layer. In more details, the first neurons form a transient structure called the pre-plate (PP); afterwards, when the earliest migrating cortical neurons reach the PP, they form the CP which divides the PP into a superficial marginal zone (MZ; layer I of the post-natal cortex) and a deeper subplate (SP; below layer VI) (**Fig. 1.1.2, Bottom**) [reviewed in Molyneaux et al., 2007; Rakic, 2006].

During the formation of the six-layer mature neocortex a major role is played by Cajal-Retzius cells, which are the main source of Reelin, a large extracellular glycoprotein. It is essential for newborn projection neurons in order to radially migrate from the VZ and SVZ to the pia, and detach from the RGC scaffolds to reach their final destination. In the six layers of cortical plate, newborn neurons are arranged in an "inside-out" manner, meaning that the later born neurons migrate over the earlier born ones (**Fig. 1.1.2, Bottom**). Hence, progenitor cells give rise to initially deeper layer neurons (VI and V), followed by superficial upper layer neurons (IV, III, and II) [reviewed in Molyneaux et al., 2007; Rakic, 2006]. Once finished the neurogenic phase, RGCs also generate astrocytes, oligodendrocytes, and ependymal cells (gliogenic phase) [Rakic, 2006].

In vertebrates, *Foxg1* is one of the first gene expressed and restricted in the telencephalic field. Its expression persists in the telencephalon from embryonic to adulthood stages, and mutations in *Foxg1* alleles leads to severe brain disabilities [Wong et al., 2019]. In the last 30 years, many studies investigated *Foxg1* roles in the control of telencephalic development and of cortico-cerebral histogenesis, whereas little is so far known about its involvement in the post-natal cortex. For these reasons, *Foxg1* is the main subject of this PhD thesis, focusing on its role in post-mitotic cortico-cerebral neurons.

1.2. *Foxg1*: structure and function of the gene

Forkhead box G1 (*FOXG1*)[3] is a member of the large family of forkhead box (FOX) genes, encoding for a telencephalic regulatory transcription factor. The FOX family is characterized by a highly conserved 80-110 aminoacids long DNA-binding motif, termed "winged-helix" or "forkhead" domain (FHD). Structurally, the FHD consists of 3 α-helices (helical sections) and 1 β-hairpin (1 loop and 2 β-strands; winged sections) (**Fig. 1.2.1, Right**). FoxG1 has been shown to act primarily as a transcriptional repressor [reviewed in Florian et al., 2012].

The 489[4] aminoacids long human FOXG1 transcription factor is encoded by only 1 intron-less coding region located in chromosome 14q12. In addition to the DNA-binding motif, FOXG1 protein presents other two functional domains to recruit transcriptional corepressors, the 10-residue Groucho/TLE-binding domain (GBD), and the 23-residue KDM5B (formerly JARID1B)-binding domain (JBD) [reviewed in Florian et al., 2012] (**Fig. 1.2.1, Left**). FoxG1 protein sequence from FHD to the C-terminal portion is highly conserved (96%) in vertebrates, whereas the N-terminal region varies among species. In particular, mammals are characterized by histidine-proline-glutamine repeats (HPQ rich domain), which were selectively expanded in the primate species [Bredenkamp et al., 2007].

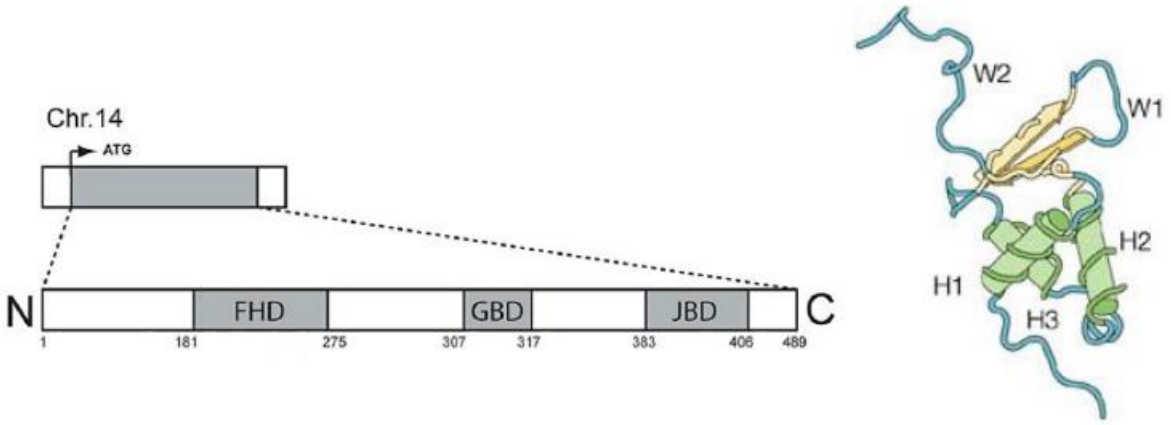

Fig. 1.2.1. *FOXG1* gene locus and protein domains. (Left): representation of *FOXG1* locus and of three functional domains (FHD, GBD, JBD). Adapted from Florian et al., 2012. **(Right)**: example structure of the FHD domain, showing helical (H) sections and winged (W) sections. Adapted from Coffer and Burgering, 2004.

[3] It was formerly named Brain Factor-1 (BF-1) and renamed *Foxg1* for mouse, *FOXG1* for human, and *FoxG1* for other chordates.

[4] The murine *Foxg1* gene is located in chromosome 12 and encoded for a 481 aminoacids long transcription factor.

In vertebrates, *FoxG1* plays non-redundant and pleiotropic roles in brain development. It induces the formation of the telencephalon, then regulates the rostro-caudal and the dorso (pallial)-ventral (subpallial) specification. Moreover, *FoxG1* is involved in the regulation of neural precursors proliferation and neural cell differentiation, as well as neuronal migration, cerebral cortex patterning and layering. All this places *FOXG1* as a key telencephalic regulator and help understanding why even a moderate alteration in its gene expression level may deeply impact neurodevelopmental processes and higher cognitive functions, leading to neurological disorders [Danesin and Houart 2012; Florian et al., 2012; Wong et al., 2019] (**Fig. 1.2.2**).

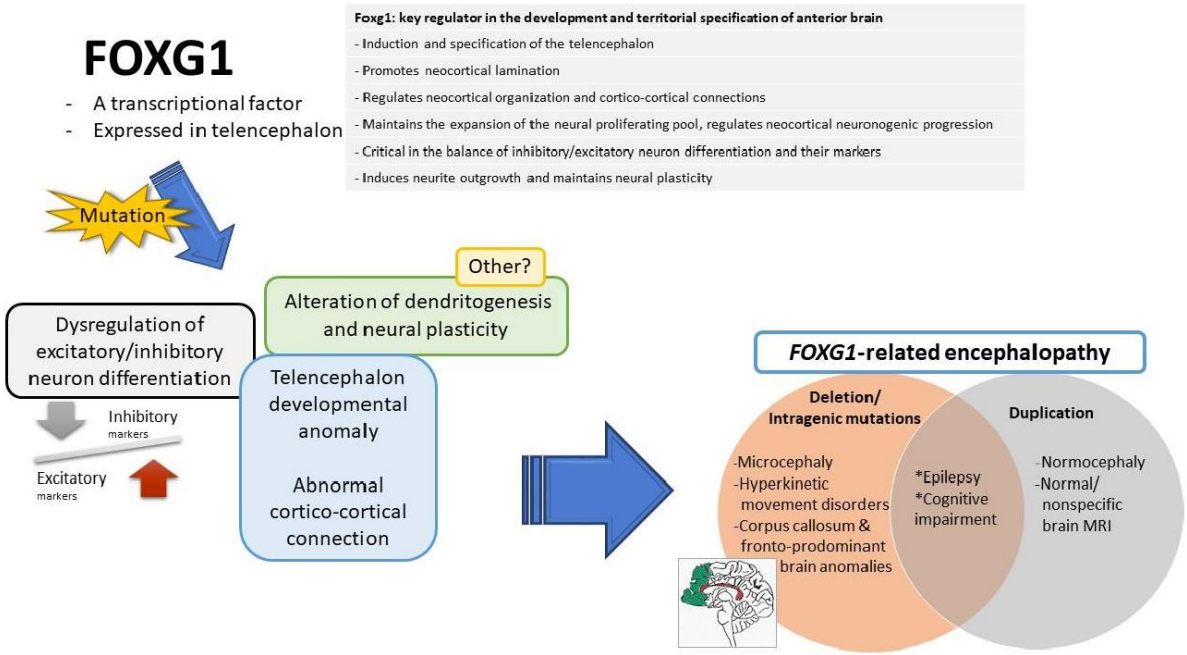

Fig. 1.2.2. Schematic view of Foxg1 roles. Taken from Wong et al., 2019.

1.3. *Foxg1* in the telencephalic specification and patterning

At E8.0-8.5 of mouse development, in the anterior edge of the neural plate starts the expression of *Foxg1*. It is induced by the rostral Fgf8 secretion from the ANR, afterwards Foxg1 expression gradually expands caudally according to a high ventral/anterior to low dorsal/posterior gradient (**Fig. 1.3.1**). At the end of the embryonic development, *Foxg1* is highly expressed in most of telencephalon except the cortical-hem, and persists into adult telencephalic derivatives, including olfactory bulbs, basal ganglia, hippocampus, and cerebral cortex [reviewed in Kumamoto and Hanashima, 2017].

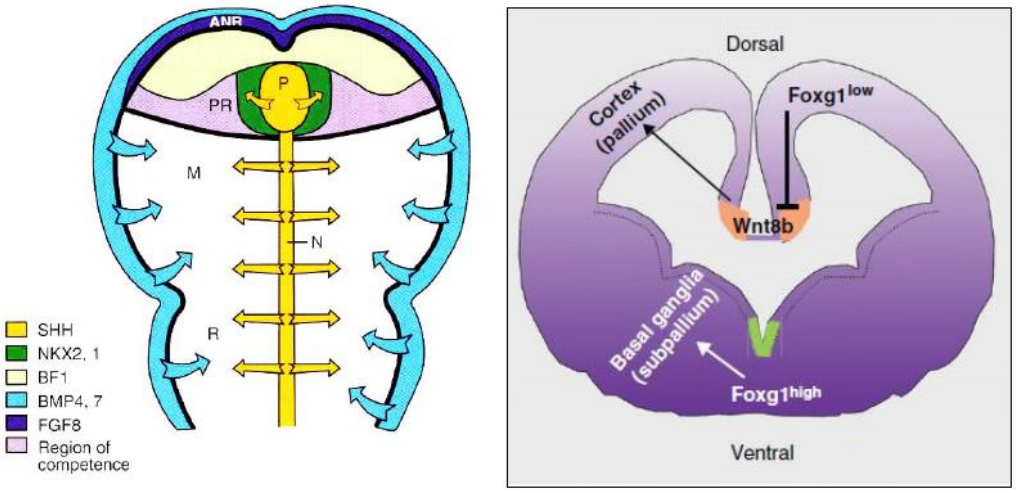

Fig. 1.3.1. Foxg1 induction and expression gradient in the developing telencephalon. (Left): ligands that allow the induction and expression regulation of *Foxg1* in the anterior neural plate. Taken from http://www.md.ucl.ac.be/didac/anat110/Brain/patterning%20forebrain.png. **(Right)**: *Foxg1* is highly expressed in the ventral part of the telencephalon where induce ventral cell fates. Dorsally, low *Foxg1* expression limits Wnt dorsalizing function, thanks inhibition and so restriction of *Wnt8b* expression to the roof plate. Adapted from Danesin and Houart, 2012.

Foxg1 regulates the dorso-ventral patterning of the telencephalon by integrating several signaling centers. Both Foxg1 and Shh promote *Fgf8* expression in the ANR. In particular, Foxg1 directly promotes *Fgf8* expression, whereas Shh indirectly promotes it by inhibiting the Gli3 repression of *Fgf8*. Moreover, the zinc-finger transcription factor Gli3 plays a dorsalizing function, thus Shh induces a ventral telencephalic identity by preventing the dorsalization. Finally, both Foxg1 and Fgf8 are required to complete the development of telencephalon forming a positive feedback loop [reviewed in Danesin and Houart, 2012].

Foxg1 is also required to restrict dorsal fates and to limit expression of Bmp and Wnt ligands of the roof plate, regulating dorsal (pallial) development. Bmps are required for the formation of the cortical-hem, which - in turn - promotes the development of the adjacent hippocampus, probably, via the secretion of Wnt ligands. The early telencephalic roof plate is a critical signaling center for pallial differentiation. Foxg1 inhibits the *Wnt8b* expression through direct transcriptional repression, restricting its domains to the roof plate. Therefore, Foxg1 limits Wnt dorsalizing activity, confining it in the pallium [reviewed in Danesin and Houart, 2012] (**Fig. 1.3.1, Right**; **Fig. 1.3.2**).

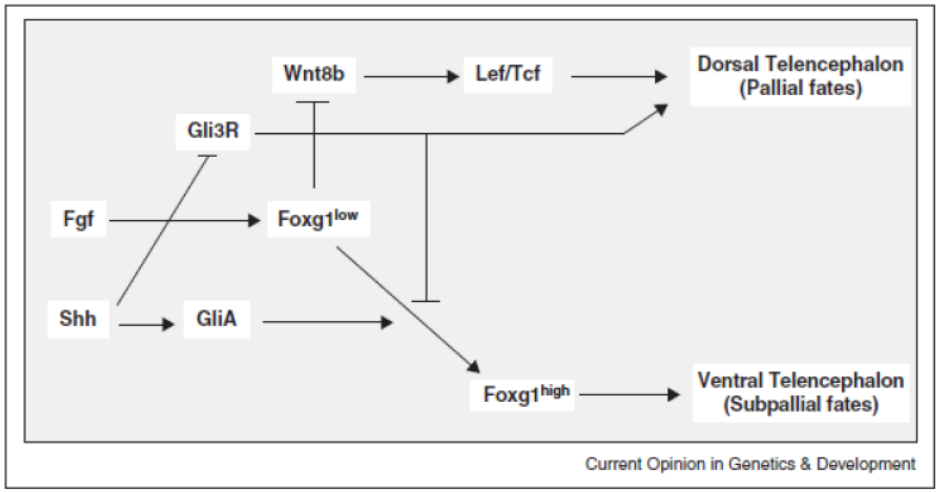

Fig. 1.3.2. Network of signaling pathways that involve Foxg1. Gli3 is present in two form: Gli3 repressor (Gli3R) and Gli3 activator (GliA). Gli3R is predominantly expressed in the dorsal telencephalon and is required for the dorsal pallial fates. Shh stimulates the conversion of Gli3R to the GliA form, leading to a higher *Foxg1* expression that in turn drives ventral subpallial fates. Taken from Danesin and Houart, 2012.

Finally, *Foxg1*-null mice fail to express peculiar markers of neocortical field. More in details, the subpallium is not formed, while the dorsal telencephalon, reduced in size, acquires molecular properties of archicortex and cortical hem, transforming ventral identity into more dorsal fates (**Fig. 1.3.3**). These defects are accompanied by a perturbation of signaling centres: dorsalizing signals (e.g. BMP4) expand ventrally and the ventralizing ligands (i.e. Shh) are lost [Xuan et al., 1995; Hanashima et al., 2004; Muzio and Mallamaci, 2005].

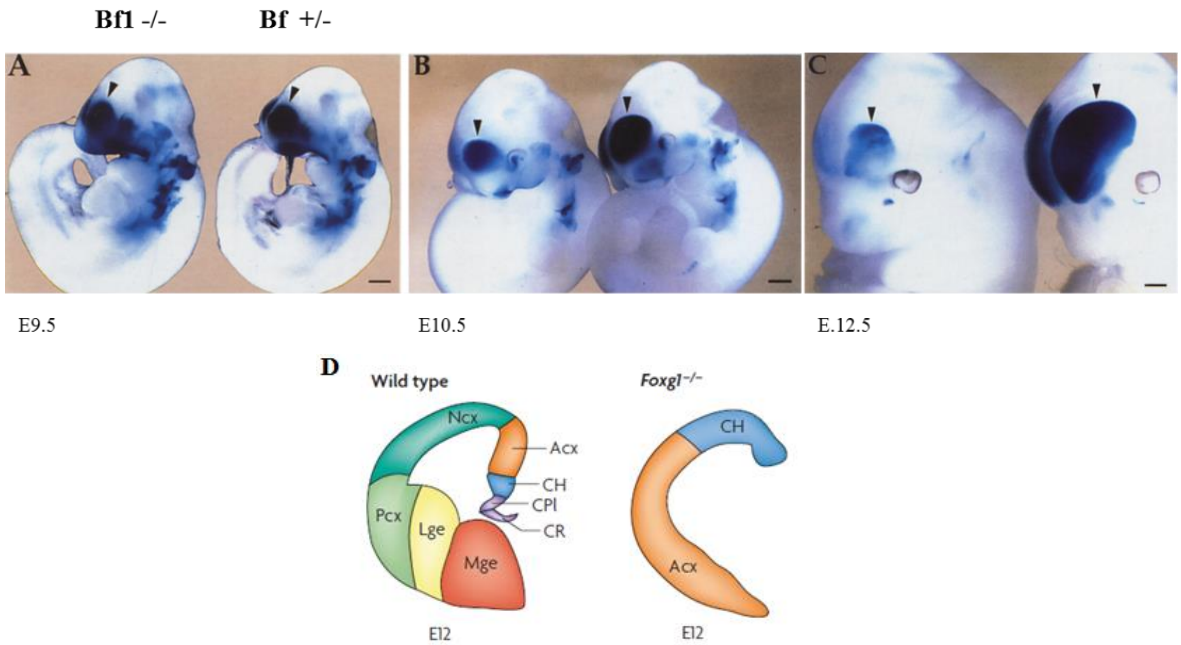

Fig. 1.3.3. The telencephalon in the loss of function (LOF) for *Foxg1*. (A-C): the telencephalon is reduced in size between E9.5 and E12.5. Adapted from Xuan et al., 1995. **(D)**: at E12 the subpallium is not formed, and the most of telencephalon acquires mainly archicortical identity. Adapted from Molyneaux et al., 2007.

1.4. The *Foxg1* role in neurogenesis and neuronal differentiation

Immediately after the telencephalic specification, neural stem cells within the VZ and SVZ undergo a period of rapid proliferation generating a disproportionate expansion of telencephalic vesicles relative to other structures. This is then followed by a gradual deceleration of cell cycle causing the exit and the differentiation of neural cells (Takahashi et al., 1995). This second phase, named neurogenesis, generates the most of neurons that will populate the post-natal telencephalon. The neurogenesis is a tight controlled process in order to ensure a correct final output of neurons at the right time and place. In this context, *Foxg1* plays a pivotal role regulating the balance between proliferation and differentiation of telencephalic neural precursors, and temporally controlling the production of specific neuronal subtypes within the cerebral cortex.

In *Foxg1*-null mice, the telencephalon is reduced in size (from E10.5; **Fig. 1.3.3A-C**) due to reduction of proliferative rate and increased differentiation [Xuan et al., 1995]. These mice die shortly after birth. More in details, telencephalic precursors show early lengthening of the cell cycle and more occurrence of exit from it [Xuan et al., 1995; Hanashima et al., 2002; Martynoga et al., 2005]. Conversely, gain of function (GOF) for *Foxg1* stimulates their proliferation, inhibits differentiation [Ahlgren et al., 2003; Bourguignon et al., 1998; Brancaccio et al., 2010; Hardcastle et al., 2000] and increases cell survival [Dastidar et al., 2011].

In order to stimulate proliferation, *Foxg1* inhibits the anti-proliferative activity of Transforming Growth Factor β (TGF-β) signaling in telencephalic progenitors. Interestingly, it has been shown that Foxg1 controls this pathway by a DNA-binding-independent mechanism. *In vitro* and *in vivo* studies showed that a mutant form of Foxg1 in its DNA-binding domain ($Foxg1^{NHAA}$; mutations from N165 and H169 to alanines) is again able to increase proliferation of neural stem cells but to not repress neuronal differentiation [Duo et al. 2000; Hanashima et al., 2002]. More in details, Foxg1 binds to and blocks the Smad-FoxO transcriptional complex, downstream the TGF-β signaling. This reduces the expression of cell cycle inhibitor $p21^{Cip1}$, preventing cell cycle exit of neural stem cells. TLE co-repressor protein contributes to inhibit the TGF-β pathway by interaction with Foxg1. Moreover, Foxg1 interacts with Foxh2 (FAST-2) to block the FAST-Smad complex formation, thereby repressing the TGF-β responsive transcriptions and allowing cell proliferation. Finally, the DNA-binding defective form of Foxg1 is not able to repress the expression of *Bmps* and *Wnts* (genes normally associated with an increased differentiation [Li et al., 1998; Mabie et al., 1999]), demonstrating a direct involvement of Foxg1 through the FHD domain.

To conclude, these studies demonstrate that:

- the pro-proliferative function of Foxg1 is based on DNA-binding-independent mechanisms, via protein-protein interactions;
- the neuronal anti-differentiative function requires the DNA-binding activity of Foxg1.

While enlarging telencephalic structures via control of cell cycle kinetics, Foxg1 also orchestrates the laminar specification of neocortex and the radial migration of newborn neurons from the VZ to the cortical plate (**Fig. 1.4.1**). These events follow a precise time and spatial order. The first step in neuronal corticogenesis is the transition from earliest-born Cajal-Retzius (CR) cells to deep-layer neurons. *Foxg1*-null mice show a premature cortical neurogenesis of early neuronal subtypes (i.e. CR cells) at the expense of later ones (**Fig. 1.4.1, Left**). Therefore, *Foxg1* represses CR cell fate, promoting the proper transition of pallial precursors to deep-layer neurons [Hanashima et al., 2004; Shen et al., 2006]. In particular, *Foxg1* sustains the activation of neuronal differential program of layer V. *Fezf2* transcription factor gene is the main determinant of layer V identity. It results inhibited by *Tbr1*, a transcription factor expressed in the majority of neocortical glutamatergic neurons at their birth. As demonstrated by Toma et al. [2014], Foxg1 represses *Tbr1* removing the inhibition on *Fezf2* (**Fig. 1.4.1, Right**).

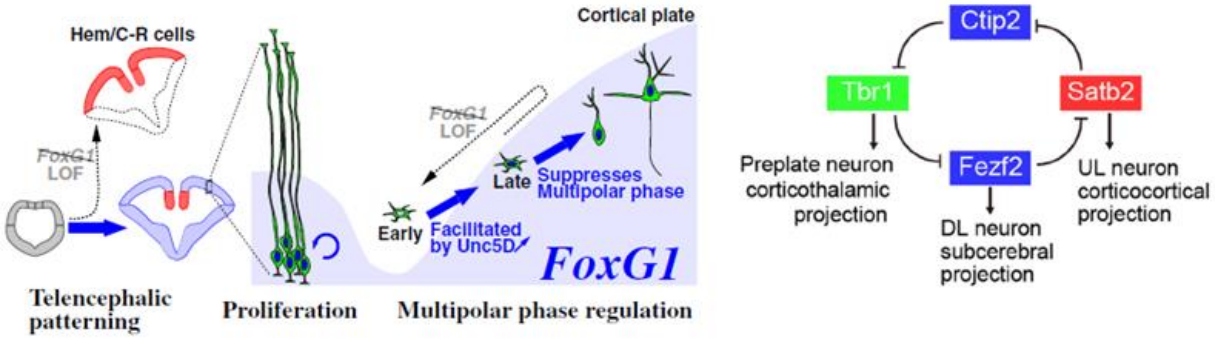

Fig. 1.4.1. The dynamic expression of *Foxg1* impacts the neuronal migration and laminar specification into the neocortex. (Left): in the first steps of telencephalic development *Foxg1* is highly expressed promoting the proliferation of neural precursors and inhibiting CR cells. Subsequently, its expression declines allowing neuronal differentiation, and then re-starts during the multipolar phase and for a proper laminar position. *Foxg1* expression is indicated with a blue wave, whereas the function with blue arrows. Adapted from Miyoshi and Fishell, 2012. **(Right)**: Schematic model of identified genetic interactions between the layer-subtype transcription factors. Adapted from Toma et al., 2014.

Concerning the radial migration, *Foxg1* is required to allow newborn neurons to entering in cortical plate. In the intermediate zone, pyramidal neuron precursors detach from the radial glia scaffold and initiate to extend their axons, assuming transiently a characteristic "multipolar" morphology, successively they enter the cortical plate. It has been demonstrated that *Foxg1* is transiently downregulated in post-mitotic multipolar precursors allowing the activation of *Unc5D*, which is crucial for transition from early to late phase. Moreover, the reactivation of *Foxg1* expression in these neurons is crucial for the proper migration into the cortical plate. Experiments in *Foxg1* loss-of-function (LOF) demonstrated that when multipolar cells failed to re-express Foxg1, they permanently lost their ability to enter into the cortical plate [Miyoshi and Fishell, 2012] (**Fig. 1.4.1, Left**). Then, *Foxg1* remains highly expressed in post-migratory neurons where is needed for the formation of the corpus callosum and cortical laminar structure [Cargnin et al., 2018].

Therefore, *Foxg1* dosage is critical at distinct developmental stages in the control of cortical neuronal generation and axonal outgrowth, thus for neuronal circuit formation.

1.5. The *Foxg1* role in the excitatory/inhibitory balance and in the control of neuronal electrical activity

The differential expression of *Foxg1* between the dorsal^{low} and ventral^{high} telencephalic precursors is fundamental in the balance of excitatory and inhibitory neurons in the mature cerebral cortex. Changes in this balance are at the basis of human neurological disorders ranging from epileptic seizures to autism spectrum disorders (ASD), including West and Rett syndromes.

In mice, it was demonstrated that *Foxg1* regulates the GABAergic interneuron development. Specifically, *in vitro* experiments showed that *Foxg1*-depleted interneuron precursors from MGE cultures developed shorter neurites and fewer branches [Yang et al., 2017]. Moreover, *in vivo* experiments showed that *Foxg1*-depleted interneurons, displayed migration defects, and mice were characterized by increased seizure susceptibility [Shen et al., 2019].

In induced pluripotent stem cell (IPSC)-derived cortical organoids[5] from ASD patients showing an overexpression of *FOXG1* is observed an increased generation of GABAergic interneurons, due to the proliferative role of *FOXG1* on ventral telencephalic precursors [Mariani et al., 2015]. Moreover, the precise endogenous dosage control of FOXG1 protein levels via CRISPR/Cas9 and SMASh[6] (small molecule-assisted shut-off) technology, showed that if FOXG1 expression declines to as little as 30% of standard level, MGE induction and GABAergic interneuron development in telencephalon organoids are suppressed [Zhu et al., 2019].

Differently from previous findings, neurons derived from iPSCs originating from patients with FOXG1 mutations, show increased levels of inhibitory synaptic markers and decreased levels of excitatory ones. That includes an upregulation of *Grid1* (orphan glutamate receptor δ-1 subunit) encoding for a synaptic cell adhesion protein which shifts the balance excitatory/inhibitory synapses towards the inhibitory one [Patriarchi et al., 2016]. However, it is still not clear how this imbalance is linked with seizures observed in *FOXG1* patients.

Foxg1 continues to be highly expressed in post-mitotic neural cells even after the embryonic development of telencephalic structures, at post-natal and adult stages. This suggests that *Foxg1* may play a key role in high cognitive functions and neural plasticity.

[5] Organoids can recapitulate the human first trimester cortical development *in vitro*. Used as a substitute for human brain developmental model.
[6] It takes advantage of a self-removing degron fused with the protein of interest. In the presence of specific small molecules, it is not able to self-cleave, and thus, it allows the degradation of protein [Chung et al., 2015].

Chiola et al. [2019] demonstrated, both *in vitro* and *in vivo*, that *Foxg1* promotes dendritic elongation and arborization of post-mitotic glutamatergic pyramidal neurons, mainly via Hes1/pCreb1 pathway, and increases spine densities *in vitro*. Moreover, Foxg1 increases the electrical activity of neocortical pyramidal neurons, and in turn, is itself regulated by electrical stimulation [Tigani et al., 2020]. At the molecular level, *Foxg1*-overexpressing post-mitotic neocortical neurons show alteration of specific gene-sets involved in neuronal activity/excitability, such as genes encoding for voltage-gated Na+ and Ca2+ ion channels, intracellular Ca2+ flux mediators, and glutamate- and GABA-gated ion channels [Tigani et al., 2020; dataset by Artimagnella and Mallamaci, 2020].

Regarding neural plasticity, a study recently showed that the conditional knockout (cKO) of *Foxg1* in adult *Camk2α*-positive neurons resulted in impairment of spatial learning and memory, as well as a deficiency in social behavior. These results were accompanied with a significant decrease of evoked post-synaptic currents (eEPSCs) in CA1 pyramidal neurons, as well as in the reduction of NMDA receptor activity, and thus the impairment of long-term potentiation (LTP). A possible cellular mechanism which underlies the altered synaptic transmission, is the fact that the cKO of *Foxg1* in mature neurons leads to decreased dendritic arborization, axonal maintenance and spine density [Yu et al., 2019].

Altogether, these findings suggest the fundamental role of *Foxg1* in the regulation of cortical excitability.

1.6. *Foxg1* and astrogenesis

While in the midst of neuronogenesis, neural stem cells start to originate astrocyte-committed progenitors, so initiating astrogenesis, which reaches its peak after neurogenesis completion. The neuron-to-astrocyte progenitor switching is a tightly controlled developmental step. *Foxg1* affects neurogenesis via different cellular and molecular mechanisms (as shown above), that in turn impact on astrogenesis.

Both in murine and in human cells, neural stem cells restricted *Foxg1* overexpression leads to a reduction of astroglial output, and conversely promotes neurogenesis [Brancaccio et al., 2010; Falcone et al., 2019]. The *in vitro* as well as *in vivo Foxg1* anti-astrogenic activity is mainly due to inhibition of neural stem cell-to-astrocyte progenitor transition. From a mechanistic point of view, there are at least three distinct processes which occur: 1) downregulation of key transcription factor genes directing the neural stem cell-to-astrocyte progenitor progression, such as *Couptf1*, *Zbtb20*, *Sox9*, and *Nfia*; 2) direct transrepression of genes which drive the astroglial differentiation program (e.g., *Gfap* and *S100b*); 3) and *Foxg1*-dependent modulation of key pathways controlling astroglial genes (IL6/Jak2/Stat1,3, Bmp/Smad1,5,8, Dll1/Notch1^{ICD}). Finally, Foxg1 concentration within neocortical neural stem cells progressively decline, moving from the neuronogenic to the gliogenic phase, suggesting that such decline may be instrumental in proper temporal articulation of neural stem cells developmental choices [Falcone et al., 2019].

Furthermore, it was also demonstrated that the *Foxg1* overexpression inhibits astrocyte differentiation and can trigger de-differentiation to a proliferative neural stem cell state [Bulstrode et al., 2017; Santo et al., unpublished]. The anti-astrogenic activity of *Foxg1* combined with the promotion of neural stem cell self-renewal led to identify it as a key determinant in Glioblastoma multiforme tumor [Bulstrode et al., 2017; Dali et al., 2018].

1.7. *F*oxg1-related syndrome

As described until now, the expression level of *FOXG1* gene is finely regulated in each step of telencephalon development and neuronal differentiation. Therefore, in humans even a subtle change in its expression may impact many developmental pathways and processes leading to a wide range of rare neurological disorders. They include a congenital variant of Rett's syndrome, West's syndrome, autism spectrum disorders (ASD) and schizophrenia [reviewed in Kumamoto and Hanashima, 2017]. To date, more than 120 different *FOXG1* mutations have been reported, categorizable as: deletions/intragenic loss-of-function mutations, and duplications. Although the phenotype produced by *FOXG1* mutations overlaps with the previous cited developmental disorders, it is now considered that individuals harboring these mutations belong to a distinct clinical category, termed "*FOXG1* Syndrome", characterized by specific features. Differently from the Rett's syndrome, that prevalently affects female children, *FOXG1*-related disorders have been identified in both female and male patients [reviewed in Wong et al., 2019].

FOXG1-related deletions/intragenic mutations

The first description of *FOXG1* mutation was reported by Shoichet et al. [2005] in a 7-years-old girl with a global development delay and cognitive deficit. In this case, the patient presented a balanced *de novo* translocation t(2; 14)(p22;q12) with a neighboring 720-kb inversion in chromosome 14q12 that disrupts the *FOXG1* transcript. More in details, children with *FOXG1* deletions/intragenic mutations develop post-natal microcephaly, severe psychomotor delay, dyskinesia and hyperkinetic movements, language deficits, visual impairment, sleep disturbance, stereotypies, epilepsy, and severe cognitive disabilities [reviewed in Hou et al., 2020]. Moreover, brain magnetic resonance imaging (MRI) shows cerebral malformation, which includes the combination of frontal gyrus simplification with severe myelination delay, and a thinner corpus callosum. Regarding epilepsy, it is present in the majority of individuals with *FOXG1* deletions. The onset of seizures occurs in the first 3 years of age, ranging from 2 days to 14 years. They include infantile spams, focal seizures, generalized tonic-clonic seizures, and myoclonic seizures. Finally, the electroencephalogram (EEG) may show focal or multifocal epileptiform discharges without a specific pattern [reviewed in Wong et al., 2019].

At the genomic level, the most of mutations are *de novo*, including frameshift, missense, and nonsense mutations. However, some of them are inherited from clinically unaffected parents with somatic mosaicism [Diebold et al., 2014]. The *FOXG1* mutations are distributed all along the gene from the N-terminal to the C-terminal region. Interestingly, some deletions involve also

FOXG1-regulatory regions, affecting its expression level. A cohort study [Mitter et al., 2017] involving 83 individuals showed that the most severe phenotypes were associated with frameshift and nonsense mutations (generating commonly a truncated form of FOXG1) in the N-terminus and in the forkhead domain. In contrast, milder phenotypes were associated with missense mutations in the first part of the forkhead domain (181-194aa) and deletions in the regulatory regions [reviewed in Wong et al., 2019].

FOXG1-related duplications

There are few reports (21 cases) of children with *FOXG1* duplications. They present typically a normal brain size, and non-specific alteration of brain in MRI. However, they have different clinical characteristics in term of epilepsy, movement disorders, and neurodevelopment compared to children with *FOXG1* loss-of-function mutations. The common phenotype is characterized by a severe developmental delay and autistic behaviors associated with an absence or a delay of speech. Epilepsy in these individuals has different features from that due to deletions. The age of onset is younger, around 3-7 months of age. Commonly, patients present infantile spasms, the EEG shows hypsarrhythmia, and ranges from normal to focal or multifocal epileptiform discharges [reviewed in Wong et al., 2019].

Duplications are typically *de novo* and ranges between 3.1 and 33.9Mb on chromosome 14q12. However, patients with *FOXG1* duplications are not always severely impaired as those with *FOXG1* deletions. Some of them display normal phenotype and development, and no epilepsy. A possible explanation for the phenotypic variabilities could be: 1) the big size of duplications, which may involve different regulatory elements and other genes; 2) a possible incomplete penetrance of *FOXG1* duplication; 3) and genetic mosaicism [reviewed in Wong et al., 2019].

1.8. Beyond the nuclear function: cytoplasmic roles of Foxg1 in neuronal differentiation

Until now, we presented Foxg1 as a classical transcriptional factor that works into the nucleus to regulate, with both direct (DNA-dependent) and/or indirect (DNA-independent) mechanisms, the expression of many genes involved in telencephalic development. However, recent studies have been demonstrated that Foxg1 protein is also localized in the cytoplasm of post-mitotic neural cells, where it serves not fully understood roles in neuronal differentiation.

The first evidence that Foxg1 is not only confined into the nucleus was published in [2007] from Regad et al. In frog and mouse forebrain, they showed that Foxg1 is nuclear in progenitor cells and cytoplasmic in early neuronal differentiation areas, such as the mammalian superficial layer I (i.e. Cajal-Retzius cells) and deep layer VI neurons. This different subcellular localization is regulated at post-translational level. Specifically, two reciprocal pathways, Casein Kinase I (CKI) and FGF signaling, recognize different serine/threonine sites in Foxg1 protein sequence, determining its final cellular compartment. CKI phosphorylates Foxg1 at the N-term Ser19 site promoting the nuclear localization of Foxg1. Indeed, in neurons the replacement of Ser19 with a non-phosphorylated alanine residue, or the pharmacological inhibition of the CKI signaling, resulted in a cytoplasmic localization of Foxg1, and altered neurogenic activity. Conversely, the FGF signaling promotes the Foxg1 nuclear export thanks to the phosphorylation of Thr226 site within the fork-head domain. This phosphorylation is specifically mediated by the PI3K-Akt pathway. Indeed, *in vitro* studies showed that Foxg1 failed to exit the nucleus, in response to FGF2, under inhibitors of Akt (**Fig. 1.8.1**). Same results were obtained *in vivo*, confirming the post-translational regulation of Foxg1 and its subcellular localization.

In conclusion, this study proposes that the nuclear export may act as a post-translational repression of Foxg1 from nuclear functions (such as those involved in positive effect on proliferation), promoting the differentiative status.

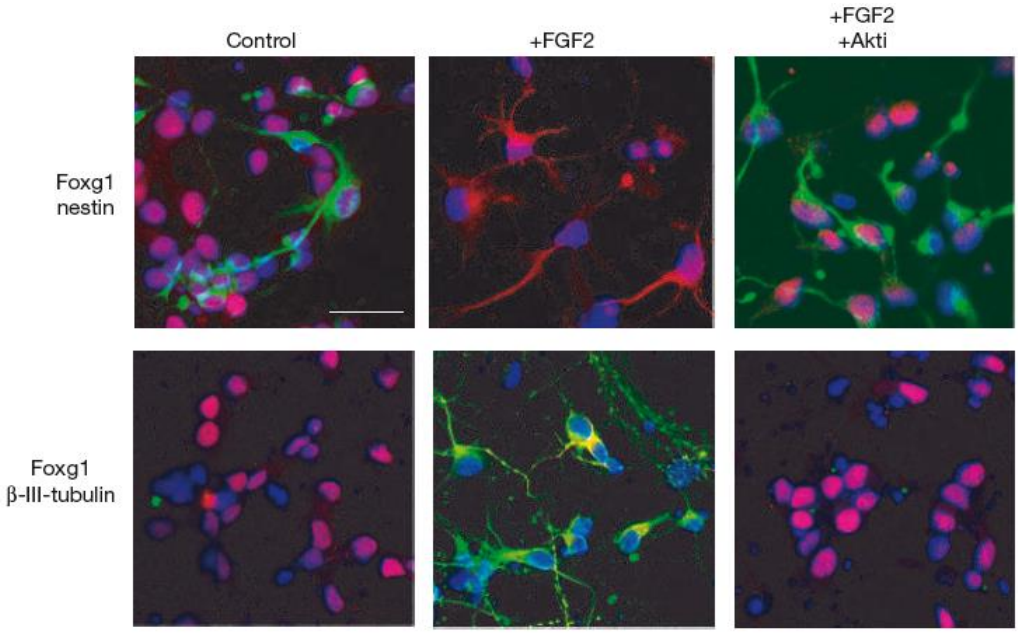

Fig. 1.8.1. The subcellular localization of Foxg1 in mouse cortical progenitors and differentiated neurons. After treatment with Fgf2, nestin is lost and Foxg1 is observed in the cytoplasm, colocalizing with β-III-tubulin. These changes do not take place in the presence of Akt inhibitors (+Akti). Foxg1 is shown in red, nestin and β-III-tubulin in green. Scale bar, 100 μm. Adapted from Regad et al., 2007.

Second, more recently, another study [Pancrazi et al., 2015] confirmed the cytoplasmic expression of Foxg1 and showed even the mitochondrial localization in post-mitotic neural cells. Specifically, it has been shown that Foxg1 protein is involved in proteolytic cleavage at N-terminal, generating three main forms: the full-length protein (FL-Foxg1, 481aa), the mitochondrial fraction (mt-Foxg1, 272-481aa), and the smallest cytosolic one (cyt-Foxg1, 315-481aa). The mitochondrial translocation of Foxg1 seems to be membrane-potential-dependent, where 277-302aa region plays a critical role for mitochondrial localization. Moreover, overexpression of the FL-Foxg1 form promoted mitochondrial fission, cellular proliferation, and enhanced mitochondrial membrane potential. Conversely, the specific overexpression of mt-Foxg1 increased mitochondrial fusion and it is involved in neuronal differentiation (**Fig. 1.8.2**).

Considering that mitochondria are, in addition to their energetic role, also implicated in the control of brain development and neuroplasticity [Gioran et al., 2014; Mattson et al., 2008], this work reveals a possible link among Foxg1, mitochondrial function, neuronal differentiation, and plasticity.

Third, it has been shown that Foxg1 is directly involved in post-transcriptional regulation. In N2a cells, mass-spectrometry analysis and co-immunoprecipitation assays revealed that FOXG1 interacts with the RNA helicase DDX5, which recruits FOXG1 to the DROSHA complex. This

interaction affects miRNA biogenesis, specially of miR200 family members which resulted down-regulated by small RNA-seq of hippocampal cells from adult *Foxg1* heterozygous mice, suggesting that Foxg1 promotes mir200 biogenesis [Weise et al., 2019]. Interestingly, *Foxg1* itself is a target of miR200, suggesting a feedback loop in the regulation of *Foxg1* expression [Zeng et al., 2016]. Moreover, the intersection of RNA-seq following miR200 overexpression in N2a cells with RNA-seq of *Foxg1* heterozygous hippocampus, showed an overlap of 35 target genes. Among them, the *Prkar2b* gene, encoding for the protein kinase cAMP-dependent regulatory type II beta (PRKAR2B), inhibits post-synaptic function by attenuating the PKA activity. This suggests that the increased level of *Prkar2b* observed upon *Foxg1*-LOF may contribute to neuronal dysfunction of synaptic transmission [Weise et al., 2019] (**Fig. 1.8.2**). This work shows that Foxg1 may be implicated in the control of synaptic function via post-transcriptional mechanisms, opening new avenues in the *FOXG1* syndrome.

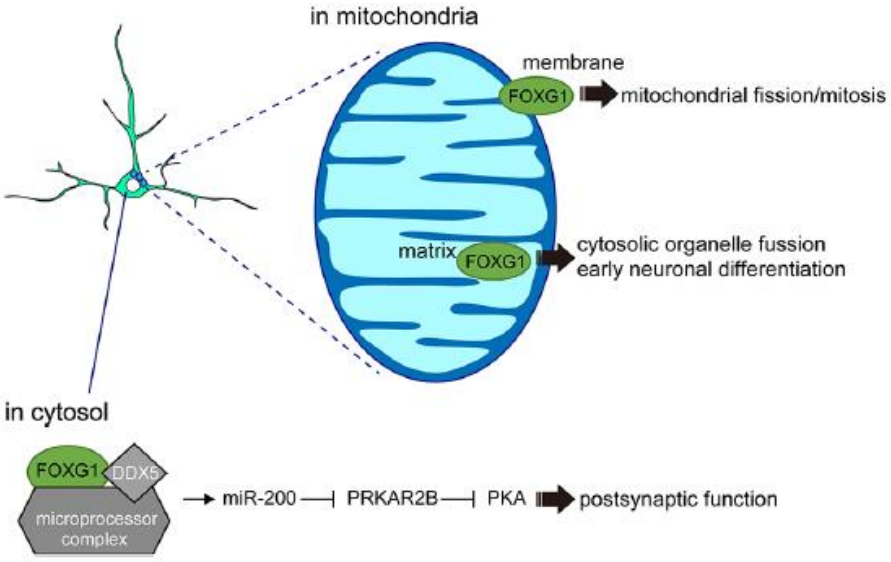

Fig. 1.8.2. Non-nuclear functions of *FOXG1*. Taken from Hou et al., 2020.

Fourth, further evidence that Foxg1 may be implicated in cytoplasmic roles derived from high-throughput mass-spectrometry experiments, which have been revealed as FOXG1 seems to interact with many non-nuclear factors. Specifically, Weise et al. [2019] discovered in N2a cells the direct involvement of FOXG1 in pathways related to RNA metabolism, i.e. pre-mRNA splicing, mRNA transport and RNA degradation, as well as to ribosome biogenesis. Moreover, the "Biogrid" protein-protein interaction database [www.thebiogrid.org] reports that human

FOXG1 binds to key factors of splicing (e.g. SNRNP200), mRNA nucleo-cytoplasm translocation and mRNA motility (e.g. NUP205, MYO9B), and of mRNA translation (e.g. PUM1, LARP1, EEF1D, EEF1G, VARS).

Finally, aminoacid-sequence analysis of human FOXG1 (as well as of murine Foxg1, and many other orthologues) reveals a motif very similar to eIF4E-binding module consensus sequence, classically present in translation regulators and further reported in selected homeoproteins (HPs) [Brunet et al., 2007] (**Fig. 1.8.3**). The consensus module consists in seven residues: Y(X)4LΦ (where X is any aminoacid and Φ is any hydrophobic aminoacid). In human FOXG1 protein the hypothetical module is localized from 374 to 380 aa, just upstream to JBD-binding domain (**Fig. 1.8.4**), and it results very similar to consensus sequence, except for the last residue, which is not an apolar aminoacid [*personal observation*].

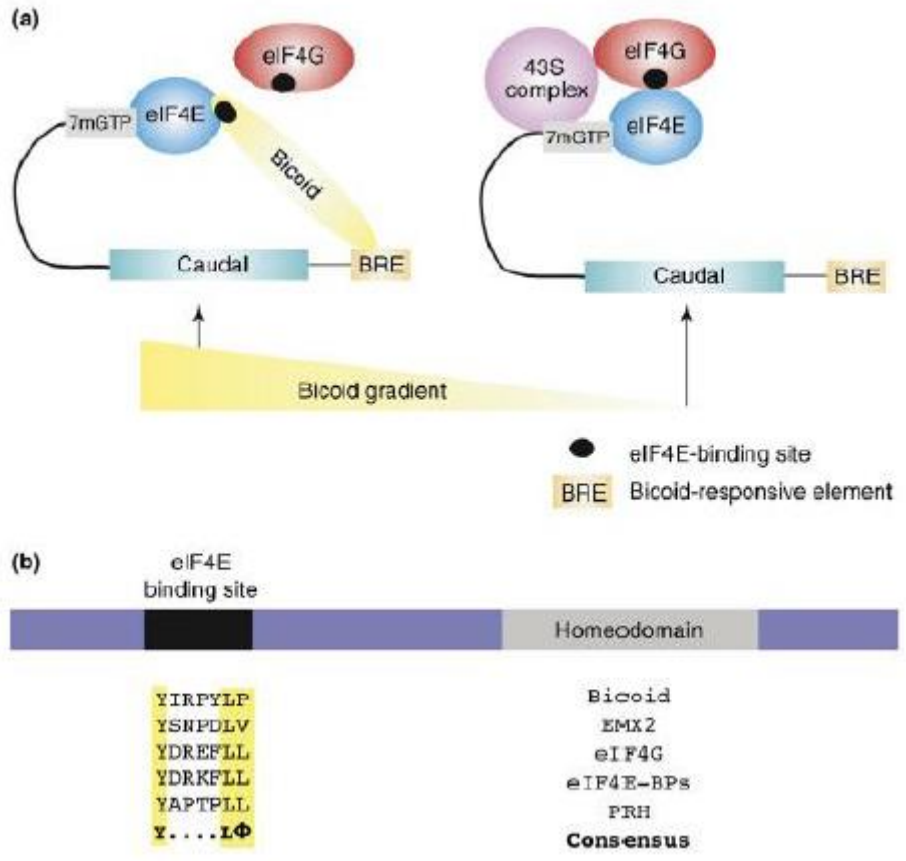

Fig. 1.8.3. Interaction among HPs and the translational machinery. (a): Bicoid inhibits caudal mRNA via chelating eIF4E. **(b)**: eIF4E binding sites in established translational modulators and HPs. Taken from Brunet et al., 2007.

FOXG1 protein sequence

MLDMGDRKEVKMIPKSSFSINSLVPEAVQNDNHHASHGHHNSHHPQHHHHHHHHHHH
PPPPAPQPPPPPQQQQPPPPPPPAPQPPQTRGAPAADDDKGPQQLLLPPPPPPPPAA
ALDGAKADGLGGKGEPGGGPGELAPVGPDEKEKGAGAGGEEKKGAGEGGKDGEGGKE
GEKKNGKYEKPPFSYNALIMMAIRQSPEKRLTLNGIYEFIMKNFPYYRENKQGWQNS
IRHNLSLNKCFVKVPRHYDDPGKGNYWMLDPSSDDVFIGGTTGKLRRRSTTSRAKLA
FKRGARLTSTGLTFMDRAGSLYWPMSPFLSLHHPRASSTLSYNGTTSAYPSHPMPYS
SVLTQNSLGNNHSFSTANGLSVDRLVNGEIP**YATHHLT**AAALAASVPCGLSVPCSGT
YSLNPCSVNLLAGQTSYFFPHVPHPSMTSQSSTSMSARAASSSTSPQAPSTLPCESL
RPSLPSFTTGLSGGLSDYFTHQNQGSSSNPLIH

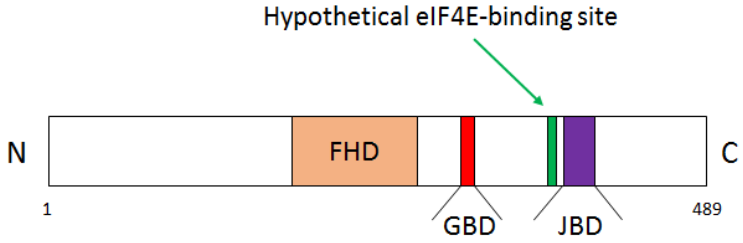

Fig. 1.8.4. FOXG1 protein sequence and its domains. In green is indicated the hypothetical 7 long aminoacids eIF4E-binding site. Red letter means the conserved aminoacid residue compared to the consensus module.

Altogether, this evidence strongly suggests that Foxg1 may be directly involved in post-transcriptional and translational mechanisms of neural cells. Since Foxg1 is involved in the regulation of neuronal activity in post-natal and adult neurons, these new mechanisms might be on the basis of Foxg1 regulation on synaptic transmission.

1.9. The NMDA receptor and synaptic plasticity

To date, it is known that NMDA receptors (NMDARs), triggering the glutamatergic transmission, are crucial for neuronal communication and to induce activity-dependent synaptic plasticity, that is thought to underlie higher cognitive functions. NMDARs are glutamate-gated ion channels formed by four subunits (heterotetrameric receptors): two GluN1 main subunits; and other two regulatory subunits (containing the glutamate binding site), which define their biophysical and pharmacological properties. GluN1 is encoded by the *Grin*1 gene, which presents eight alternative splicing variants; instead, regulatory subunits are encoded by different genes: four genes for GluN2 subunits (GluN2A/*Grin2a*, GluN2B/*Grin2b*, GluN2C/*Grin2c*, GluN2D/*Grin2d*); and two genes for GluN3 subunits (GluN3A/*Grin3a*, GluN3B/*Grin3b*). The combination of these subunits theoretically originates more than 60 possibilities, but only 9 receptor subtypes have been described, forming di-heteromeric or tri-heteromeric NMDARs. Structurally, all seven GluN subunits consist of four distinct domains[7] [reviewed in Paoletti et al., 2013]:

- NTD, the N-terminal domain which is mainly involved in the allosteric regulation of NMDA receptor.
- ABD, the agonist-binding domain which binds glutamate in GluN2 subunits and glycine (or D-serine) in GluN1 and GluN3 subunits. NTD and ABD are in the extracellular region.
- TMD, the transmembrane domain which consists in three transmembrane helices and a pore loop that forms the ion selectivity filter.
- CTD, the intracellular C-terminal domain is the region that most varies among each GluN subunits and within the alternative isoforms of GluN1 subunit. The CTD is quite long, and involved in receptor trafficking, anchoring and coupling to signaling molecules.

The *Grin1* gene

Grin1 is the gene encoding for the main subunit of NMDA receptor, GluN1. It is abundantly expressed in the brain (neocortex, hippocampus, thalamus, striatum and cerebellum) and in the spinal cord [Prybylowski et al., 2001]. *Grin1* presents a total of 22 exons[8] and a complex pattern of alternative splicing, which involves exon 4, 20, 21 and 22 (also termed N1, C1, C2, and C2', respectively), generating eight *Grin1* transcript variants (**Fig. 1.9.1**). The exon 22 is generated

[7] The structure of a full NMDA receptor (GluN1-GluN2B) was described the first time by Karakas and Furukawa [2014].
[8] This count is made projecting in the *Grin1* gene locus all exons generated from the alternative splicing (from Ensembl database).

via the splicing out of exon 21, because its deletion removes the first stop codon and forms a new open reading frame before the second stop codon. Isoforms-containing exon 4 possess the additional extracellular cassette N1 (21aa) that increases current amplitude and reduces affinity for agonists, affecting the NMDAR's gating and pharmacological properties. Isoforms derived from C-terminal exons present CTDs of variable length and differential trafficking properties. Those splice variants presenting both C1 (37aa) and C2 (38aa) cassettes are also indicated as long GluN1, whereas those including only the C2' cassette (22aa) are also indicated as short GluN1. The C1 cassette contains an endoplasmic reticulum retention signal (RRR), thus GluN1 variants that have the C1 cassette present significantly less surface expression than those without C1. Conversely, the C2' cassette, that includes the terminal PDZ-interacting domain[9], confers increased surface expression [reviewed in Lau and Zukin, 2007; Vrajova´ et al., 2010].

Finally, there are some differences in localization and developmental expression of *Grin1* spliced variants. In the embryonic stage, the first isoforms to be expressed are those lacking N1 cassette, which, instead, appear in the post-natal phase. Moreover, GluN1 variants harboring the C2 cassette is widely distributed in the brain, whereas those containing both C1 and C2 cassette are concentrated in more rostral regions, including the neocortex and hippocampus [Zukin and Bennett, 1995].

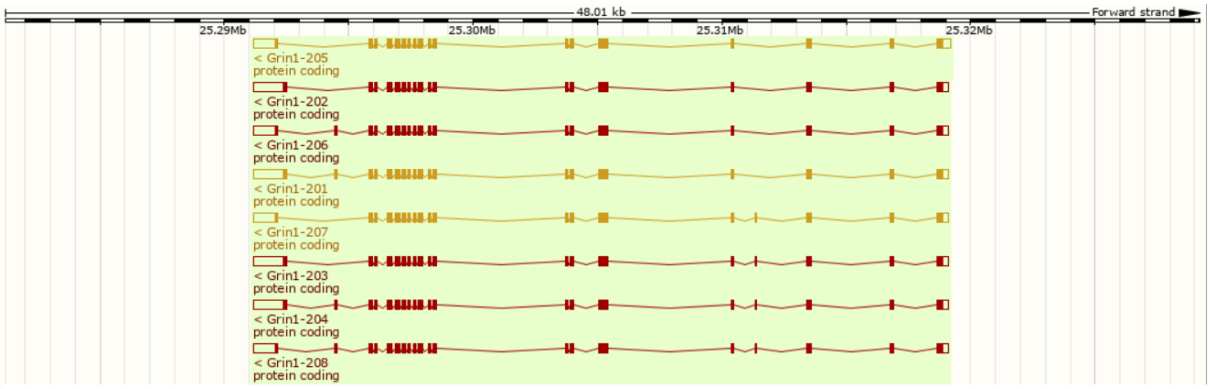

Fig. 1.9.1. Grin1 gene locus with its alternative splicing isoforms. Image taken from Ensembl database.

[9] The PDZ domain mediates the association between NMDARs and scaffolding proteins of post-synaptic densities, promoting receptor delivery to membrane.

Regulatory NMDAR subunits

The expression of regulatory subunits is regulated in time and space of CNS. Specifically, in neocortex GluN2A and GluN2B are the major regulatory subunits. For this reason, we continue description of NMDARs focusing on those composed by these two regulatory subunits (this sub-paragraph is extensively reviewed in [Paoletti et al., 2013]; for more details about other regulatory subunits please refer to the review).

According to the subunit composition of NMDARs, they show different biophysical, pharmacological and signaling attributes.

- Permeation properties: di-heteromeric NMDARs including GluN2A or GluN2B subunits generate high-conductance channel openings with high sensitivity to Mg^{2+} blockade and Ca^{2+} permeability.
- Gating properties: GluN2A-containing NMDA receptors have a higher open probability than GluN2B-containing ones but the lowest sensitivity to glutamate and glycine. Finally, the glutamate deactivation kinetics, which govern the excitatory post-synaptic current (EPSC) decay, is faster in GluN1/GluN2A receptors than GluN1/GluN2B ones. Interestingly, this kinetics is also influenced by GluN1 isoforms, in particular exon 4-containing GluN1 isoforms decay faster than those that do not contain it. EPSC decay is a crucial parameter in the control of synaptic integration.
- Pharmacological properties: NMDARs are modulated by different substances, such as protons, polyamines and Zn^{2+}. GluN2B-containing receptors are preferentially inhibited by protons and enhanced by polyamines. By contrast, GluN2A-containing receptors are antagonized by Zn^{2+} ions with higher sensitivity compared to GluN1/GluN2B receptors. These pharmacological properties are useful to distinguish NMDARs subunit composition. For this purpose, synthetic drugs were also developed, such as ifenprodil and derivatives (e.g. Ro 25-6981), acting as GluN2B-specific antagonists, whereas TCN-201 is a GluN2A-specific antagonist, reducing glycine potency.
- Trafficking and signaling properties: the CTD domain is the site of many subunit-specific regulations that affect receptor trafficking and signaling. NMDARs subunits are co-synthesized and assembled in the endoplasmic reticulum (ER). Their export from ER and the transport to synapses varies according to GluN1 C-terminal isoforms. Generally, this process is regulated by neuronal activity (see below). Moreover, numerous kinases phosphorylate specific sites of GluN2 subunits, participating in the subunit-specific trafficking and intracellular signaling. In particular, Ca^{2+}/calmodulin-dependent protein kinase II (CaMKII), which has a crucial role in

LTP induction, strongly interacts with the CTD of GluN2B subunit compared to that of GluN2A, suggesting that GluN2B-CaMKII interaction is implicated in synaptic plasticity.

Activity-dependent NMDARs regulation

Neuronal activity regulates the subunit composition of NMDARs, and this occurs during development, as well as in mature neurons. GluN2B is predominantly expressed during the embryonic development, whereas at the birth there is the so called "NMDAR developmental switch", in which GluN2A expression increase, while GluN2B remains low and quite constant. This time window coincides with synapse maturation, circuit refinement and acquisition of learning abilities. Moreover, the post-natal GluN2B-to-GluN2A switch is also driven by neuronal activity and/or experience-dependent plasticity, indeed synaptic activity promotes GluN2A trafficking at the synapse, and then insertion of GluN2A-containing NMDARs. By contrast, neuronal activity increases the synaptic clearance of GluN2B-containing receptors. In a similar way, even at mature synapses NMDARs are dynamically regulated by synaptic activity [reviewed in Lau and Zukin, 2007]:

- LTP promotes insertions of NMDARs, in particular of GluN2A-containing receptors, as well as lateral diffusion of them from extrasynaptic sites [Grosshans et al., 2002] (**Fig. 1.9.2a**).
- Conversely, LTD promotes endocytosis of NMDARs, a lateral displacement of them from synaptic sites, and a general destabilization of synapse structure [Morishita et al., 2005; Snyder et al., 2001] (**Fig. 1.9.2b**).
- Activity blockade enhances the levels of GluN2B subunit, and thus the presence at synaptic membrane of GluN1/GluN2B receptors. Moreover, it promotes splicing out of GluN1 exon 21 (C2) and splicing in of exon 22 (C2', short GluN1) [Ehlers et al., 2003; Mu et al., 2003] (**Fig. 1.9.3**).
- Chronic activity enhances the levels of Glun2A subunits, the proteasomal degradation of GluN1 and GluN2B subunits, favoring the switch from GluN2B-containing to GluN2A-containing NMDARs. Moreover, it promotes the splicing in of GluN1 exon 21 (C2, long GluN1) [Ehlers et al., 2003; Mu et al., 2003] (**Fig. 1.9.3**).

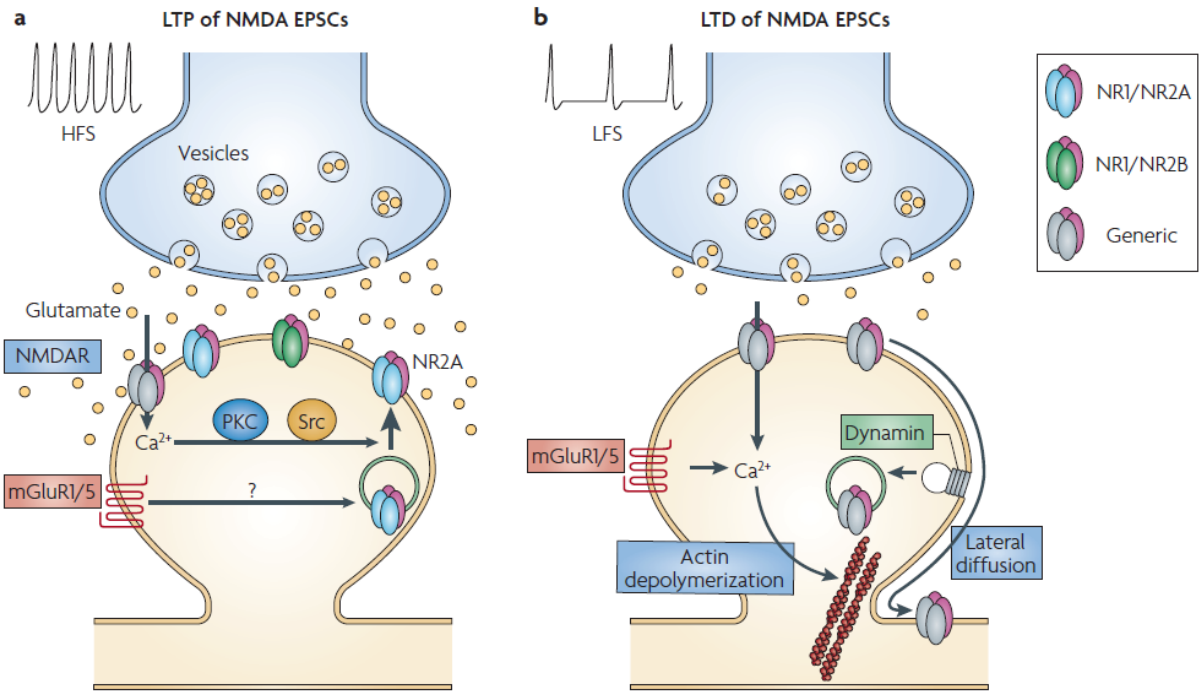

Fig. 1.9.2. LTP and LTD effects on NMDARs. (a) LTP. **(b)** LTD. Image taken from Lau and Zukin 2007.

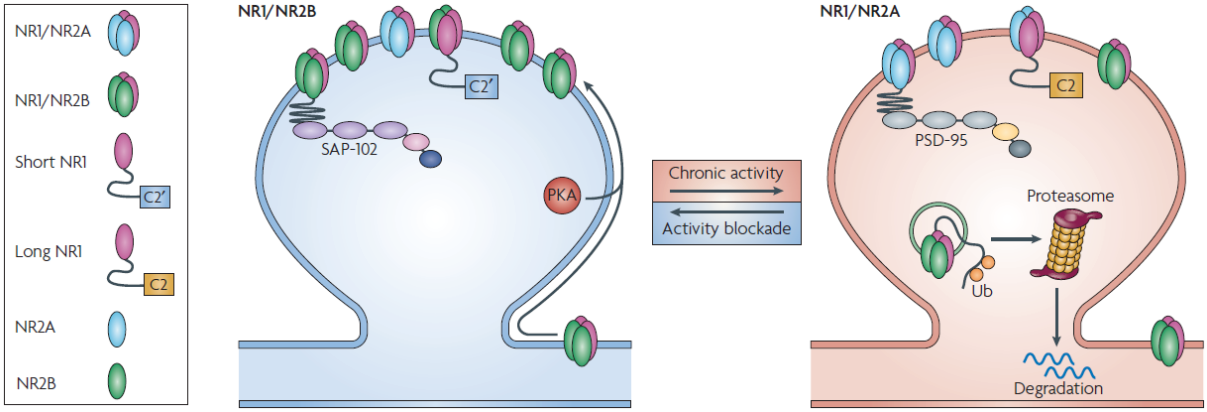

Fig. 1.9.3. Effects of activity blockade and chronic activity on NMDARs. Image taken from Lau and Zukin 2007.

Activity-dependent translation of GluN1 and GluN2A subunits

A number of studies investigated in deep about changes in NMDAR subunits expression after plasticity induction. In many of them it has been reported that there are specific waves of NMDAR subunit rises after high-frequency stimulation (HFS). In more details, in hippocampal slices and cultures, GluN1 and GluN2A subunit levels increased, reaching the peak 70 minutes after HFS, whereas GluN2B remained constant. Moreover, both GluN1 and GluN2A subunits were increased in dendrites of hippocampal cultures 30-75 minutes after KCl pulses, which mimic plasticity induction. Interestingly, looking at 90 minutes post-stimulation subunit levels did not differ from unstimulated neurons, suggesting the implication of degradation mechanisms [reviewed in Baez et al., 2018].

From a mechanistic point of view, a dendritic localization of *GluN2A* mRNA, characterized by a short polyA tail and inefficiently translated, was observed. After stimulation by NMDA, a polyA polymerase (Gld2) catalyzes the addition of A nucleotide in the tail of *GluN2A* mRNA, leading to translational enhancement of it. However, a similar mechanism was not reported for GluN1 [Udagawa et al., 2012]. Another study showed that cycloheximide (CHX)[10] treatment did not alter GluN1 increase in dendrites, but significantly blocked the increase of GluN2A subunits. However, at the level of neuronal soma, the increase of both GluN2A and GluN1 levels were blocked adding CHX before KCl pulses. Conversely, the addition of actinomycin D (ActD)[11] partially affected only GluN1 subunits [Cercato et al., 2017].

Altogether, these results suggest that GluN2A-containing NMDARs increase in dendrites after plasticity induction, through local translation of GluN2A subunits. Conversely subject of translational (and to some extent also transcriptional) plasticity-driven upregulation, GluN1 subunits are generated at neuronal soma ER, from which they are available to be transported in dendrites to assemble GluN2A-containing NMDA receptors.

NMDARs and CNS disorders

Many neurological and neuropsychiatry disorders are linked to NMDAR subunits alteration levels. In **Fig. 1.9.4** a partial list of such diseases is reported, with the subunit type implicated, and the therapeutics treatments available to date.

[10] CHX is an inhibitor of protein synthesis. It binds to the exit E-site of ribosomes and blocks translational elongation.
[11] ActD is a transcriptional inhibitor. It binds to DNA at the level of transcription initiation complex, blocking RNA polymerase elongation.

Disease indications	Key NMDAR-subunit related alterations	Therapeutic treatments
Cerebral ischaemia and traumatic brain injury	Excessive activation of NMDA receptors (NMDARs), especially extrasynaptic GluN2B-containing receptors, owing to increased extracellular glutamate levels. Hyperactivation of NMDARs leads to neuronal death	• GluN2B-selective antagonists • Peptides disrupting GluN2B-interacting partners
Pain	GluN2B-containing receptors are majorly implicated, and alterations include overexpression and altered phosphorylation state of GluN2B. GluN2A-containing receptors can also be involved	GluN2B-selective antagonists
Alzheimer's disease	Activation of GluN2B-containing NMDARs mediates amyloid-β (Aβ)-induced alterations in synaptic plasticity and synapse loss, enhanced production of Aβ- and tau-induced excitotoxicity	NMDAR antagonist (memantine) or GluN2B-selective antagonists
Huntington's disease	Activation of extrasynaptic GluN2B-containing NMDARs increases mutant huntingtin protein-induced excitotoxicity	NMDAR antagonists or GluN2B-selective antagonists
Parkinsons's disease (dyskinesia)	Enhanced synaptic GluN2A expression and redistribution of GluN2B-containing receptors from synaptic to extrasynaptic locations	• GluN2B-selective antagonists • Potential interest for interventions targeting GluN2A subunits
Depression	Inhibitors of NMDARs, in particular GluN2B-containing receptors, induce rapid (hours) and sustained (days) reduction in depressive symptoms	NMDAR antagonists (ketamine) or GluN2B-selective antagonists
White matter injury	NMDAR activation leads to oligodendrocyte damage and loss of the myelin sheath. Specific involvement of GluN2C and/or GluN3A subunits	Potential interest for GluN2C- or GluN3A-selective antagonists
Autism spectrum disorders	Either reduced or enhanced NMDAR function is implicated. Mechanisms are unclear and there is no clear subunit specificity	Potential interest for NMDAR antagonists or NMDAR potentiators
Cognitive impairments	Reduced expression of NMDARs, especially GluN2B-containing receptors, correlates with decline in cognitive functions	Potential interest for NMDAR potentiators
Schizophrenia	Reduced NMDAR presence and/or activity, probably in GABAergic inhibitory neurons, which leads to an imbalance in neural network activity. Suggestions for a preferential loss of GluN2A-containing receptors	• NMDAR potentiators • D-serine, glycine and glycine transporter 1 inhibitors • Potential interest for GluN2A-selective potentiators

Fig. 1.9.4. NMDAR subunits involved in some CNS disorders, and their therapeutic treatments. Image adapted from Paoletti et al., 2013.

1.10. Methodologies to study protein translation

The central dogma of molecular biology describes the sequential flow of genetic information from DNA, via messenger RNA (mRNA), to proteins, which execute the most of biological functions in organisms. The entire proteome of a cell at any given time depends on four main regulatory steps: epigenetic and transcriptional regulation, which impact on mRNA synthesis; mRNA degradation/stability; translational control, which affects protein synthesis; and finally, protein degradation. The amplitude of translational regulation exceeds the sum of transcription, mRNA degradation and protein degradation [Schwanhausser et al., 2011]. Therefore, regulation of protein translation constitutes a crucial step in control of gene expression. However, due to technological difficulties, such as (1) complexity of translational machinery (with the involvement of both proteins and RNA molecules), and (2) the rapid response of it to environment (in the order of few minutes), little is known about the translation control respect to transcriptional regulation. Only in recent years thanks to advances in next-generation sequencing, proteomics methods, and microscopy-based tools it is possible to accurately monitor protein translation rates, from single mRNA molecules to global scale, and with high spatio-temporal resolution.

Next-generation sequencing-based methods

Translation initiation is supposed to often be the rate-limiting step in translational regulation, therefore these methods measure the association of mRNAs with translating ribosomes, as an index for protein synthesis. There are three main techniques:

- Polysome profiling (developed in the 1960s) is obtained by purifying polysomes through a sucrose gradient ultracentrifugation, and assessing relative mRNA enrichment levels in the polysomal fraction. This technique is useful to detect large changes in translation [Arava et al., 2003]. However, the polysomal fraction may be contaminated by other large ribonucleoprotein (RNPs) complexes, and it does not reveal exact Open Reading Frame (ORF) sites in a mRNA[12].
- Ribosome profiling (Ribo-seq) [Ingolia et al., 2009] takes advantage of mild nuclease treatment to degrade mRNA with exception of 20-35 nt long ribosome protected mRNA fragments (known as ribosome footprints, RFPs). These RFPs can be identified and quantified with single nucleotide resolution by RNA-seq, revealing ribosome positions and densities on each transcript (**Fig. 1.10.1A**). This technique allows to infer on alternative start codons (including non-AUG initiation sites), uORFs, stop codon bypasses, and translational pausing. In contrast, the RFP

[12] About half of all transcripts of a cell harbors additional ORFs in the 5' UTR of mRNAs that are known as upstream ORFs (uORFs) [Wethmar et al., 2014].

density is proportional to the translation initiation rate and inversely proportional to elongation velocity, meaning that high RFPs not necessarily represent translational activity. Moreover, Ribo-seq is not easy, costly and time consuming. It requires a large amount of starting material, and due to short length of RFPs is needed high sequencing to obtain sufficient coverage of mRNAs (>100 million reads per sample) and computational abilities to filter (supposed) false positives out (many RFPs maps to non-coding RNAs) [as reviewed in Zhao et al., 2019].

- Translating Ribosome Affinity Purification (TRAP-seq) [Zhou et al., 2013] takes advantage of immunoprecipitation, as an alternative to sedimentation, of epitope tagged ribosomal proteins (e.g. EGFP-Rpl10a) in order to purify "translating" ribosomes. Thanks to dedicated model organisms, which transgenically express tagged ribosomes, TRAP-seq can be used for cell-specific *in vivo* analysis of translation (**Fig. 1.10.1B**). Similarly to Ribo-seq, also this technique requires a large amount of starting materials.

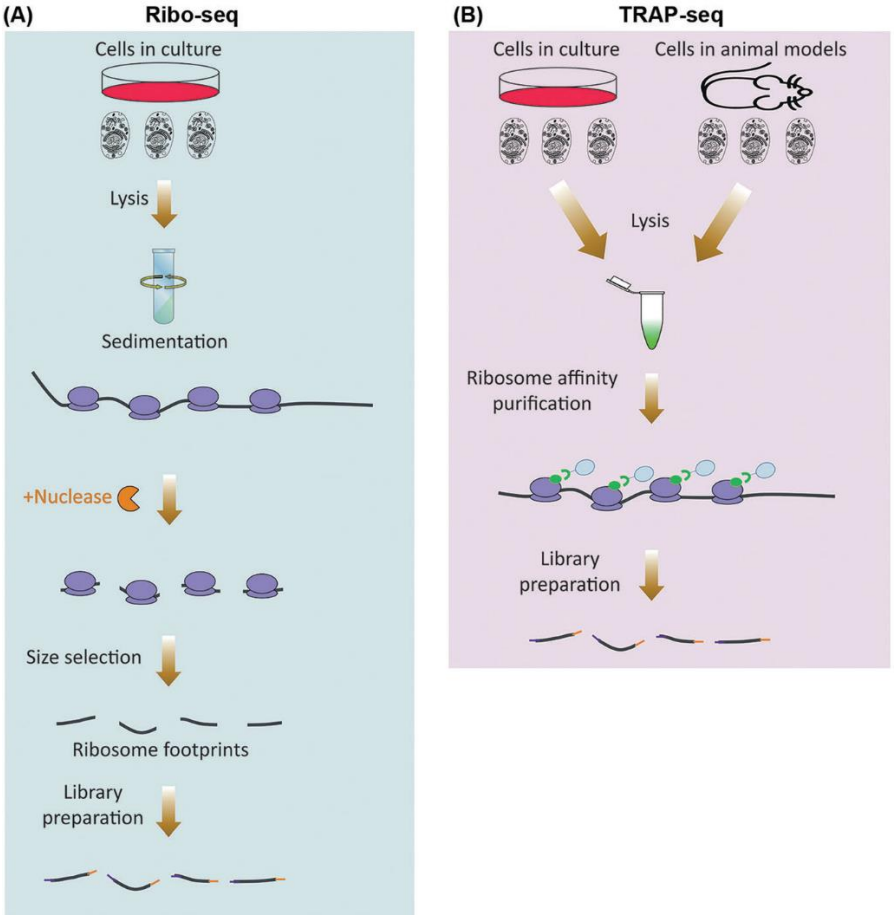

Fig. 1.10.1. Next-generation sequencing-based methods. (A) Ribo-seq. **(B)** TRAP-seq. Adapted from Dermit et al., 2017.

These techniques have a high temporal resolution giving an instantaneous snapshot of the translatome (mRNA fraction bound to ribosomes). Thanks to these methods can be calculated the translation efficiency of each gene by measuring and comparing the levels of total *gene-of-interest*-mRNA and its ribosome-associated mRNA fraction [Rodrigues et al., 2020]. However, more ribosome-associated mRNAs does not always mean more translation.

Proteomics-based methods

These techniques allow to study translation identifying and quantifying nascent proteins. For this purpose, the nascent protein chain is labeled through pulses of chemical conjugates, non-canonical or isotopologue aminoacids. Then, they are purified and quantified via mass-spectrometry (MS) (**Fig. 1.10.2**).

- Pulsed-Stable Isotope Labeling of Aminoacids in Culture (p-SILAC) [Ong et al., 2002; Selbach et al., 2008] utilizes pulses of stable isotopes of arginine (Arg) and lysine (Lys) added into the cell culture medium in order to label newly-synthesized proteins. The comparing of labeled with non-labeled peptides provides accurate quantification. However, p-SILAC requires prolonged pulses (in the order of hours, >10h) to achieve sufficient abundance of labeled peptides. This timescale is longer than translation process of a general protein (in the order of minutes), thus limiting the temporal resolution [as reviewed in Dermit et al., 2017 and Zhao et al., 2019].
- Bio-Orthogonal Non-Canonical Aminoacid Tagging (BONCAT) [Dieterich et al., 2007] utilizes pulses of azidohomoalanine (AHA, a methionine analogue) which is incorporated into nascent proteins in the position of its canonical counterpart. AHA contains an active azide moiety that allows Click-chemistry with tags such as biotin. Tagged proteins are then purified and quantified via MS. The Click-chemistry can be possible also with fluorescent molecules, this method is known as FUNCAT (Fluorescent Non-Canonical Aminoacid Tagging) [Dieterich et al., 2010] and allows visualization of newly-synthesized proteins also *in vivo* [Hinz et al., 2012].

Limits of BONCAT are the small temporal resolution due to need for incorporation of pulsed AHA into proteins, as well as the problem that it requires depletion of the endogenous methionine, possibly alterating translational dynamics. Last, some proteins lack of methionine itself.

- Puromycin-associated Nascent CHain Proteomics (PUNCH-P) [Aviner et al., 2014] takes advantage of a biotinylated variant of puromycin[13] (Biotin-Puro) in order to purify nascent proteins that have incorporated it in their chain. Peculiarity of this method is the fact that polysomes are

[13] Puromycin is an antibiotic, similar to an amino acyl-tRNA molecule, which occupies the acceptor site of the ribosome and inhibits translation elongation. In this process, puromycin is incorporated into the nascent polypeptide, leading to detach of newly-synthesized protein from translational machinery.

first isolated by sedimentation, then nascent proteins are labeled under cell-free condition (at high efficiency), purified by streptavidin conjugated beads, and finally quantified by MS. PUNCH-P provides an instantaneous snapshot of the translatome (high temporal resolution) and a high depth of analysis. In contrast, prior lysis and purification of translating ribosomes results in loss of any spatial regulation that may influence translation process in live cells. Finally, it requires a large amount of starting material [as reviewed in Dermit et al., 2017].

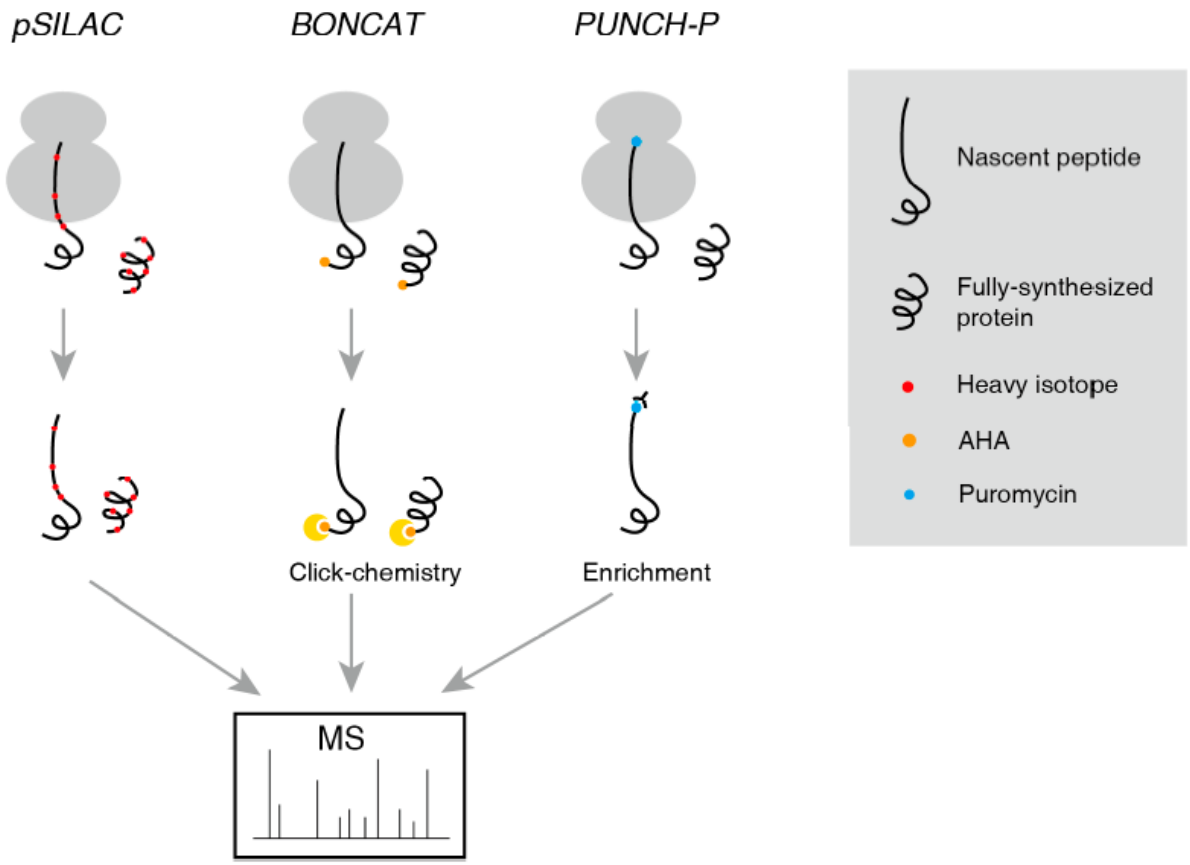

Fig. 1.10.2. Proteomics-based methods. Adapted from Zhao et al., 2019.

Puro-PLA

Alternatively to proteomics methods, puromycinylated peptides can be also revealed using an anti-puromycin antibody via fluorescent microscopy, western blot or fluorescent-activated cell sorting (FACS) [Schmidt et al., 2009]. Among them, a variant of the proximity ligation assay (PLA) [Söderberg et al., 2006] uses puromycin (Puro-PLA; [tom Dieck et al., 2015]) to detect in space and in time the translation of a *single* protein. The PLA was originally developed to detect *in situ* low expressed protein and protein interaction via microscopy. It uses a pair of oligonucleotide-labeled secondary antibodies which form a circle DNA, through a ligation step, only if they are in close proximity to each other (maximum a distance of 40nm). The circle DNA

template is required for the rolling-circle amplification by a DNA polymerase, which produces concatemeric sequences. Finally, fluorochromes-coupled oligos hybridize to the complementary sequences within concatemers, allowing up to 1000-fold amplified and localized signal. Therefore, the Puro-PLA utilizes two primary antibodies, one which binds to protein of interest, and the other one which binds to puromycin, in this way the proximity ligation assay run only in the protein of interest showing where and how much protein synthesis is produced in the temporal window of puromycinylation (**Fig. 1.10.3**)

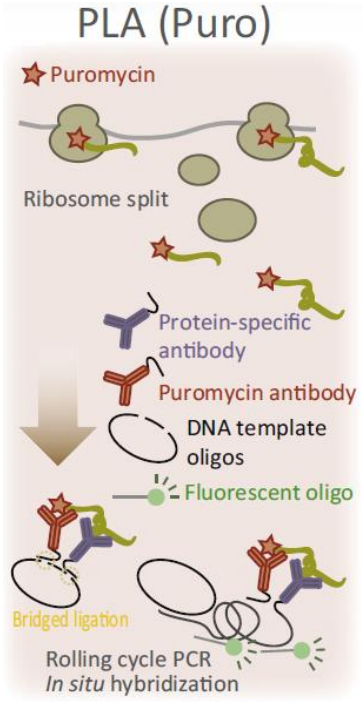

Fig. 1.10.3 Puromycin-proximity ligation assay (Puro-PLA). Adapted from Iwasaki and Ingolia, 2017.

Live-cell imaging methods

The abovementioned methods allow assessment of protein translation rates at specific time points. Recent imaging technologies can help to continuously monitor translation of *single* mRNA in *living* cells.

- Photoconvertible Fluorescent Reporters (PFRs, such as mEos3.2 molecule) [Zhang et al., 2012] fused to protein of interest allow to follow in the space and in time the protein synthesis of such protein, via fluorescence live imaging. Generally, PFRs are born "black" or "of a defined color" and, thanks to exposure at light of specific wavelength, they get converted into "a different color". In such way, it is possible to monitor where and how much newly-synthesized protein of interest is translated, eliminating the noisy contribution of previously synthesized protein.

However, it does not always easy transduce the fused protein-of-interest-PFR in case of big protein, or to use this technology *in vivo*.

- Translating mRNA Imaging by Coat protein Knock-off (TRICK) [Halstead et al., 2015] allows to monitor the first round of translation in live imaging. This is achieved tagging a target mRNA with two different RNA hairpin repeats recognized by distinct exogenous fluorescent RNA-binding proteins. Specifically, the first repeat is localized at 3'UTR and it is recognized by RFP-MS2 bacteriophage coat proteins, the second one is added within the ORF region of the same mRNA and it is recognized by GFP-PP7 bacteriophage coat proteins. After its transcription, the mRNA appears as a yellow spot (both red and green signals are visible), whereas during the first round of translation, the ribosome that moves along the mRNA knock the GFP-PP7 coat proteins off the ORF region, resulting in a change of color from yellow to red (**Fig. 1.10.4A**). This technique allows visualization of translation initiation of single mRNA molecule; however, it has a low signal to noise ratio, and cannot be used to measure rates of protein translation.

- Nascent Chain Tracking (NCT), known also as Single-molecule Imaging of Nascent Peptides (SINAPS) [Wu et al., 2016], instead allows to study translation dynamics in live cells, visualizing nascent protein chains associated with their cognate mRNAs. NCT/SINAPS tags both the target mRNA, at 3'UTR with RNA hairpin repeats recognized by RFP tagged coat proteins, and the target protein at N-terminal with epitope repeats recognized by intracellular GFP fluorescent antibodies. In this way, all single mRNA molecules are visualized in red, and as newly synthesized proteins exit the ribosomes during translation, the red signal becomes yellow (**Fig. 1.10.4B**). Moreover, the GFP fluorescent intensity can be used to estimate the translation rate of a single mRNA. In the future, NCT/SINAPS may be largely adapted for *in vivo* use. Limits are the insertions of artificial sequences on both mRNA and protein of interest that may modify their physiological metabolism.

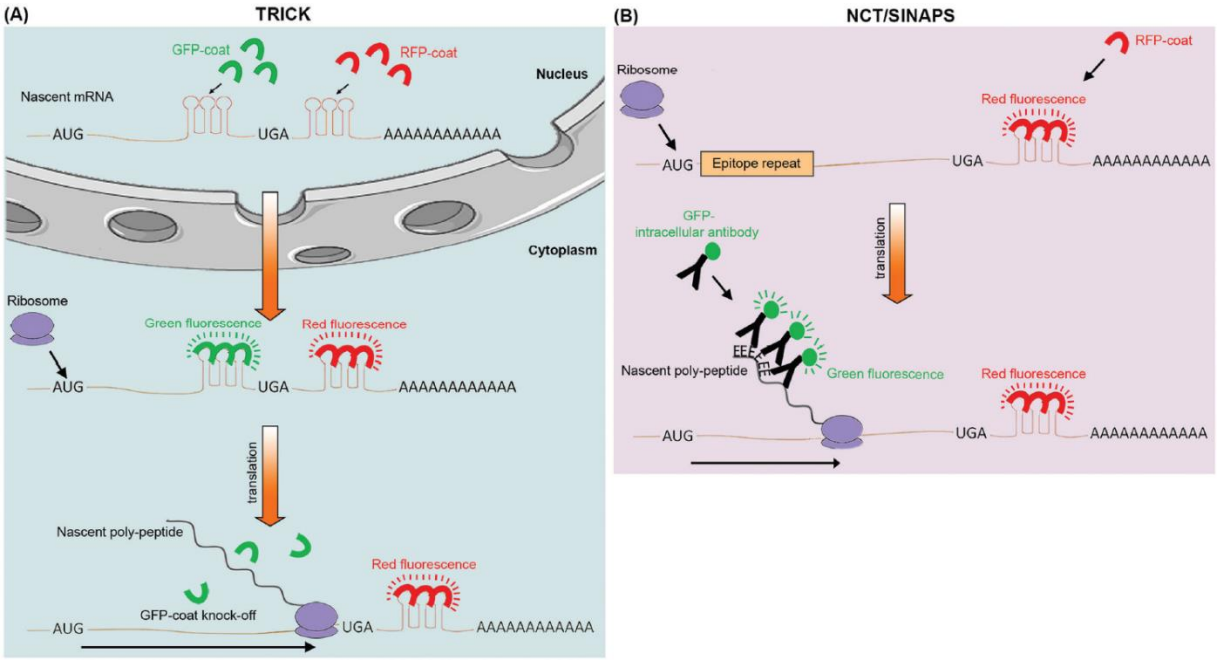

Fig. 1.10.4. Live-cell imaging methods. (A) TRICK. **(B)** NCT/SINAPS. They are not high-throughput compatible. Adapted from Dermit et al., 2017.

2. AIM OF THE THESIS

Main aim of this study was to investigate Foxg1 implication in translational control within neocortical glutamatergic neurons.

The study was primarily run on Grin1, paying special attention to molecular mechanisms mediating Foxg1 control of its translation and potential impact of such control on neuronal plasticity.

These subjects were mainly investigated in primary neocortical cultures, engineered by lentiviral somatic transgenesis, and molecularly profiled by a set of up-to-date technologies.

3. MATERIALS AND METHODS

3.1. Animal handling

Animal handling and subsequent procedures were in accordance with European and Italian laws (European Parliament and Council Directive of 22 September 2010 (2010/63/EU); Italian Government Degree of 04 March 2014, no.26). Experimental protocols were approved by SISSA OpBA (Institutional SISSA Committee for Animal Care) and authorized by the Italian Ministery of Health. Wild type (*wt*) CD1 strain mice (purchased from Envigo Laboratories, Italy), transgenic Gt(ROSA)26Sor$^{tm1.1(CAG-EGFP/Rpl10a,-birA)Wtp}$/J mice (named later *Rpl10a*$^{EGFP-Rpl10a/+}$) [Zhou et al., 2013] (founders purchased from Jackson Laboratories, USA, and maintained following their instructions), and *wt* Wistar rats used in this study were housed at the SISSA animal facility. Embryos were obtained mating male mice and *wt* female mice, and they were staged by timed breeding and vaginal plug inspection. *Rpl10a*$^{EGFP-Rpl10a/+}$ mouse embryos were distinguished from their *wt* littermates by inspection under fluorescence microscope. Pregnant female mice were killed by cervical dislocation. Rat pups were anesthetized with CO_2 and sacrificed by decapitation. Cortices were dissected out in sterile ice-cold 1X PBS (Gibco) supplemented with 0.6% D-glucose.

3.2. Lentiviral vectors

Self-inactivating lentiviral vectors (LV) were generated and titrated as previously described (Brancaccio et al., 2010). Plasmids employed in this study include:

- LV_pU6_shFoxg1 (Sigma SHCLND-NM_008241, TRCN0000081746).
- LV_pU6_shCtrl [Chiola et al., 2019].
- LV_pPgk1_rtTA2S-M2 [Spigoni et al., 2010].
- LV_pPgk1_EGFP [Brancaccio et al., 2010].
- LV_TREt_Foxg1 [Raciti et al. 2013].
- LV_TREt_PLAP [Falcone et al., 2019].
- LV_pPgk1_mCherry [Falcone et al. 2019].
- LV_TREt_Foxg1-EGFP

Starting from "LV_TREt_Foxg1", we replaced the SrfI/ApaI fragment (including the last 161nt of Foxg1-cds) with "SrfI_Foxg1(cds-3'term)-EGFP_ApaI" fragment, detailed in Table S3.

- LV_CMV_Flag-eIF4E (lentivirus of second generation; Addgene plasmid #38239).
- CMV_Flag_GFP (Addgene plasmid #60360).

- CMV_Flag-Gephyrin (gift from Cherubini E. Lab).
- LV_CMV_EEF1G-V5 (DNASU Plasmid Repository, HsCD00434091).
- LV_CMV_EEF1D-V5 (DNASU Plasmid Repository, HsCD00444454).
- LV_CMV_PUM1-V5 (DNASU Plasmid Repository, HsCD00438817).
- LVrc_TREt-pl-BGHpA

Starting from "LV_pPgk1_EGFP", we replaced the pPgk1_EGFP_WPRE fragment with a TREt_polylinker_BGHpA fragment, cloned from 3'LTR to 5'LTR direction (reverse complement).

- LVrc_TREt_Flag-rnoGrin1-203-HA

We transferred the *rnoGrin1-203* mRNA tagged by 3xFlag N-term epitope and 3xHA C-term epitope ("Flag-rnoGrin1-203-HA" fragment, detailed in Table S3) into XhoI(destroyed)/XbaI-cut "LVrc_TREt-pl-BGHpA.

- LVrc_TREt_rnoGrin1-203*.full

We transferred the *rnoGrin1-203* mRNA harboring a STOP codon and a polylinker after the codon 30 ("rnoGrin1-203*.full" fragment, detailed in Table S3) into XhoI(destroyed)/XbaI-cut "LVrc_TREt-pl-BGHpA", detailed in Table S3.

- LVrc_TREt_rnoGrin1-203*.d1 (5'utr deletion)

Starting from "LVrc_TREt_rnoGrin1-203*.full", we removed the BstBI/PmeI fragment, and we reconstructed the original Kozak(GAGCTC)-1-30aa-STOP sequence of "rnoGrin1-203*", via ds-oligos BstBI/PmeI ends.

- LVrc_TREt_rnoGrin1-203*.d2 (cds1 deletion)

Starting from "LVrc_TREt_rnoGrin1-203*.full", we removed the AccIII/AccIII fragment.

- LVrc_TREt_rnoGrin1-203*.d3 (cds2-3'utr deletion)

Starting from "LVrc_TREt_rnoGrin1-203*.full", we removed the KpnI/KpnI fragment.

- LVrc_TREt_rnoGrin1-203*.d4 (3'utr deletion)

Starting from "LVrc_TREt_rnoGrin1-203*.full", we removed the PshAI/BamHI fragment.

- LVrc_TREt_rnoGrin1-203*.d5 (cds3 deletion)

Starting from "LVrc_TREt_rnoGrin1-203*.full", we removed the PmeI/PshAI fragment.

3.3. Primary cortico-cerebral cell culture

Cortical tissue from E16.5 mice was chopped to small pieces for 5 minutes (min), in the smallest volume of ice-cold 1X PBS - 0,6% D-glucose - 5mg/ml DNaseI (Roche) solution. After chemical digestion in 2.5X trypsin (Gibco) - 2mg/ml DNaseI for 5 min, and its inhibition with DMEM-glutaMAX (Gibco) - 10% FBS (Euroclone) - 1X Pen-Strep, cells were spinned down

and transferred to differentiative medium [Neurobasal-A, 1X Glutamax (Gibco), 1X B27 supplement (Invitrogen), 25μM L-glutamate (Sigma), 25μM β-Mercaptoethanol (Gibco), 2% FBS, 1X Pen/Strept (Gibco), 10pg/ml fungizone (Gibco)]. Cells were counted and plated as followings: in case of RNA profiling, and western blot experiments, cortico-cerebral cells were plated onto 0.1mg/ml poly-L-Lysine (Sigma) pre-treated 12-multiwell plates (Falcon) at $8x10^5$ cells/well in 0.6-0.8 ml differentiative medium; in case of immunofluorescence, and PLA experiments, cortico-cerebral cells were plated onto 0.1mg/ml poly-L-Lysine (Sigma) pre-treated 12mmØ glass coverslips in 24-multiwell plates (Falcon) at $1x10^5$ cells/well in 0.6-0.8 ml differentiative medium. In general, when indicated, lentiviral infection was done at DIV1. TetON regulated transgenes were activated by 2μg/ml doxycyclin (Clontech, 631311) administration, as illustrated in each Figure. Where required, 10μM Cytosine β-D-arabinofuranoside (AraC; Sigma) was acutely added to the medium at DIV1. Cells were kept in culture 8 days.

3.4. Primary hippocampal cell culture and live-imaging

Specifically for Fig. 1G,H, hippocampal tissue from P2 Wister rats was chopped to small pieces and chemical digested. Dissociated cells were plated at $4×10^4$ cells/ml onto 35mm glass dishes (Ibidi) pre-treated with 0.5mg/ml poly-D-lysine (Sigma) for 1 h at 37°C, in Minimum Essential Medium (MEM) with GlutaMAX™ supplemented with 10% FBS, 0.6% D-glucose, 15 mM Hepes, 0.1mg/ml apo-transferrin, 30μg/ml insulin, 0.1 μg/ml D-biotin, 1 μM vitamin B12 (all from Sigma), and 2.5 μg/ml gentamycin (Invitrogen). At DIV2, hippocampal neurons were engineered with "LV_pPgk1_ rtTA2S-M2" and "LV_TREt_Foxg1-EGFP" transgenes. At DIV4, the expression of *Foxg1-EGFP* chimera was activated by administration of 2μg/ml doxycycline. Finally, at DIV7, 50nM Mitotracker dye (Life Technologies, M7512) was added to hippocampal cultures, and confocal images were acquired after 30 min. The fluorescent imaging was done with a confocal microscope (NIKON A1R) equipped with 488nm and 594nm laser excitation light, and an incubator to maintain, during live acquisition, 37°C, 5% CO_2, and 95% humidity. The objective used to visualize the cells was the 60×oil immersion objective (N.A. 1.40).

3.5. HEK293T cell culture

HEK293T cells were used for lentiviral production, quantitative titration (Brancaccio et al. 2010), and to evaluate protein-protein interactions via co-immunoprecipitation (co-IP) and proximity ligation assay (PLA). In case of co-IP assay, HEK293T cells were cultured in DMEM-glutaMAX - 10% FBS - 1X Pen-Strep on 6-multiwell plates at $1.2x10^6$ cells/well. Cells were

kept in culture for 3 days. In case of PLA, HEK293T cells were cultured in DMEM-glutaMAX - 10% FBS - 1X Pen-Strep onto 0.1mg/ml poly-L-Lysine pre-treated 12mmØ glass coverslips in 24-multiwell plates at $3x10^5$ cells/well. Cells were kept in culture for 2 days. In both experiments, plasmid transfection was done by LipoD293 (SignaGen laboratories, SL100668) at DIV1 according to manufacturer's instructions.

3.6. Neural cell culture immunofluorescence

Neural cell cultures were fixed by ice-cold 4% PFA for 15-20 min and washed 3 times in 1X PBS. Samples were subsequently treated with blocking mix (1X PBS; 10% FBS; 1mg/ml BSA; 0.1% Triton X-100) for at least 1 hour at room temperature (RT). After that, incubation with primary antibodies was performed in blocking mix, overnight at 4°C. The day after, samples were washed 3 times in 1X PBS - 0.1% Triton X-100 for 5 minutes and then incubated with secondary antibodies in blocking mix, for 2 hours at RT. Samples were finally washed 3 times in 1X PBS - 0.1% Triton X-100 for 5 minutes, and subsequently counterstained with DAPI (4', 6'-diamidino-2- phenylindole) and mounted in Vectashield Mounting Medium (Vector). The following primary antibodies were used: anti-Tubβ3, mouse monoclonal, (clone Tuj1, Covance, MMS-435P, 1:1000); anti-Foxg1, rabbit polyclonal (gift from G.Corte, 1:200); anti-Psd95, mouse monoclonal (clone 6G6-1C9, Abcam, ab2723, 1:500); anti-Smi312, mouse monoclonal (Abcam, ab24574, 1:1000); anti-Flag, mouse monoclonal (clone M2, Sigma, F1804, 1:1000); anti-HA, rabbit monoclonal (clone 3F10, Roche, 11867423001, 1:500). Secondary antibodies were conjugates of Alexa Fluor 488, and Alexa Fluor 594 (Invitrogen, 1:600).

3.7. Proximity ligation assay (PLA) and puro-PLA

The PLA assay was performed according to manufacturer's instructions (Duolink™ PLA Technology, Sigma). Briefly, cells were fixed for 15-20 min in ice-cold 4% PFA, washed 3 times in 1X PBS, permeabilized in 1X PBS - 0.1% Triton X-100 for 1h at RT, blocked for 1 h at 37°C in Duolink blocking buffer and incubated for 3h at RT with mouse and rabbit primary antibodies, indicated in dedicated Figures; in case of HEK293T cells, negative controls were done omitting either antibodies. Afterwards, samples were washed 3 times for 5 min in Duolink buffer A, then incubated for 1 h at 37°C in Duolink anti-mouse MINUS and anti-rabbit PLUS probes diluted 1:5 in Duolink antibody dilution buffer. Samples were next washed 3 times for 5 min in buffer A, incubated for 30 min at 37°C in Duolink ligase diluted 1:40 in 1X ligation buffer, washed again 3 times in buffer A, and incubated for 100 min at 37°C in Duolink polymerase diluted 1:80 in 1X green or red amplification buffer. Finally, samples were washed 2

times for 10 min in Duolink buffer B, and 1 time in 1:100 buffer B for 1 min, and mounted in Duolink mounting medium with DAPI. The next day confocal images were acquired.

In case of puro-PLA, when indicated cortico-cerebral cells were pulsed for 15 min with 1μM puromycin (Sigma, P8833), or with 1X PBS as negative control, then cells were immediately fixed in ice-cold 4% PFA.

The following primary antibodies were used: anti-Grin1, rabbit monoclonal [EPR2481(2)] (Abcam, ab109182, 1:500); anti-Foxg1 ChIP-grade, rabbit polyclonal (Abcam, ab18259, 1:500); anti-puromycin, mouse monoclonal (clone 12D10, Millipore, MABE343, 1:1000); anti-V5, mouse monoclonal (SV5-Pk1, Abcam, ab27671, 1:1000); anti-Flag, mouse monoclonal (clone M2, Sigma, F1804, 1:1000).

3.8. Neural activity modulation protocol

Cortico-cerebral cultures were set up as described above (to see "Primary cortico-cerebral cell culture") and as detailed in Fig. 7A. At DIV8, cells were differently treated according to specific activity modulation protocol. This required the acutely administration of 1μM TTX (Latoxan, L8503) for 1.5h, then media was removed, and cells were treated with 4 pulses of 55mM KCl - 1X PBS media for 3 min ("KCl/TTX" samples) or with 4 "pulses" of simply 1X PBS media ("PBS/TTX" samples). Time distance of each pulse was of 10 min in which cells received the previous conditioned media containing the 1μM TTX. After the last pulse, cells were treated with conditioned media containing 1μM TTX and 1μM puromycin for 15 min. "Unstimulated" samples were cells without any kind of treatment, except for the last 15 min of 1μM puromycin.

3.9. Image acquisition and analysis

Immunoprofiled cultured cells were photographed on a Nikon Eclipse TI microscope, equipped with a 40X objective through the Hamamatsu 1394 ORCA-285 camera (Fig. 4), and with 40X-oil objective through the Nikon C1 confocal system (Figs 1A-F,3,5,7). Photos were collected as 1344x1024 pixel images for Fig. 4, or as 3μm Z-stacks (step of 0.3μm), 3μm Z-stacks (step of 1μm), 4μm Z-stacks (step of 1μm) of 1024x1024 pixel images for Fig. 1, Fig. 5, and Figs 3,7, respectively. All images were analyzed with Volocity 5.5.1 and Microsoft Excel softwares, and processed using ImageJ-Fiji and Adobe Photoshop CS6 softwares. Details about image analysis are provided in legend of each Figure.

3.10. Total RNA extraction

Total RNA was extracted from cells (Figs 2D, 4B) using TRIzol Reagent (Thermofisher) according to the manufacturer's instructions. RNA was precipitated using isopropanol and GlycoBlue (Ambion) overnight at -80°C. After two washes with 75% ethanol, the RNA was resuspended in 20µl sterile nuclease-free deionized water. Agarose gel electrophoresis and spectrophotometric measurements (NanoDrop ND-1000) were employed to estimate its concentration, quality and purity.

3.11. Translating Ribosome Affinity Purification (TRAP) assay

The TRAP assay was performed as previously described [Ainsley et al., 2014; Heiman et al., 2014] with modifications. For each TRAP reaction, 10µg of anti-GFP antibody, purchased from the Monoclonal Antibody Core Facility at the Memorial Sloan-Kettering Cancer Center (purified form of HtzGFP-19C8), were covalently bound to 1mg magnetic epoxy beads (Dynabeads Antibody Coupling kit, Life Technologies, 14311D), according to manufacturer's protocols, followed by BSA treatment to reduce non-specific binding. Antibody-coupled beads were prepared at the concentration of 1mg/100µl. Cortico-cerebral cells, derived from *Rpl10a*$^{EGFP\text{-}Rpl10a/+}$ embryos, were set up as described above (to see "Primary cortico-cerebral cell culture") and as detailed in Fig. 2A. At DIV8, cells were treated by addition to media of 0.1mg/ml cycloheximide (CHX; Sigma, C7698) at 37°C for 15 min. Then, cells were washed two times with ice-cold 1X PBS containing 0.1mg/ml CHX. For each well (12-multiwell plate) was added 75µl ice-cold lysis buffer for 10 min on ice. Afterwards, cells were scraped and lysed by vigorously pipetting up and down without the creation of bubbles. The lysate derived from two wells (about $1.6x10^6$ cells; corresponding to biological sample), was firstly centrifuged at 2000g for 10 min and then centrifuged at 20000g for 10 min at 4°C, after addiction to each sample of 1/9 volume of 300mM DHPC (Avanti Polar Lipids). The resulting supernatant of each sample was incubated with 100µl antibody-coupled beads for 1h at 4°C on roller-shaker. After incubation, beads were collected with a magnet: the immunoprecipitated component (IP) was washed four times with 1ml of ice-cold high-salt buffer; the supernatant component (SN) of each sample was stored on ice. [Lysis buffer: 20mM HEPES (Ambion), 150mM KCl (Ambion), 10mM $MgCl_2$ (Ambion), 1%(vol/vol) NP-40 (Thermo Fisher Scientific), 1X EDTA-free protease inhibitors (Roche), 0.5mM DTT (Invitrogen), 0.1mg/ml cycloheximide, 10µl/ml rRNasin (Promega), 10µl/ml Superasin (Applied Biosystems). High-salt buffer: 20mM HEPES, 350mM KCl, 10mM $MgCl_2$, 1%(vol/vol) NP-40, 1X EDTA-free protease inhibitors, 0.5mM DTT, 0.1mg/ml cycloheximide].

For each sample, RNA of SN and IP components were extracted with Trizol® LS reagent (Thermofisher) according to manufacturer's instructions. A back extraction was used to improve yield. RNA was precipitated using NaOAc, isopropanol and GlycoBlue overnight at -80°C. After two washes with 75% ethanol, the RNA was resuspended in 10µl sterile nuclease-free deionized water. Agarose gel electrophoresis and spectrophotometric measurements (NanoDrop ND-1000) were employed to estimate quantity, quality and purity of the resulting RNA.

3.12. RNA immunoprecipitation (RIP) assay

Cortico-cerebral cells were set up as described above (to see "Primary cortico-cerebral cell culture") and as detailed in Fig. 6A. For each RIP reaction, 10µl of protein A/G Dynabeads (Thermofisher, 492024) were coupled with 10µg of anti-protein of interest (POI; anti-Foxg1 ChIP-grade, rabbit polyclonal, Abcam, ab18259; anti-GFP, rabbit polyclonal, Abcam, ab290), or 10µg of rabbit IgG (Millipore, 12370) as control, according to manufacturer's protocols. Preclearing beads were prepared omitting antibody coupling. At DIV8, cells were washed once with ice-cold 1X PBS. For each well (12-multiwell plate) was added 75ul ice-cold lysis buffer for 10 min on ice. Afterwards, cells were scraped and lysed by vigorously pipetting up and down without the creation of bubbles. The lysate derived from 10 wells (about $8x10^6$ cells; corresponding to pair anti-POI/IgG biological samples), was twice "pipetted up and down and kept 10 min on ice", then it was centrifuged at 2000g for 10 min at 4°C, and then centrifuged at 16000g for 10 min at 4°C. The resulting supernatant of each sample was incubated with preclearing beads (pre-equilibrated in lysis buffer) for 30 min at 4°C on roller-shaker. Then, preclearing beads were separated with a magnet, and supernatant was incubated with antibody-coupled beads (pre-equilibrated in lysis buffer), overnight at 4°C on roller-shaker. The 10% of supernatant (Input, IN-RIP) was stored on ice. The day after, beads were collected with a magnet and washed five times with 0.5ml of ice-cold high-salt buffer. [Lysis buffer: 25mM TRIS-HCl, 150mM KCl (Ambion), 10mM $MgCl_2$ (Ambion), 1%(vol/vol) NP-40 (Thermo Fisher Scientific), 1X EDTA-free protease inhibitors (Roche), 0.5mM DTT (Invitrogen), 10ul/ml rRNasin (Promega), 10ul/ml Superasin (Applied Biosystems). High-salt buffer: 25mM TRIS-HCl, 350mM KCl (Ambion), 10mM $MgCl_2$ (Ambion), 1%(vol/vol) NP-40 (Thermo Fisher Scientific), 1X EDTA-free protease inhibitors (Roche), 0.5mM DTT (Invitrogen)]. For each sample, RNA immunoprecipitated (IP-RIP) and Input were extracted with Trizol® LS reagent according to manufacturer's instructions. A back extraction was used to improve yield. RNA was precipitated using isopropanol and GlycoBlue overnight at -80°C. After two washes with 75% ethanol,

the RNA was resuspended in 10ul sterile nuclease-free deionized water. Agarose gel electrophoresis and spectrophotometric measurements (NanoDrop ND-1000) were employed to estimate quantity, quality and purity of the resulting RNA.

3.13. DNase treatment, Reverse Transcription and Real-Time quantitative PCR

RNA preparations from total RNA samples, TRAP-SN component, and RIP-derived samples were treated by TURBO™ DNase (2U/μl) (Ambion) for 1h at 37°C, following manufacturer's instructions. cDNA was produced by reverse transcription (RT) by SuperscriptIII™ (Invitrogen) according to manufacturer's instructions (1/10 volume TRAP-IP, 1/10 volume TRAP-SN DNA-free, 1/6 volume IP- and IN-RIP DNA-free, 0.5μg total RNA DNA-free), in the presence of random hexamers. Then, the RT reaction was diluted 1:3 (in case of TRAP samples) or 1:5 (in case of RIP, and total RNA samples), and 1-2μl of the resulting cDNA was used as substrate of any subsequent quantitative PCR (qPCR) reaction. Limited to intron-less amplicons and for TRAP-derived IP component, and RIP-derived samples, negative control PCRs were run on RT(-) RNA preparations. qPCR reactions were performed by the SsoAdvanced SYBR Green Supermix^{TM} platform (Biorad), according to manufacturer's instructions. For each transcript under examination and each sample, cDNA was qPCR-analyzed in technical triplicate, and results averaged. In case of total RNA and TRAP samples, mRNA levels were normalized against *Rpl10a* mRNA [Zhou et al., 2010]. In addition, for TRAP samples, averages of IP-mRNAi / SN-mRNAi ratios was evaluated for each i-sample. In case of RIP samples, IP-RIP was normalized against IN-RIP. Data analysis was done by Excel software.

The following oligonucleotides have been employed in this study:

Psd95/F: GCCGTGGCAGCCCTGAAGAACACA
Psd95/R: GCTGCTATGACTGATCTCATTGTCCAGG
Foxg1(*5utr*)/F: TAGAAGCTGAAGAGGAGGTGGAGTGC
Foxg1(*5utr*)/R: CAGACCCAAACAGTCCCGAAATAAAGC
Gria1/F: TCCATGTGATCGAAATGAAGCATGATGGAATCC
Gria1/R: CGATGTAGGTTCTATTCTGGACGCTTGAGTTG
pan-Grin1/F: CGAGGATACCAGATGTCCACCAGACTAAAGA
pan-Grin1/R: CTTGACAGGGTCACCATTGACTGTGAACT
ex20-Grin1/F: CCGTGAACGTGTGGAGGAAGAACCT
ex20-Grin1/R: GTGTCTTTGGAGGACCTACGTCTCTTG
Grid1/F: AAGGACTGACTCTCAAAGTGGTGACTGTCTT
Grid1/R: CCTTAGCCAGTGCATCCAGCACATCTATG
Gabra1/F: AAACCAGTATGACCTTCTTGGACAAACAGTTGAC
Gabra1/R: GTGGAAGTGAGTCGTCATAACCACATATTCTC

Slc17a6/F: TTTTGCTGGAAAATCCCTCGGACAGATCTACA
Slc17a6/R: CTTACCGTCCTCTGTCAGCTCGATGG
Bdnf2c/F: CTTTGGGAAATGCAAGTGTTTATCACCAGGAT
Bdnf4/F: CTGCCTTGATGTTTACTTTGACAAGTAGTGACTG
Bdnf(2c,4)/R: GCCTTCATGCAACCGAAGTATGAAATAACCATAG
Rpl10a/F: CAGCAGCACTGTGATGAAGCCAAGG
Rpl10a/R: GGGATCTGCTTAATCAGAGACTCAGAGG
Foxg1(cds)/F: GACAAGAAGAACGGCAAGTACGAGAAGC
Foxg1(cds)/R: GAACTCATAGATGCCATTGAGCGTCAGG
F-rnoGrin1-H/F: ACCTCCACCCTGGCCTCCAGCTT
F-rnoGrin1-H/R: GGGATAGCCAGCGTAATCTGGAACATC
rnoGrin1.d1/F: AGATCGCCCTCGACTTCGAAGAGC
rnoGrin1.f1/F: GTCGCACTCGCGCAACCCAGAG
rnoGrin1.f1-d1/R: CTCAGCACCGCCTCGAGTCCG
rnoGrin1.d2-d5-f2-f5/F: CCCAAGATCGTCAACATCGGCTGAGT
rnoGrin1.d2/R: ACTTCTGTGAAGCCTCAAACTCCAGCA
rnoGrin1.d5/R: TCCTCCCTCTCAATAGCGCGTCG
rnoGrin1.f2-f5/R: TGTGGGTGACAGAAGTGGCGTTGAG
rnoGrin1.d3/F: CTGGCCGTGTGGAATTCAATGAGGATG
rnoGrin1.d4/F: TGCAGGATAGAAAGAGTGGTAGAGCAGA
rnoGrin1.f3-f4/F: CAGTGGTGATGCCTAAAGGAATGTCAG
rnoGrin1.d3-d4-f3-f4/R: GGGCAAACAACAGATGGCTGGCAACT

3.14. TRAP-seq profiling

TRAP-derived IP samples, produced as described in "Translating Ribosome Affinity Purification (TRAP) assay" section, were sequenced by IGA Technology Services Srl. Libraries were produced using retrotranscribed cDNA previously amplified by Ovation Ultralow Library System V2 (NuGEN Technologies, Inc.). Library size and integrity were assessed using the Agilent Bioanalyzer (Santa Clara, CA) or Caliper GX (PerkinElmer, MA). Sequencing was performed by Illumina HiSeq 2500 (Illumina, San Diego, CA) and 20M paired-end reads (2x125) per replicate were generated. Bioinformatic analysis was execute by a commercial operator (Sequentia, Barcelona, Spain), as here described. Quality control of the sequenced reads was performed with the software FASTQC v0.11.5, then low quality bases and adapters were removed with the software BBDuk version 35.85, setting a minimum base quality of 30 and a minimum read length of 35 bp. The high-quality reads were mapped against the *Mus musculus* reference genome (mm10, Ensembl 38.91), using STAR v2.7.3a in local mode. The read counting was performed with the software FeatureCounts v2.0.0 while the statistical analyses were performed with R. The raw counts were normalized using the TMM method implemented in the algorithm HTSFilter, and differential expression analysis was performed with edgeR, applying a batch correction. Genes with an FDR value lower or equal than 0.05 were considered statistically significant.

3.15. TRAP-seq/RNA-seq comparison, and Gene Ontology (GO)

Starting from data of "TRAP-seq profiling" and total RNA-seq (previously published by Tigani et al., 2020; Zenodo dataset: Artimagnella and Mallamaci, 2020), genes with low expression level (<1st quartile log_2CPM) in both datasets were removed from the analysis. For each gene was compared the log_2FC(trapRNAseq) with log_2FC(totalRNAseq) (= Δlog_2FC), and – in a first analysis – they were filtered IF "$\Delta log_2FC \neq 0$" AND ["log_2FC(trapRNAseq)≠0" OR "logFC(totRNAseq)≠0" (in both cases, with $p<0.05$ and FDR<0.05)]. GO analysis was performed by [http://geneontology.org/] tool, using PANTHER classification system.

3.16. Co-Immunoprecipitation (co-IP) assay

HEK293T cell lines were cultured and transfected as described in "cell lines" section, and as detailed in Fig. 5A,C. After three days, cells were washed in 1X PBS and lysed with 500µl of CHAPS buffer, supplemented with 1X protease inhibitors (Roche). Total cell lysates were centrifuged at 12000g for 10 min at 4°C, to remove debris. For each sample, the 4% of supernatant was saved as Input (IN), the remaining part was incubated with anti-Flag-conjugated resin for 3h at 4 °C, following manufacturer's instructions (FLAG Immunoprecipitation Kit, Sigma). Then, the precipitated resin (IP) was washed 4 times in 1X wash buffer, and finally it was denatured at 95 °C for 5 min in 1X sample buffer (supplemented with 0.5% β-Mercaptoethanol), as well as Input sample. Afterwards, IP and IN samples were processed for western blot analysis.

3.17. Protein degradation assay

Cortico-cerebral cells were set up as described above (to see "Primary cortico-cerebral cell cultures") and as detailed in Fig. 3A. At DIV8, cells were treated with 50µg/ml cycloheximide (CHX). Four points were analyzed, the starting point t0 and then 6, 10, 14 hours after CHX administration. For each point samples were lysed in CHAPS buffer, supplemented with 1X protease inhibitors, and stored at -80°C. All samples were centrifuged at 12000g for 10 min at 4°C, to remove debris, and then processed for western blot analysis.

3.18. Western blot analysis

Western blot analysis was performed according to standard methods. Total cell lysates in CHAPS buffer were quantified by BCA protein assay kit (Fisher Scientific, 10678484) (except for co-IP samples), and denatured at 95°C for 5 min, prior to loading. 20-30µg of proteins were loaded per each lane on a 10% acrylamide - 0.1% SDS gel. Afterwards, proteins were transferred

to nitrocellulose membrane. Membranes were incubated 1h in 1X TBS-Tween containing 5% non-fat dry milk, before to be exposed at primary antibodies at 4°C overnight. Then, membranes were washed 3 times in 1X TBS-Tween, incubated 1h with HRP-conjugated secondary antibodies (DAKO, 1:2000) in 1X TBS-Tween containing 5% non-fat dry milk, at room temperature, washed again 3 times, and finally revealed by an ECL kit (GE Healthcare, GERPN2109). The following primary antibodies were used: anti-Foxg1, rabbit polyclonal (gift from G.Corte, 1:2000); anti-Flag, mouse monoclonal (clone M2, Sigma, F1804, 1:1000); anti-Grin1, rabbit monoclonal [EPR2481(2)] (Abcam, ab109182, 1:5000); anti-β-Actin HRP-conjugated mouse monoclonal (Sigma, A3854, 1:20000). Images were acquired by Alliance LD2–77.WL apparatus (Uvitec, Cambridge), and analyzed by Uvitec NineAlliance software.

3.19. Statistical analysis

When not otherwise stated, experiments were performed at least in biological triplicate. Statistical tests employed for result evaluation, and definitions of *n* (biological replicate) are provided in each Figure.

4. RESULTS

4.1. Foxg1 promotes *Grin1*-mRNA translation in neocortical neurons

Mainly known as a transcription factor involved in rostral brain patterning [Kumamoto and Hanashima, 2017], Foxg1 was also previously reported to be in the *cytoplasm* of olfactory placode and early-born neocortical neurons [Regad et al., 2007], as well as in the cytoplasm and mitochondria of a hippocampal neuronal line and whole brain homogenates [Pancrazi et al., 2015]. Consistently, we also found a prominent cytoplasmic Foxg1 immunoreactivity in the majority of neurons from DIV8 cultures of murine E16.5 neocortical precursors (**Fig. 1A-F**) as well as in DIV7 cultures of rat P2 hippocampal precursors (**Fig. 1G,H**). In the former case, Foxg1 was specifically detectable in neuronal soma, as well as in punctate-Psd95^{+} dendrites (**Fig. 1C,D**) and Smi312^{+} axons (**Fig. 1E,F**).

Next, three high-throughput screenings, in HEK293T, yeast and N2A cells [Li et al., 2015; Stelzl et al., 2005; and Weise et al., 2019, respectively] showed that FOXG1 may interact with a number of factors implicated in translation. In addition, we noticed that Foxg1 harbors a YATHHLT motif (at 366-372 position), conserved among vertebrates (not shown) and reminiscent of the eIF4E-binding motif detectable in eIF4-BP, eIF4G and other effectors [Nédélec et al., 2004].

All these observations suggested us that Foxg1 might also be involved in control of mRNA translation.

To cast light on this issue, we selected a small sample of genes undergoing translational regulation [Dörrbaum et al., 2020; Baez et al., 2018] and/or being implicated in neuronal activity, and we evaluated the impact of *Foxg1* expression level on ribosomal engagement of their mRNAs. For this purpose, we used neocortical neurons obtained from E16.5 *Rpl10a*$^{EGFP\text{-}Rpl10a/+}$ mouse embryos [Zhou et al., 2013], engineered to overexpress *Foxg1* (*Foxg1*-OE) or a *PLAP* control. Four days after transgenes activation, at DIV8, they were profiled by Translating Ribosome Affinity Purification (TRAP)-qRTPCR (**Fig. 2A, left**). Specifically, we purified ribosome-associated RNA (IP component) from supernatant cellular RNA (SN component), and profiled them by qRT-PCR, paying attention to eight candidate genes (*Grid1*, *Grin1, Slc17a6*, *Gria1*, *Gabra1*, *Bdnf - 2c* and *4* isoforms -, *Psd95*, and *Foxg1)*. Upon normalization against *Rpl10a*-mRNA, IP/SN ratios were averaged and further normalized against *Plap* controls. *Grid1* and *Grin1* IP/SN ratios were upregulated in *Foxg1*-OE samples (+50.7±16.2%, with p<0.01 and

n=6,6; and +34.7±7.0%, with $p<0.01$ and *n*=6,6, respectively), suggesting that Foxg1 may promote ribosomal engagement of their mRNAs. The same index was not affected in the remaining cases (**Fig. 2B**).

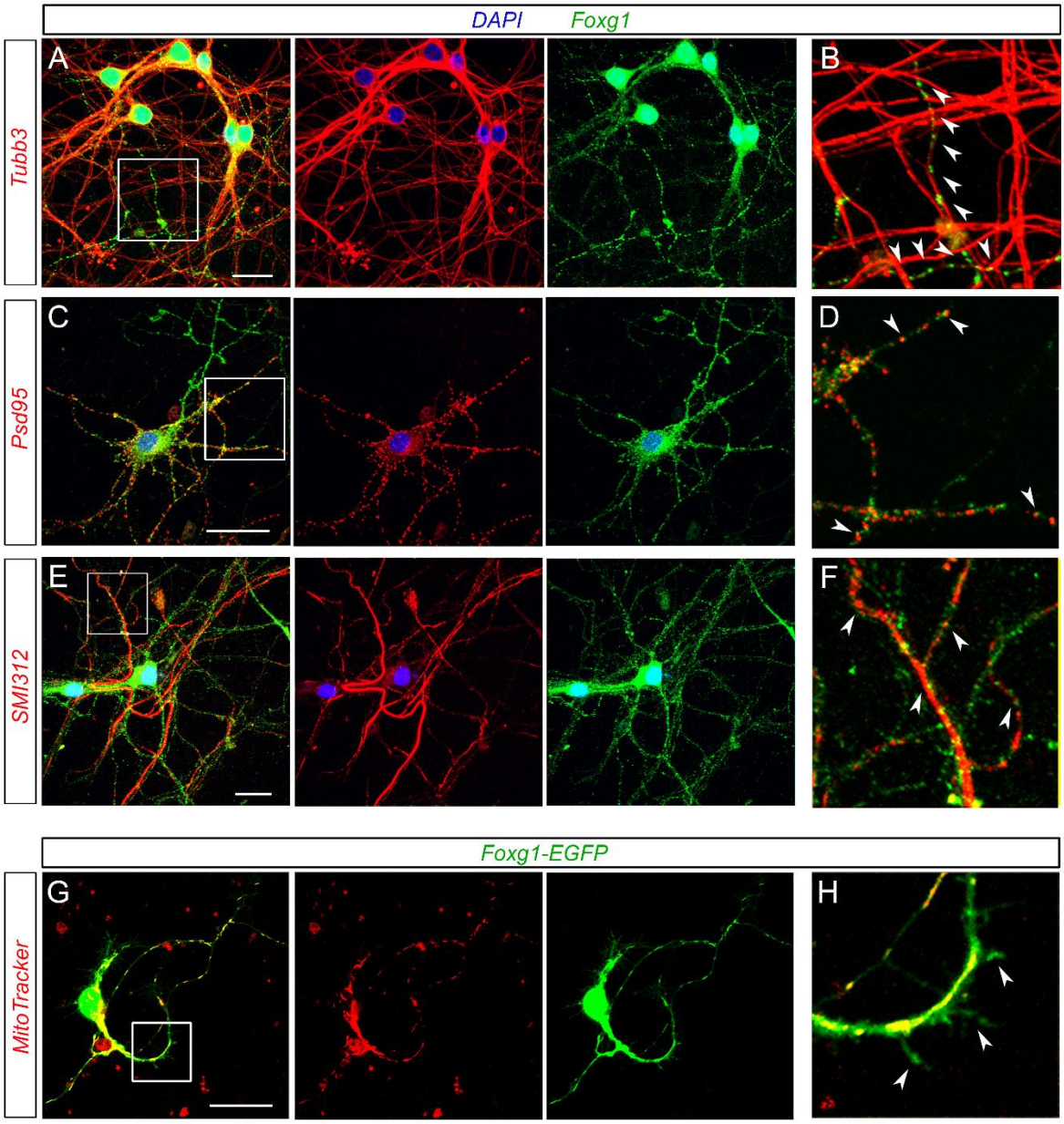

Figure 1. Neuronal, subcellular Foxg1 localization. (A-F) Preparations obtained by dissociation of E16.5 murine neocortices were cultured up to day in vitro 8 (DIV8), under a pro-differentiative medium supplemented with AraC. They were co-immunoprofiled for Foxg1 and, alternatively, Tubb3 (A, B), Psd95 (C,D), and SMI312 antigen (E,F), by confocal microscopy. Arrowheads point to Foxg1 immunoreactive grains adjacent to Tubb3-positive bundles (B), Psd95-positive spots (D), and SMI312-positive bundles (F). **(G, H)** Preparations obtained by dissociation of P2 rat hippocampi were cultured up to DIV7, under a pro-differentiative medium. Such cultures were transduced at DIV2 by lentiviral vectors driving p(Pgk1)/TetON-controlled Foxg1/EGFP expression, preterminally labelled by the red MitoTracker dye for 30 min, and finally profiled by live-confocal microscopy. Arrowheads in (H) point to cytoplasmic Foxg1-EGFP signal which does not co-localize with mitochondria. High power magnifications of (A,C,E,G) panel insets are in (B,D,F,H), respectively. Scalebars, 20µm.

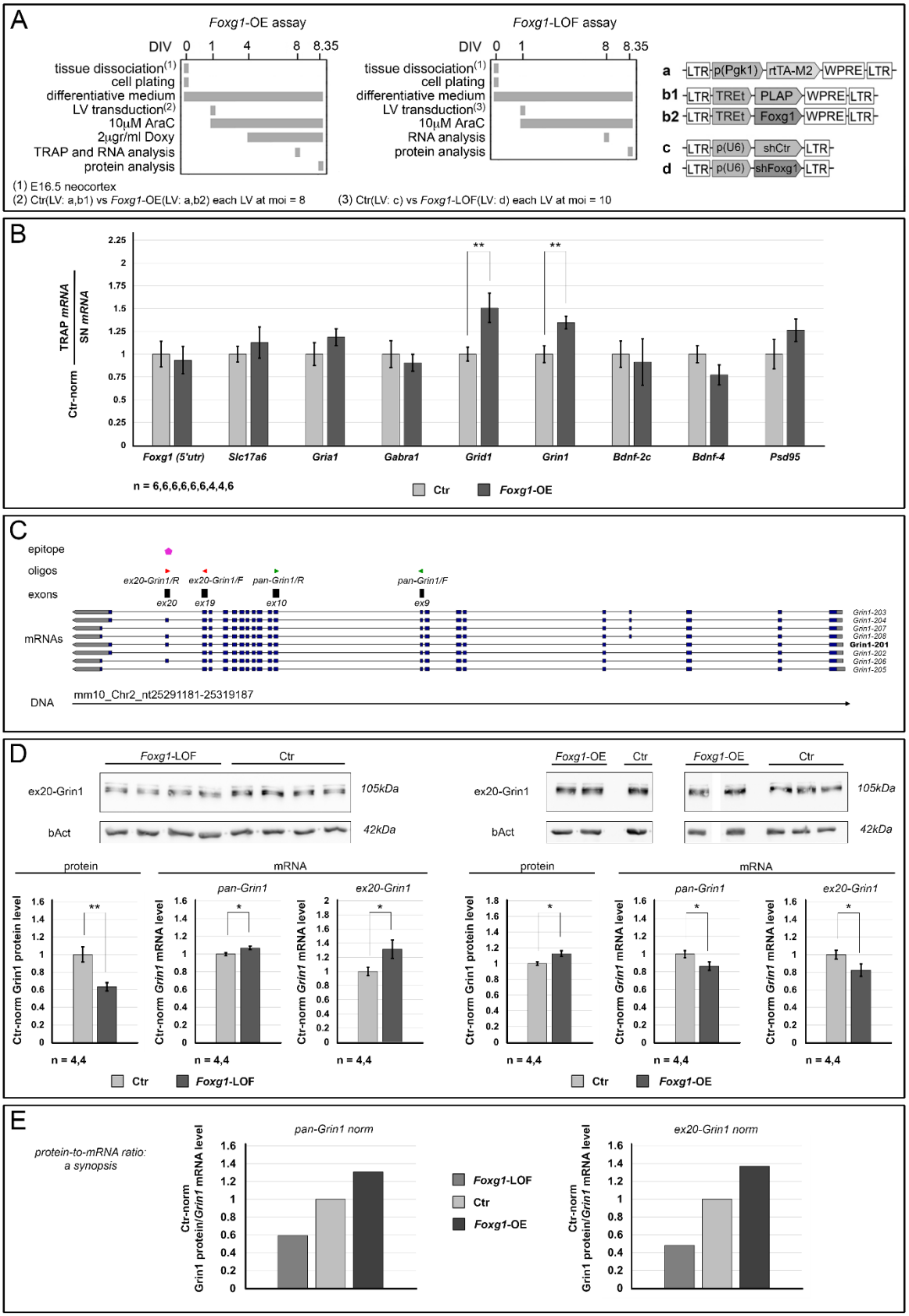

Figure 2. Impact of *Foxg1* manipulation on ribosomal allocation and protein output of selected neuronal transcripts. (A) Protocols and lentiviral vectors used to engineer neocortical cultures to conditionally overexpress *Foxg1* (Foxg1-OE, left panel) or reduce its level (*Foxg1*-LOF, right panel). **(B)** Comparative, Translating Ribosome Affinity Purification (TRAP) quantification of ribosome-associated

mRNA fraction (TRAP-mRNA) and its supernatant fraction (SN-mRNA), referring to selected neuronal transcripts, in *Foxg1*-OE cultures. mRNA levels measured by qRT-PCR, and double normalized, against *Rpl10a*-mRNA and controls. **(C)** *Grin1* gene locus with the main polypeptide-encoding transcripts originating from it. The top polygon represents the protein epitope recognized by the anti-Grin1 antibody used in Western blot assays. Arrowheads indicate oligos used to quantify *Grin1*-mRNA, distinguishing between ex20-*Grin1* isoforms and pan-*Grin1* isoforms. **(D)** Western blot analysis of Grin1 protein and qRT-PCR quantification of pan-*Grin1* and ex20-*Grin1* mRNA isoforms, upon *Foxg1*-LOF (left) and *Foxg1*-OE (right) manipulations. Protein levels double normalized against bAct and controls, mRNA levels against *Rpl10a*-mRNA and controls. **(E)** Progression of "normalized Grin1-protein" - to - "normalized *Grin1*-mRNA" ratio upon *Foxg1* manipulation, referring to pan-*Grin1* mRNA (left graph) or ex20-*Grin1*-mRNA (right graph). Throughout figure, *n* is the number of biological replicates, i.e. independently cultured and engineered preparations, originating from a common neural cell pool. Statistical evaluation of results was performed by one-way ANOVA, one-tailed and unpaired. * $p<0.05$, ** $p<0.01$. Errors bars indicate s.e.m.

To corroborate this finding and explore its biological meaning, we focused our attention on *Grin1* gene, encoding for the main subunit of NMDA receptor. To this aim, we evaluated its protein-to-mRNA ratio upon artificial modulation of Foxg1 expression levels. Tests were run in cultures of E16.5+DIV8 murine neocortical neurons, engineered to conditionally overexpress *Foxg1* (**Fig. 2A, lef**t) or reduce its level (*Foxg1*-LOF) (**Fig. 2A, right**). Grin1 protein was quantified via WB, by a monoclonal antibody recognizing an epitope encoded by *Grin1*-exon 20. *Grin1*-mRNA was measured via qRTPCR, by two oligonucleotide pairs, detecting all *Grin1* isoforms (*pan-Grin1*) or exon20-containing ones (*ex20-Grin1*) (**Fig. 2C**). Normalized against bAct, Grin1 protein was decreased (-36.7±4.7%, with $p<0.005$ and $n=4,4$) and increased (+12.8±3.8%, with $p<0.02$ and $n=4,4$), following down- and up-regulation of *Foxg1*, respectively. Opposite trends were displayed by *pan-Grin1*-mRNA (+6.9±2.0, with $p<0.02$ and $n=4,4$, in *Foxg1*-LOF samples; -13.7±4.7%, with $p<0.04$ and $n=4,4$, in *Foxg1*-OE ones). Remarkably, such opposite trends were even more pronounced in case of *ex20-Grin1*-mRNA (+31.5±13.0%, with $p<0.04$ and $n=4,4$, in *Foxg1*-LOF samples; -17.7±7.0%, with $p<0.05$ and $n=4,4$ in *Foxg1*-OE ones) (**Fig. 2D**). Finally, to get a comprehensive index of post-transcriptional *Foxg1* impact on Grin1 level, we calculated the "Grin1-protein/*Grin1*-mRNA" ratios peculiar to *Foxg1*-misexpressing cultures and normalized them against their controls. Such ratios ranged from 0.59 (*Foxg1*-LOF) to 1.31 (*Foxg1*-OE), referring to *pan-Grin1*-mRNA, from 0.48 (*Foxg1*-LOF) to 1.37 (*Foxg1*-OE), taking specifically into account *ex20-Grin1*-mRNA (**Fig. 2E**). All that suggests that *Foxg1* exerts a robust positive impact on post-transcriptional Grin1-protein tuning.

Next question was: does *Foxg1* enhance (1) translation of *Grin1*-mRNA and/or (2) does it diminish degradation of Grin1 protein?

As for (1), we evaluated Grin1 translation rates in E16.5+DIV8 neocortical cultures made *Foxg1*-LOF by RNAi. To this aim, we terminally pulsed these cultures with puromycin and we measured levels of nascent Grin1 ((n)Grin1) protein, via anti-Grin1/anti-puromycin-driven proximity ligation assay (PLA) (**Fig. 3A, left**). Compared to controls, (n)Grin1 was dramatically decreased in *Foxg1*-LOF samples. (n)Grin1^{+} spots per cell were reduced by -88.7±3.1% (p<4.0*10^{-7}, n=4,4), cumulative (n)Grin1 immunofluorescence per cell by -92.7±0.8% (p<4.0*10^{-5}, n=4,4) (**Fig. 3B**). Taking also into account the concomitant +31.5% upregulation of ex20-*Grin1*-mRNA occurring in the same samples (see **Fig. 2D**), this means that *Foxg1* strongly promotes *Grin1*-mRNA translation.

As for (2), we evaluated Grin1 degradation rates in similar *Foxg1*-LOF neocortical samples. To this aim, we blocked translation by cycloheximide and we monitored time course progression of previously synthesized Grin1 protein over 14 hours (**Fig. 3A, right**). Remarkably, Grin1 degradation rate resulted to be not increased, but - rather - slightly decreased upon *Foxg1* downregulation. Specifically, the Grin1(t)/Grin1(0) ratio equalled e$^{-0.046*hours}$ and e$^{-0.074*hours}$ in *Foxg1*-LOF cultures and controls, respectively (with p<0.048, n=3,3,3,3) (**Fig. 3C**). This result rules out that the *Foxg1*-dependent increase of "Grin1-protein/*Grin1*-mRNA ratio" referred above (**Fig. 2E**) may be due to *Foxg1* inhibition of Grin1 protein degradation.

To corroborate this inference and tentatively identify translation steps sensitive to *Foxg1* levels, we took advantage of a TetON-controlled transgene, encoding for a $^{N\text{-}term}$Flag-rnoGrin1-$^{C\text{-}term}$HA chimera. We delivered it to *Foxg1*-LOF and control E16.5 neocortical cultures and acutely activated it by doxyclycline. 12 hours later, we evaluated levels of *Flag-rnoGrin1-HA*-mRNA, by qRTPCR, as well as of Flag and HA epitopes, by quantitative immunofluorescence (qIF) (**Fig. 4A**). Normalized against *Foxg1*-LOF samples, controls displayed a pronounced downregulation of *Flag-rnoGrin1-HA*-mRNA (-35.0±14.3%, with p<0.042 and n=3,3), and poorly affected Flag and HA epitope levels (**Fig. 4B**, a-c graphs, and **4C**). Next, we calculated the resulting "Flag epitope/*Flag-rnoGrin1-HA*-mRNA" and "HA epitope/Flag epitope" ratios, as presumptive indices of translation initiation and polypeptide elongation, respectively. Both were upregulated in controls compared to *Foxg1*-LOF samples, by +45.2% and +16.0±3.7%, respectively (the latter with p<0.001 and n=55,68) (**Fig. 4B**, d,e graphs, and **4C**). This confirms the positive *Foxg1* impact on *Grin1*-mRNA translation. It further suggests that *Foxg1* may promote both initiation and elongation of the Grin1 polypeptide.

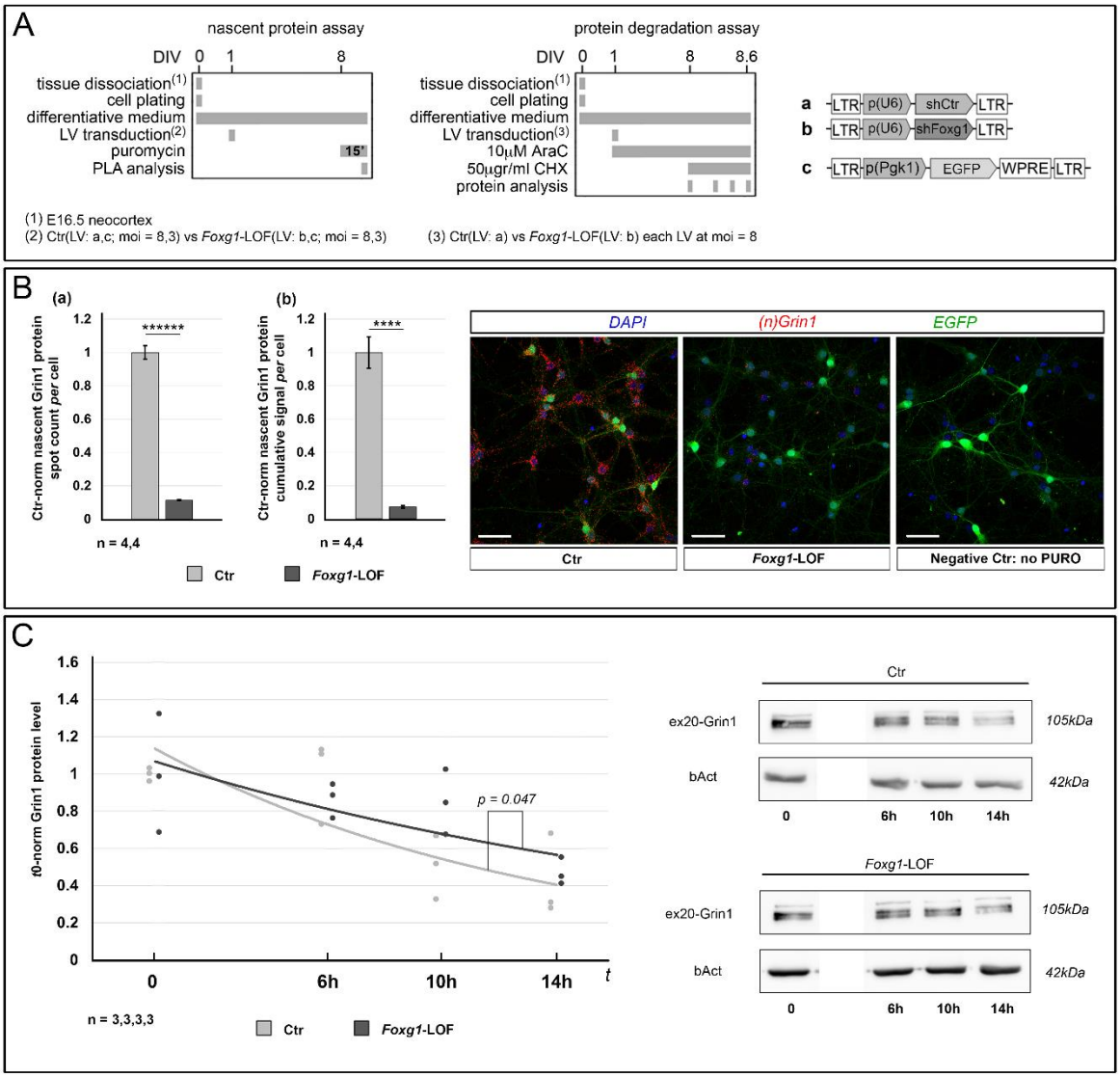

Figure 3. Evaluation of nascent Grin1 protein and Grin1-protein degradation rate in *Foxg1*-LOF neurons. (A) Protocols and lentiviruses employed for this analysis. **(B)** (Left) Graphs representing quantitative confocal immunofluorescence (qIF) evaluation of nascent Grin1 protein, (n)Grin1, performed upon *Foxg1* down-regulation, preterminal (15 min) puromycin administration and final anti-Grin1/anti-puromycin-driven proximity ligation assay (PLA). As indices of (n)Grin1 levels, shown are the average number of signal-spots per cell (graph a), and the average cumulative qIF signal per cell (graph b). Results normalized against controls. Neuron cell silhouettes were identified by direct EGFP fluorescence. Error bars indicate s.e.m. Statistical evaluation of results performed by one-way ANOVA, one-tailed and unpaired. **** $p<10^{-4}$, ****** $p<10^{-6}$. (Right) Examples of primary data employed for this analysis. Scalebars, 50μm. **(C)** (Left) Graph representing time course progression of Grin1-protein levels, evaluated by western blot, upon *Foxg1* down-regulation and subsequent cycloheximide (CHX) blockade of translation. For each genotype, results double normalized, against ($t=t_i$)bAct protein levels and (t=0) average values. Superimposed, exponential trendlines. Statistical evaluation of results performed by ANCOVA test. (Right) Examples of primary data employed for this analysis. Throughout figure, *n* is the number of biological replicates, i.e. independently cultured and engineered preparations, originating from a common neural cell pool.

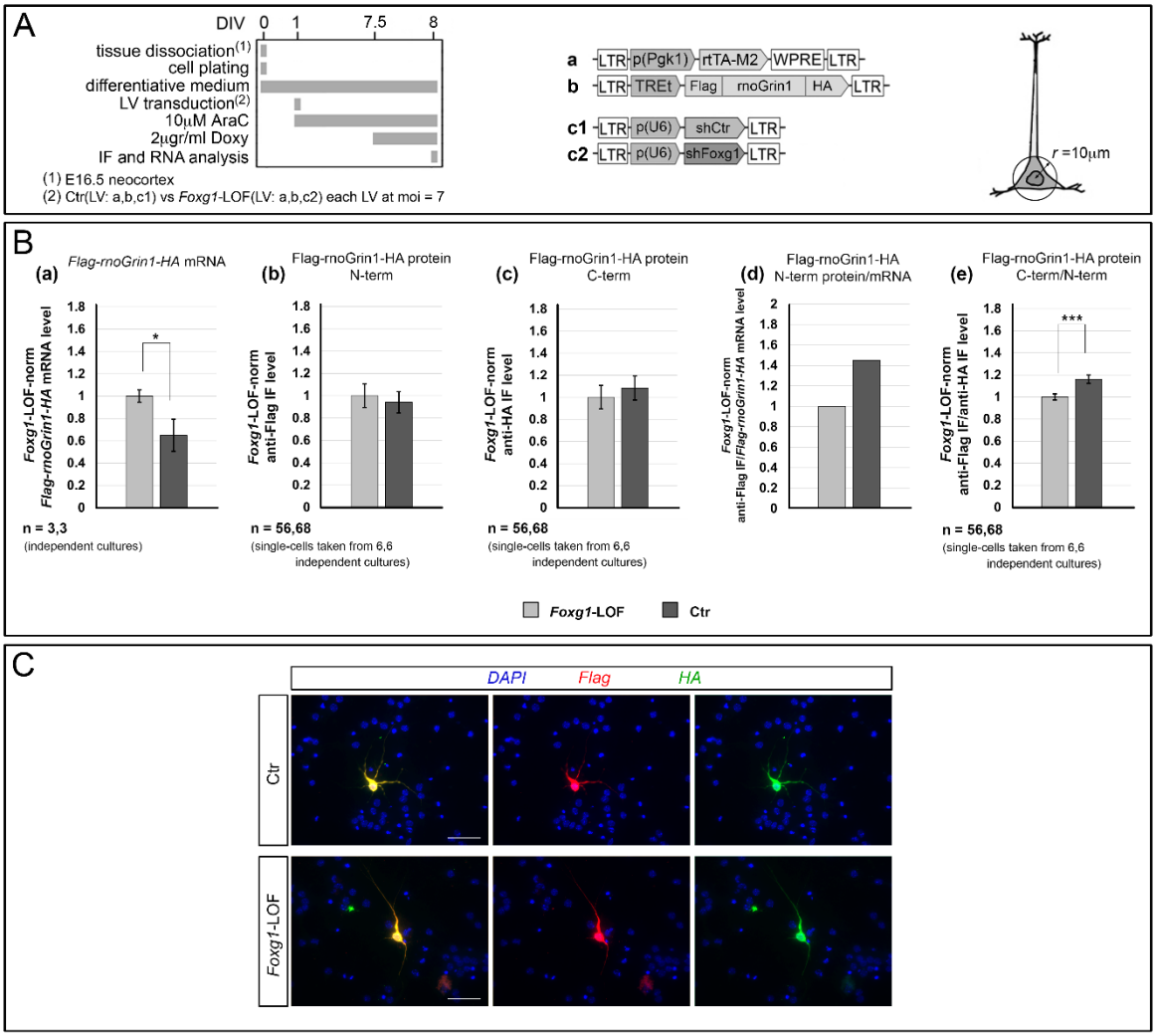

Figure 4. Evaluation of *Grin1* translational initiation and elongation rates by means of a heterologous *Flag-rnoGrin1-HA* sensor in *Foxg1*-LOF neurons. (A) Protocols (*left*) and lentiviral vectors (*mid*) used to make neocortical cultures *Foxg1*-LOF and profile mRNA and protein outputs of their doxycycline-activatable, *Flag-rnoGrin1-HA* transgene. The silhouette (*right*) represents an idealized pyramidal cell, where the somatic cytoplasm subject of IF protein quantification is highlighted in pale grey **(B)** Graphs showing: (a) qRT-PCR quantification of *Flag-rnoGrin1-HA*-mRNA levels in bulk cultures, primarily normalized against *Rpl10a*-mRNA; (b,c) single-cell IF quantification of average N-term-Flag and C-term-HA signals detectable in neuronal somata; (d) "N-term-Flag to *Flag-rnoGrin1-HA*-mRNA" ratio, as an index of rnoGrin1 translational initiation; (e) "C-term-HA to N-term-Flag" ratio, as an index of rnoGrin1 translational elongation. In all five graphs, results normalized against *Foxg1*-LOF samples. *n* is the number of biological replicates. These are: (a) independently cultured and engineered preparations, originating from a common neural cell pool; (b,c,e) single-cells, evenly taken from multiple, independent *Foxg1*-LOF and control cultures. Statistical evaluation of results was performed by one-way ANOVA, one-tailed and unpaired. * $p<0.05$, *** $p<0.001$. Errors bars indicate s.e.m. **(C)** Example of anti-Flag and anti-HA immunostainings in *Foxg1*-LOF and control cultures. Scalebars, 50µm.

4.2. Foxg1 physically interacts with *Grin1*-mRNA and selected translation factors

We have shown that Foxg1 enhances translation of Grin1. Next question was: does Foxg1 act in this context (1) as a canonical nuclear transcription factor, tuning expression of translation factor genes or (2) straightly as a cytoplasmic "translation modulator"? Previous Foxg1 interaction screening reports [Li et al., 2015; Stelzl et al., 2005; Weise et al., 2019] as well as limited responsivity of translation factors' mRNA levels to *Foxg1* overexpression (**Table S1**) suggested us that type (2) mechanisms might be prevailing.

To cast light on this issue, we took advantage of HEK293T preparations, expressing Foxg1 and distinct translation-related, putative interactors of it, tagged by V5 or Flag. We specifically focused on EIF4E, EEF1D, EEF1G, PUM1, evaluating their interaction with Foxg1 by quantitative proximity ligation assay (qPLA), driven by anti-Foxg1 and anti-tag antibodies (**Fig. 5A**). Normalized against their technical controls, EIF4E, EEF1D and PUM1 gave robust PLA signals [3.2±0.4 (with $p<0.02$ and $n=2,3$), 3.6±0.4 (with $p<0.01$ and $n=2,3$), and 2.4 (with $n=1,1$), respectively], suggesting that their interaction with Foxg1 is genuine. As for EEF1G, its signal hardly overcome the corresponding controls (**Fig. 5B**).

To confirm Foxg1/EIF4E interaction (not included in previously published interaction reports), we further interrogated HEK293T cells cotransfected with Foxg1- and Flag-EIF4E-encoding transgenes, via quantitative-immunoprecipitation-western blot (qIP-WB). Tentative negative controls were set by replacing *Flag-EIF4E* via *Flag-Gephyrin* and *Flag-GFP* transgenes (**Fig. 5A**). Immunoprecipitated by anti-Flag and probed upon WB separation by anti-Foxg1, lysates of *Foxg1/Flag-EIF4E*-transduced cells specifically gave a robust Foxg1 enrichment. Normalized against *Foxg1/Flag-Gephyrin*- and *Foxg1/Flag-GFP*-transduced controls, such enrichment equalled 99.1±0.1 (with $p<2.0*10^{-6}$ and $n=2,2$) and 35.2±0.4 (with $p<2.0*10^{-4}$ and $n=2,2$), respectively (**Fig. 5C**).

In a few words, Foxg1 interacts with standard factors implicated in both translation initiation (EIF4E) and polypeptide elongation (EEF1D), as well as - possibly - with another specific factor implicated in regulation of polypeptide synthesis (PUM1).

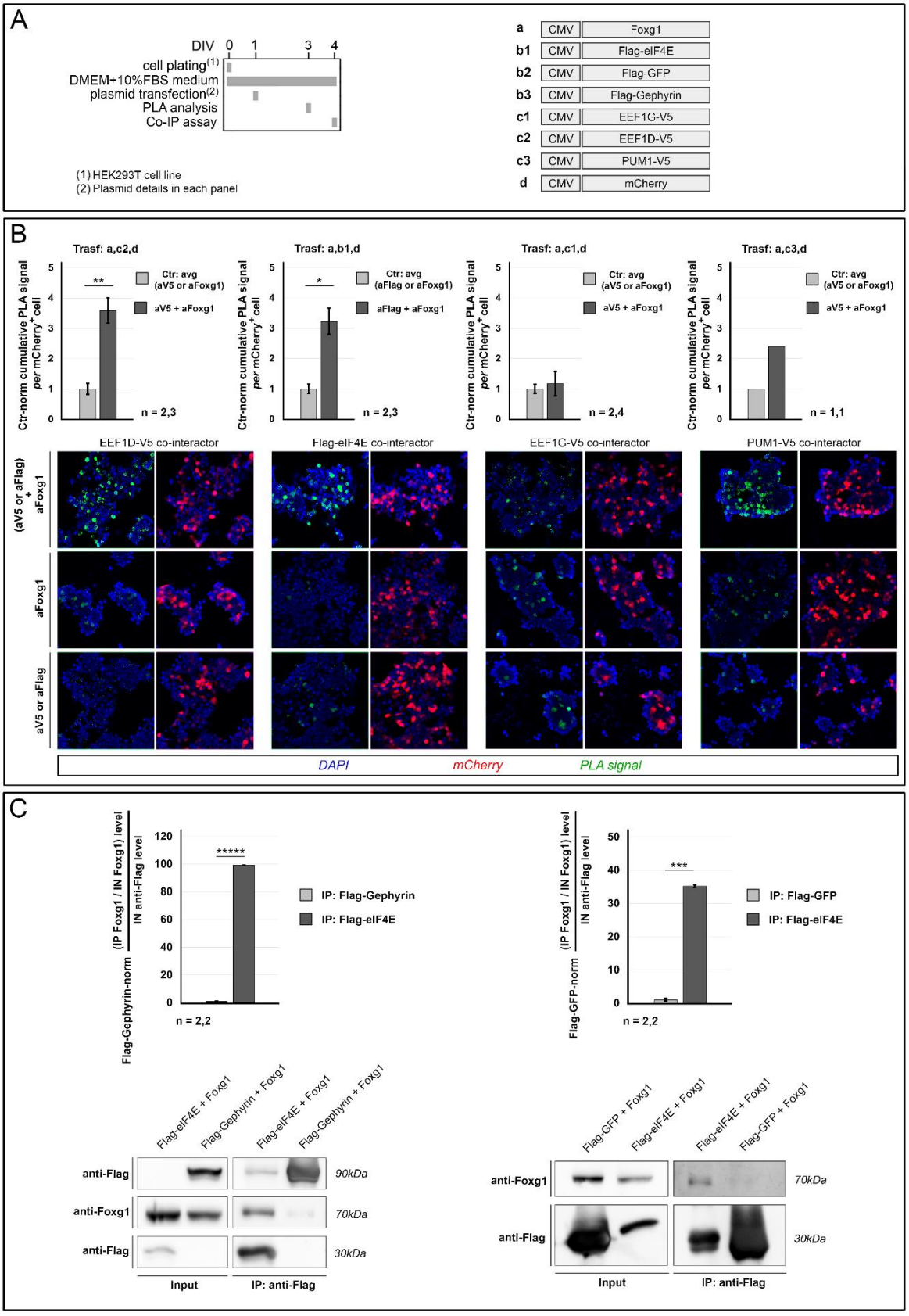

Figure 5. Assessment of Foxg1-protein interaction with selected translation factors (Transl.F) in engineered HEK293T cells, by quantitative immunoprecipitation-western blot (qIP-WB) and quantitative proximity ligation (qPLA) assays. (A) Protocols and lentiviral vectors used. **(B)** qPLA assessment of Foxg1 interaction with selected Transl.Fs: graphical representation of results (upper row)

and examples of primary data (lower row). Cells double transfected, by Foxg1- and Flag-Transl.F- or Transl.F-V5- encoding transgenes, and further transfected by an mCherry transgene, as an internal control. Interaction signals revealed by anti-Foxg1/anti-Flag- or anti-Foxg1/anti-V5-driven proximity ligation assays, mCherry revealed by direct fluorescence. For each co-transfection type, shown is the average cumulative "green" qPLA signal per transfected $mCherry^+$ cell, normalized against the average values of the two corresponding negative controls (each obtained by omitting either primary antibody). **(C)** qIP-WB assessment of Foxg1/Eif4E interaction: graphical representation of results (top row) and examples of primary data (bottom row). Cells double transfected, by Foxg1- and Flag-Eif4E-encoding transgenes (negative controls: Flag-Gephyrin and Flag-EGFP), IP by anti-Flag, immuno-detection by anti-Foxg1. Densitometric IP-protein values double normalized, against Foxg1 and Flag-protein inputs, and further normalized, against negative controls. Throughout figure, *n* is the number of biological replicates, i.e. independently cultured and engineered preparations, originating from a common cell pool. Statistical evaluation of results performed by one-way ANOVA, one-tailed and unpaired. * $p<0.05$, ** $p<0.01$, *** $p<0.001$, ***** $p<0.00001$. Errors bars indicate s.e.m.

To further support the hypothesis that Foxg1 promotes Grin1 synthesis as a translation factor, we investigated if Foxg1 interacts with *Grin1*-mRNA. To this aim, firstly, we quantified the fraction of *Grin1*-mRNA immunoprecipitated by an anti-Foxg1 antibody in lysates of E16.5+DIV8 neocortical neurons, by RNA immuno-precipitation (RIP)-qRTPCR (**Fig. 6A**). This fraction exceeded the IgG background by 17.6±7.4 folds (with $p<0.05$, $n=5,4$) (**Fig. 6B**); moreover, compared to control, it showed a declining trend upon *Foxg1* knock-down (10.3±1.5 vs 20.1±8.7, with $p<0.15$ and $n=2,2$) (**Fig. 6C**). Then, we scored for *Grin1*-mRNA enrichment RNA samples originating from *Foxg1-EGFP* overexpressing neurons, immunoprecipitated by an anti-EGFP antibody. Remarkably, such enrichment equalled 6.1±0.8, upon normalization against Plap expressing controls (with $p<0.02$, $n=2,2$) (**Fig. 6D**). Altogether these results indicate that, within neocortical neurons, *endogenous* Foxg1 protein interacts with *endogenous Grin1*-mRNA.

Next, to tentatively identify *Grin1*-mRNA domains needed to bind Foxg1 protein, we co-transduced murine neocortical neurons with TetON-controlled, intronless transgenes, encoding for the *Rattus norvegicus Grin1*-203 transcript (including exon 20 and orthologous to the murine *Grin1*-201 isoform) and artificially-deleted variants of it (**Fig. 6A**). [Within these transgenes, to prevent toxicity induced by *chronic Grin1* overexpression and potential artifacts due to differential protection of *rnoGrin1*-mRNA by translating ribosomes, a stop codon was inserted between codons 30 and 31 (*rnoGrin1*.203*)]. Then, we immunoprecipitated RNA originating from these cultures by anti-Foxg1 and normalized the IP-*Grin1*-mRNA fraction peculiar to each deletion against IP, full-length *rnoGrin1*.203*.f (**Fig. 6E**). Finally, we critically evaluated the relevance of distinct *Grin1*-mRNA segments to anti-Foxg1 immuno-precipitability. We observed

that the two variants missing the AccIII-PshAI fragment at the Grin1-cds 3' end, *rnoGrin1*.203*.d3 and *rnoGrin1*.203*.d5, specifically displayed an normalized IP fraction well below 1 (0.53±0.04 with $p<0.002$ and $n=4$, and 0.30±0.19, with $p<0.002$ and $n=2$, respectively), pointing to a pivotal role of this fragment in the interaction with Foxg1. Next, the removal of the original 3'UTR, peculiar to *rnoGrin1*.203*.d4, increased the IP fraction up to 2.39±0.13 (with $p<5*10^{-6}$ and $n=2$), suggesting that such domain may normally antagonize Foxg1 recruitment to *Grin1*-mRNA. Last, a declining IP trend was also detectable in *rnoGrin1*.203*.d1, missing the 5'UTR (0.78±0.04, with $p<0.07$ and $n=4$), further implicating the 5'UTR in Foxg1 recruitment to *Grin1*-mRNA (**Fig. 6E**). Altogether, these results corroborate the specificity of Foxg1/*Grin1*-mRNA interaction and provide a coarse-grained, tentative framework for its articulation.

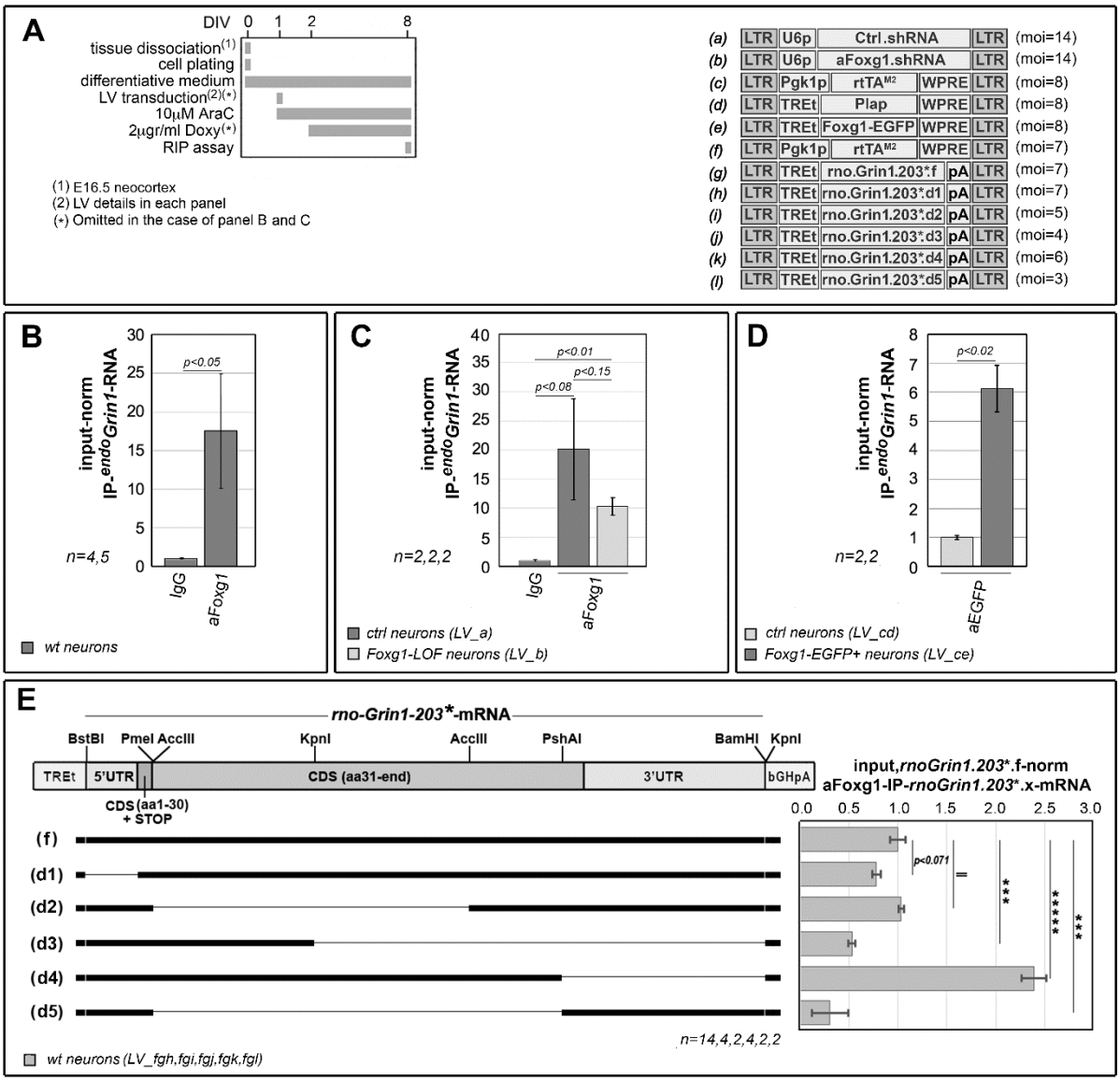

Figure 6. Assessment of Foxg1-protein/*Grin1*-mRNA interaction in neurons, by RNA immunoprecipitation (IP) qPCR (qRIP-PCR) assays. (A) Protocols and lentiviral vectors used. **(B, C)** Anti-Foxg1-IP fraction of endogenous *Grin1*-mRNA in neurons expressing naive (B) or decreased (C) levels of *Foxg1*-mRNA. Results double normalized, against input-RNA and IgG-IP samples. **(D)** Anti-EGFP-IP fraction of endogenous *Grin1*-mRNA in neurons expressing a lentivector-driven, *Foxg1-EGFP* transgene or a *Plap* control. Results double normalized, against input-RNA and control samples. **(E)** Mapping determinants of Foxg1-protein binding on a heterologous *rno-Grin1*-mRNA, encoded by a lentiviral transgene. To this aim, a number of partially overlapping deletions were generated starting from the full-length cDNA (f), by standard molecular cloning techniques, so giving rise to five distinct mutants (d1-d5). To prevent toxicity originating from *chronic*, exaggerated Grin1 expression and potential artifacts stemming from differential protection of *rnoGrin1*-mRNA by translating ribosomes, in all constructs a stop codon was inserted in a fixed position, between codons 30 and 31. To quantify the impact of each deletion, neural cultures were co-transduced with lentiviral mixes encoding for different combinations of full-length (f) and mutant (d_n) transgenes. Anti-Foxg1-IP fractions of mutant *rnoGrin1*-mRNAs, primarily normalized against the corresponding inputs, were diminished by the corresponding IgG-IP backgrounds and finally renormalized against the average full-length fraction. Trougout figure,

n is the number of biological replicates, i.e. independently cultured and engineered preparations, originating from a common neural cell pool. Statistical evaluation of results was performed by one-way ANOVA, one-tailed and unpaired. *** $p< 0.001$, ***** $p< 0.00001$. Errors bars indicate s.e.m.

4.3. Foxg1 is needed to achieve proper enhancement of *Grin1*-mRNA translation in silent neurons

Grin1 is a key player implicated in neuronal plasticity [Baez et al., 2018]. Its protein product was specifically reported to be upregulated in hippocampal neurons of adult rats having undergone open field habituation or object recognition tests. Upon delivery of an activity-stimulating protocol based on exposure to alternating K^+/TTX [Wu et al., 2001], a similar upregulation was also found in the soma of cultured hippocampal neurons, where it required *de novo* protein synthesis [Cercato et al., 2017]. To get insight into biological relevance of Foxg1 promotion of Grin1 translation, we evaluated rates of Grin1-protein synthesis in murine neocortical cultures, pretreated by an anti-*Foxg1*.shRNA or a negative control of it (NC.shRNA), and finally exposed to alternating K^+/TTX or alternating PBS/TTX, or chronically kept in control medium (= "unstimulated" samples). Grin1 synthesis rates were assessed upon preterminal puromycin culture labelling, by means of anti-Grin1/anti-puromycin-driven qPLA (**Fig. 7A**). We found that cultures treated by NC.shRNA underwent a slight, not statistically significant downregulation as well as an upregulation (+60.2±12.1%, with $p<0.01$ and $n=5,4$) of Grin1 protein synthesis rates, upon exposure to alternating K^+/TTX and alternating PBS/TTX, respectively. Moreover, we found that such synthesis rates collapsed in anti-*Foxg1*.shRNA-treated cultures. Here, normalized against "NC.shRNA-treated/unstimulated" controls, these rates equalled 0.07±0.01, 0.10±0.01 and 0.15±0.02 in case of K^+/TTX-, control medium- and PBS/TTX-treated samples, respectively. Albeit small, differences between anti-*Foxg1*.shRNA-treated samples were significant ($p<0.04$, with $n=4,4$, as for K^+/TTX-vs-control ones; $p<0.03$, with $n=4,4$, as for PBS/TTX-vs-control ones) (**Fig. 7B**). These results point to an unexpected homeostatic tuning of Grin1 translation rates, considerably higher in silenced neurons compared to K^+ stimulated ones. They further show that not only basal, but also Grin1 *de novo* synthesis triggered by electrical inactivity requires *Foxg1*.

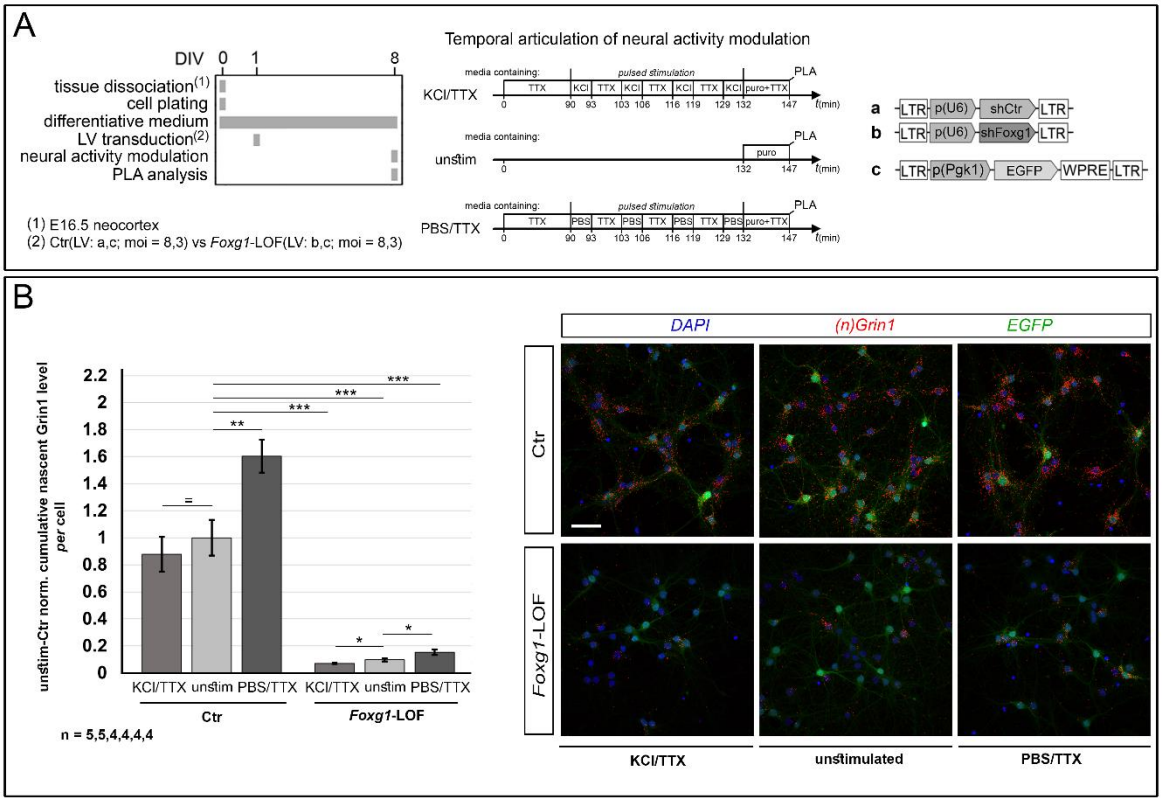

Figure 7. Foxg1 relevance to homeostatic *Grin1*-mRNA translational tuning. (A) Protocols and lentiviral vectors used. (**B**) Nascent Grin1 protein content per cell, in *Foxg1*-LOF neural cultures and "wild type" controls: graph to the left, examples of primary data to the right. Neural cultures, untreated or undergoing subterminal primary 90 min exposure to 1µM TTX, followed by a secondary alternating exposure to 1µM TTX and 55mM extracellular [K^+] ("KCl/TTX" samples) or 1µM TTX and standard medium ("PBS/TTX" samples), were terminally pulsed with 1µM puromycin. Nascent Grin1 was distinguished by anti-Grin1/anti-puromycin-driven quantitative proximity ligation assays (qPLA). Neuron cell silhouettes were identified by direct EGFP fluorescence. For each sample, the average cumulative qPLA signal per cell was normalized against the average value peculiar to unstimulated "wild-type" controls. *n* is the number of biological replicates, i.e. independently cultured and engineered preparations, originating from a common cell pool. Scalebars, 50µm. Statistical evaluation of results performed by one-way ANOVA, one-tailed and unpaired. * $p< 0.05$, ** $p< 0.01$, *** $p<0.001$. Errors bars indicate s.e.m.

4.4. General impact of *Foxg1* on mRNA ribosomal engagement

We wondered if *Foxg1* impact on translation is peculiar only to a few genes including *Grin1* or is it a pervasive phenomenon. To get a preliminary insight into this issue, we systematically sequenced ribosome-engaged-mRNA (trapRNAseq) purified from *Foxg1*-OE and control cultures, and compared it to total-mRNA originating from corresponding sister cultures (totRNAseq) [Artimagnella and Mallamaci, 2020]. Upon filtering out low-expressed genes, for each gene, we calculated $\log_2$"expression fold change" values ($\log_2$FC) peculiar to trapRNA and totRNA samples. Finally, we scored each gene on the basis of the difference between the former and the latter [$\log_2$FC(trapRNAseq)-$\log_2$FC(totRNAseq), hereafter $\Delta\log_2$FC], as a measure of *Foxg1* stimulation of ribosomal mRNA engagement and a presumptive index of *Foxg1* promotion of its translation. We found that >1000, >250, ~50 and >10 genes had $\Delta\log_2$FC greater than 0.5, 2, 4 and 6, respectively, suggesting that *Foxg1* might promote their translation. We also found larger numbers of genes with $\Delta\log_2$FC less than -0.5, -2, -4 and -6, respectively, further suggesting that in a number of cases *Foxg1* might *inhibit* translation (**Table 1**).

Evaluated against all genes transcribed in neurons, genes belonging to the "$\Delta\log_2$FC>0.5" ensemble showed statistically significant enrichments for gene ontology (GO) terms: modulation of chemical synaptic transmission, regulation of plasma membrane bounded cell projection organization, regulation of transport, signaling, cell communication, response to stimulus under the "biological process" category; gated channel activity, under the "molecular function" category; excitatory synapse, integral component of presynaptic membrane, cation channel complex, postsynaptic membrane, under the "cellular component" category. Similar GO scoring of genes belonging to the "$\Delta\log_2$FC<-0.5" ensemble did not give significant outcomes under "biological process" and "molecular function" categories, and displayed an enrichment for postsynaptic membrane, somatodendritic compartment, neuron projection under the "cellular component" category (**Table S2**).

Intriguingly, a number of genes with $\Delta\log_2$FC>0.5 resulted to have their total mRNA significantly downregulated by *Foxg1*, pointing to a likely biphasic *Foxg1* modulation (upwards and then downwards) of their final expression levels (not shown).

Table 1. Integrated totRNAseq- and trapRNAseq-profiling of *Foxg1*-OE neocortical neurons. For the compilation of this table, genes with control CPM values falling within the 1st quartile were discarded and the remaining ones were taken into account IF "$\Delta log_2FC \neq 0$" AND ["log_2FC(trapRNAseq)$\neq 0$" OR "log_2FC(totRNAseq)$\neq 0$" (in both cases, with $p<0.05$ and $FDR<0.05$)].
Δlog_2FC stands for log_2FC(trapRNAseq)-log_2FC(totRNAseq).

Δlog_2FC	*number of genes*
>0.5	1170
<-0.5	1523
>2	253
<-2	418
>4	49
<-4	100
>6	14
<-6	33

5. DISCUSSION AND CONCLUSIONS

Here, moving from pervasive expression of Foxg1 protein in axons and dendrites of neocortical pyramids (**Figure 1**), we documented an impact of *Foxg1* on ribosomal engagement of *Grin1*-mRNA (**Figure 2A,B**). Next, we showed that Foxg1 increases Grin1 protein level by enhancing translation of its mRNA, while not ameliorating its stability (**Figure 2A,C-E** and **3**). Such enhancement was apparently due to increased translational initiation and, possibly, polypeptide elongation (**Figure 4**). Mechanisms underlying these phenomena included Foxg1 protein interaction with Eif4E, Eef1d and Pum1 (**Figure 5**) as well as with *Grin1*-mRNA (**Figure 6**). Moreover, we found that *Grin1*-mRNA translation becomes particularly prominent in silent neurons and Foxg1 is needed for that (**Figure 7**). Finally, as a proof-of-principle, a dedicated TRAP-seq survey showed that, not just peculiar to *Grin1*, functional Foxg1 implication in translation apparently is a pervasive phenomenon, affecting hundreds of synaptic genes (**Table 1**).

Actually a localization of Foxg1 in the cytoplasm of early born, neocortical glutamatergic neurons was already reported [Regad et al., 2007]. Here we showed that Foxg1 may be localized in dendrites and axons of the majority of neocortical pyramids (**Figure 1A-F**) and we further documented an association of Foxg1 to glutamatergic spines (**Figure 1C,D**).

Based on higher *Grin1*-mRNA levels in ribosome-engaged- compared to total-mRNA of *Foxg1*-OE neurons (**Figure 2B**), we inferred a likely positive impact of Foxg1 on *Grin1* translation. However, hyper-recruitment of *Grin1*-mRNA to ribosomes, as documented by $^{anti\text{-}Rpl10a}$TRAP analysis, does not imply an increased synthesis of its protein product, but simply reflects an enhanced initiation of its translation by the holoribosome (*ribosomal stalling might paradoxically increase such engagement, in front of ultimately reduced protein synthesis*). Subsequently, we also found that higher *Foxg1* levels led to increased "Grin1-protein to *Grin1*-mRNA" ratios (**Figure 2E**) in the absence of Grin1-protein stabilization (**Figure 3C**), as well as to increased puromycin-tagged, nascent Grin1 (**Figure 3B**). That allowed us to definitively validate the aforesaid inference.

Concerning our tentative dissection of Foxg1 impact on polypeptide initiation and elongation via comparative immunoprofiling of two artificial epitopes appended to N- and C-terms of Grin1 (**Figure 4A**), its results require a particularly cautious interpretation. In fact, albeit providing useful information on polypeptide elongation rates (**Figure 4B,** graph e), they depend on tags

accessibility, namely a parameter hardly sensitive to dynamics of primary protein folding [Kubelka et al., 2004], however potentially sensitive to enduring, Foxg1-dependent post-transcriptional protein modifications. [Actually, replacing small, immunodetectable tags by intrinsically fluorescent polypeptides might have helped to circumvent this issue, however the potentially artifactual impact of the size of the latter on translation dynamics discouraged us from doing that].

As for molecular mechanisms underlying Foxg1 impact on *Grin1* translation, we achieved multiple pieces of evidence pointing to it as a "translation modulator". In fact, beyond Foxg1 detection in neuronal cytoplasm (**Figure 1**), we found that it interacts with selected translation factors (**Figure 5**) and binds to *Grin1*-mRNA (**Figure 6**). To note, our PLA-based investigation of Foxg1/Eef1d and Foxg1/Pum1 association confirmed results of previous high-throughput mass spectrometry (MS) screenings in HEK293T and N2A cells [Li et al., 2015; Weise et al., 2019], Foxg1 interaction with Eif4e, we proved by both IP-WB analysis and PLA, is fully novel. Similarly, while an interaction of Foxg1 with *miRNA precursors* has been already reported [Weise et al., 2019], our finding of neuronal Foxg1/*mRNA* interaction is novel. Remarkably, Foxg1 association to Eif4e and Eef1d resonate with presumptive Foxg1 implication in translation initiation and polypeptide elongation, respectively [Jackson et al., 2010; Pelletier and Sonenberg, 2019]. Conversely, we are not presently able to predict the translational impact of Foxg1/Pum1 interaction [Bohn et al., 2018].

Encoding for subunits of the heteromeric NMDA receptor, *Grin* genes undergo an intricate, multi-step regulation, needed for proper setting of integrative properties of neocortical pyramids [Paoletti et al., 2013]. Our finding that suppression of neuronal activity stimulates *Grin1*-mRNA translation is apparently at odds with Cercato et al [2017], who previously reported an enhancement of *Grin1*-mRNA translation upon neuron hyperstimulation. Different substrates employed in the two studies (E16.5+DIV8 mouse neuronal cultures and E17+DIV18 rat hippocampal cultures, respectively) might account for this discrepancy. Activity-blockade-driven, translational Grin1 upregulation might contribute to homeostatic scaling of neuronal response to glutamate [Dörrbaum et al., 2020].

Next, *Foxg1* has been recently shown to promote activity and excitability of neocortical neurons, largely via a profound impact on their transcriptome [Tigani et al., 2020]. Moreover, *Foxg1*-depleted hippocampal neurons display reduced NMDA currents and defective long-term potentiation (LTP) [Yu et al., 2019]. In this respect, *Foxg1*-dependent modulation of *Grin1* translation (**Figure 7**) might be a key mechanism accounting for both these effects. Finally,

Foxg1 is transiently upregulated by neuronal hyperactivity [Tigani et al., 2020]. In this way, *Foxg1*-dependent promotion of Grin1 translation might contribute to normal dynamic shaping of pyramid plasticity, its absence might impair such plasticity, contributing to major cognitive deficits of *FOXG1*-haploinsufficient patients [Mitter et al., 2018; Vegas et al., 2018; Wong et al., 2019].

The involvement of a transcription factor in control of mRNA translation is not novel. It has already been reported in a few cases, including Bicoid [Niessing et al., 2002], Emx2 [Nédélec et al., 2004], and En2 homeoproteins [Brunet et al., 2005]. In our case, we found that Foxg1 implication in translation is not limited to *Grin1* only, but it is a pervasive phenomenon (**Table 1**), affecting hundreds of genes, among which a substantial number encoding for synaptic effectors (**Table S2**). As said above, higher ribosomal engagement of mRNA unveiled by TRAP analysis simply reflects an enhanced *initiation* rate of translation by the holoribosome. This might straightly result in increased synthesis of its protein product. Should the ribosome stall by the kozak motif, it might alternatively pave the way to subsequent, prompt and massive completion of translation, upon the arrival of due inputs. In other words, rather than generically enhancing translation, in a fraction of cases Foxg1 might allow to get a timely (and, possibly, spatially confined) adjustment of the translational gain, strictly complying with neuronal needs. Intriguingly, in a number of cases including *Grin1*, we found that a $^{\text{trapRNA-vs-totRNA}}\Delta\log_2\text{FC}$ value well above 0 is accompanied by a substantial gene downregulation in total-mRNA samples. In these cases the very same effector, Foxg1, might promote a rapid arousal of the protein, while however limiting the temporal duration of its overexpression.

Mainly known as a classical transcription factor patterning the terminal brain and ruling its histogenesis, Foxg1 has been also detected outside the nucleus, however biological meaning of that has been clarified only to a partial extent [Hou et al., 2020]. Our finding of Foxg1 impact on translation points to this factor as a key effector, crucial to proper temporal tuning of neocortical pyramid plasticity. Interesting *per se* as well as for its profound neuropathogenic implications, this issue will be systematically investigated in a future, dedicated follow-up study.

6. SUPPLEMENTARY MATERIAL

Table S1

Translation factor genes in *Foxg1*-OE neurons (from Zenodo dataset, [Artimagnella and Mallamaci, 2020].

Locus	*log2FC*	*logCPM*	*P-value*	*FDR*	*Gene Name*	*Description*
ENSMUSG00000035530	-0.46	8.58	0.01	0.02	Eif1	eukaryotic translation initiation factor 1 [Source:MGI Symbol;Acc:MGI:105125]
ENSMUSG00000057561	0.15	6.06	0.07	0.12	Eif1a	eukaryotic translation initiation factor 1A [Source:MGI Symbol;Acc:MGI:95298]
ENSMUSG00000024841	-0.06	4.64	0.62	0.72	Eif1ad	eukaryotic translation initiation factor 1A domain containing [Source:MGI Symbol;Acc:MGI:19171
ENSMUSG00000067194	0.30	7.98	0.00	0.00	Eif1ax	eukaryotic translation initiation factor 1A, X-linked [Source:MGI Symbol;Acc:MGI:1913485]
ENSMUSG00000006941	-0.22	6.38	0.16	0.25	Eif1b	eukaryotic translation initiation factor 1B [Source:MGI Symbol;Acc:MGI:1916219]
ENSMUSG00000027810	0.17	5.44	0.05	0.09	Eif2a	eukaryotic translation initiation factor 2A [Source:MGI Symbol;Acc:MGI:1098684]
ENSMUSG00000029613	-0.26	6.43	0.00	0.00	Eif2ak1	eukaryotic translation initiation factor 2 alpha kinase 1 [Source:MGI Symbol;Acc:MGI:1353448]
ENSMUSG00000031668	0.11	5.12	0.27	0.37	Eif2ak3	eukaryotic translation initiation factor 2 alpha kinase 3 [Source:MGI Symbol;Acc:MGI:1341830]
ENSMUSG00000005102	-0.17	5.15	0.06	0.11	Eif2ak4	eukaryotic translation initiation factor 2 alpha kinase 4 [Source:MGI Symbol;Acc:MGI:1353427]
ENSMUSG00000029388	-0.12	5.33	0.25	0.35	Eif2b1	eukaryotic translation initiation factor 2B, subunit 1 (alpha) [Source:MGI Symbol;Acc:MGI:238480
ENSMUSG00000004788	-0.12	4.77	0.42	0.54	Eif2b2	eukaryotic translation initiation factor 2B, subunit 2 beta [Source:MGI Symbol;Acc:MGI:2145118]
ENSMUSG00000028683	-0.05	4.41	0.67	0.76	Eif2b3	eukaryotic translation initiation factor 2B, subunit 3 [Source:MGI Symbol;Acc:MGI:1313286]
ENSMUSG00000029145	0.01	5.39	0.95	0.97	Eif2b4	eukaryotic translation initiation factor 2B, subunit 4 delta [Source:MGI Symbol;Acc:MGI:95300]
ENSMUSG00000003235	-0.23	6.63	0.02	0.05	Eif2b5	eukaryotic translation initiation factor 2B, subunit 5 epsilon [Source:MGI Symbol;Acc:MGI:244617
ENSMUSG00000026427	-0.25	5.19	0.00	0.01	Eif2d	eukaryotic translation initiation factor 2D [Source:MGI Symbol;Acc:MGI:109342]
ENSMUSG00000021116	0.05	6.12	0.50	0.61	Eif2s1	eukaryotic translation initiation factor 2, subunit 1 alpha [Source:MGI Symbol;Acc:MGI:95299]
ENSMUSG00000074656	-0.49	7.26	0.00	0.00	Eif2s2	eukaryotic translation initiation factor 2, subunit 2 (beta) [Source:MGI Symbol;Acc:MGI:1914454]
ENSMUSG00000035150	0.16	6.21	0.36	0.47	Eif2s3x	eukaryotic translation initiation factor 2, subunit 3, structural gene X-linked [Source:MGI Symbol;
ENSMUSG00000069049	-0.89	5.39	0.00	0.00	Eif2s3y	eukaryotic translation initiation factor 2, subunit 3, structural gene Y-linked [Source:MGI Symbol;
ENSMUSG00000024991	0.10	8.34	0.29	0.40	Eif3a	eukaryotic translation initiation factor 3, subunit A [Source:MGI Symbol;Acc:MGI:95301]
ENSMUSG00000056076	-0.09	7.31	0.44	0.56	Eif3b	eukaryotic translation initiation factor 3, subunit B [Source:MGI Symbol;Acc:MGI:106478]
ENSMUSG00000030738	-0.35	8.41	0.00	0.00	Eif3c	eukaryotic translation initiation factor 3, subunit C [Source:MGI Symbol;Acc:MGI:1926966]
ENSMUSG00000016554	-0.56	6.91	0.00	0.00	Eif3d	eukaryotic translation initiation factor 3, subunit D [Source:MGI Symbol;Acc:MGI:1933181]
ENSMUSG00000022336	-0.01	6.89	0.93	0.95	Eif3e	eukaryotic translation initiation factor 3, subunit E [Source:MGI Symbol;Acc:MGI:99257]
ENSMUSG00000031029	-0.13	7.15	0.47	0.58	Eif3f	eukaryotic translation initiation factor 3, subunit F [Source:MGI Symbol;Acc:MGI:1913335]
ENSMUSG00000070319	-0.18	5.84	0.19	0.28	Eif3g	eukaryotic translation initiation factor 3, subunit G [Source:MGI Symbol;Acc:MGI:1858258]
ENSMUSG00000022312	-0.07	7.14	0.62	0.71	Eif3h	eukaryotic translation initiation factor 3, subunit H [Source:MGI Symbol;Acc:MGI:1915385]
ENSMUSG00000028798	-0.24	6.63	0.04	0.08	Eif3i	eukaryotic translation initiation factor 3, subunit I [Source:MGI Symbol;Acc:MGI:1860763]
ENSMUSG00000027236	0.12	4.40	0.23	0.33	Eif3j1	eukaryotic translation initiation factor 3, subunit J1 [Source:MGI Symbol;Acc:MGI:1925905]
ENSMUSG00000043424	-0.10	4.26	0.47	0.58	Eif3j2	eukaryotic translation initiation factor 3, subunit J2 [Source:MGI Symbol;Acc:MGI:3704486]
ENSMUSG00000053565	0.02	6.22	0.92	0.95	Eif3k	eukaryotic translation initiation factor 3, subunit K [Source:MGI Symbol;Acc:MGI:1921080]
ENSMUSG00000033047	0.06	6.77	0.43	0.55	Eif3l	eukaryotic translation initiation factor 3, subunit L [Source:MGI Symbol;Acc:MGI:2386251]
ENSMUSG00000027170	0.01	6.47	0.93	0.95	Eif3m	eukaryotic translation initiation factor 3, subunit M [Source:MGI Symbol;Acc:MGI:1351744]
ENSMUSG00000059796	-0.23	9.21	0.02	0.05	Eif4a1	eukaryotic translation initiation factor 4A1 [Source:MGI Symbol;Acc:MGI:95303]
ENSMUSG00000022884	0.35	9.54	0.00	0.00	Eif4a2	eukaryotic translation initiation factor 4A2 [Source:MGI Symbol;Acc:MGI:106906]
ENSMUSG00000025580	-0.03	5.86	0.83	0.88	Eif4a3	eukaryotic translation initiation factor 4A3 [Source:MGI Symbol;Acc:MGI:1923731]
ENSMUSG00000058655	0.28	8.23	0.00	0.00	Eif4b	eukaryotic translation initiation factor 4B [Source:MGI Symbol;Acc:MGI:95304]
ENSMUSG00000028156	-0.09	7.00	0.24	0.35	Eif4e	eukaryotic translation initiation factor 4E [Source:MGI Symbol;Acc:MGI:95305]
ENSMUSG00000026254	0.12	6.62	0.13	0.20	Eif4e2	eukaryotic translation initiation factor 4E member 2 [Source:MGI Symbol;Acc:MGI:1914440]
ENSMUSG00000093661	0.10	3.52	0.48	0.59	Eif4e3	eukaryotic translation initiation factor 4E member 3 [Source:MGI Symbol;Acc:MGI:1914142]
ENSMUSG00000031490	-2.16	3.15	0.00	0.00	Eif4ebp1	eukaryotic translation initiation factor 4E binding protein 1 [Source:MGI Symbol;Acc:MGI:103267]
ENSMUSG00000020091	-0.08	6.91	0.29	0.39	Eif4ebp2	eukaryotic translation initiation factor 4E binding protein 2 [Source:MGI Symbol;Acc:MGI:109198]
ENSMUSG00000020454	-0.02	6.08	0.85	0.90	Eif4enif1	eukaryotic translation initiation factor 4E nuclear import factor 1 [Source:MGI Symbol;Acc:MGI:19
ENSMUSG00000045983	0.08	8.77	0.38	0.49	Eif4g1	eukaryotic translation initiation factor 4, gamma 1 [Source:MGI Symbol;Acc:MGI:2384784]
ENSMUSG00000005610	0.22	10.58	0.01	0.03	Eif4g2	eukaryotic translation initiation factor 4, gamma 2 [Source:MGI Symbol;Acc:MGI:109207]
ENSMUSG00000028760	-0.22	8.12	0.08	0.14	Eif4g3	eukaryotic translation initiation factor 4 gamma, 3 [Source:MGI Symbol;Acc:MGI:1923935]
ENSMUSG00000040731	0.19	8.45	0.03	0.06	Eif4h	eukaryotic translation initiation factor 4H [Source:MGI Symbol;Acc:MGI:1341822]
ENSMUSG00000021282	0.03	7.98	0.74	0.81	Eif5	eukaryotic translation initiation factor 5 [Source:MGI Symbol;Acc:MGI:95309]
ENSMUSG00000078812	-0.11	8.37	0.46	0.57	Eif5a	eukaryotic translation initiation factor 5A [Source:MGI Symbol;Acc:MGI:106248]
ENSMUSG00000050192	0.48	4.60	0.01	0.01	Eif5a2	eukaryotic translation initiation factor 5A2 [Source:MGI Symbol;Acc:MGI:1933735]
ENSMUSG00000026083	-0.05	6.50	0.63	0.72	Eif5b	eukaryotic translation initiation factor 5B [Source:MGI Symbol;Acc:MGI:2441772]
ENSMUSG00000027613	-0.01	5.38	0.93	0.95	Eif6	eukaryotic translation initiation factor 6 [Source:MGI Symbol;Acc:MGI:1196288]
ENSMUSG00000037742	0.07	12.24	0.37	0.49	Eef1a1	eukaryotic translation elongation factor 1 alpha 1 [Source:MGI Symbol;Acc:MGI:1096881]
ENSMUSG00000016349	1.08	9.06	0.00	0.00	Eef1a2	eukaryotic translation elongation factor 1 alpha 2 [Source:MGI Symbol;Acc:MGI:1096317]
ENSMUSG00000025967	0.46	7.98	0.00	0.01	Eef1b2	eukaryotic translation elongation factor 1 beta 2 [Source:MGI Symbol;Acc:MGI:1929520]
ENSMUSG00000055762	0.01	6.21	0.97	0.98	Eef1d	eukaryotic translation elongation factor 1 delta (guanine nucleotide exchange protein) [Source:M
ENSMUSG00000001707	-0.08	5.67	0.38	0.50	Eef1e1	eukaryotic translation elongation factor 1 epsilon 1 [Source:MGI Symbol;Acc:MGI:1913393]
ENSMUSG00000071644	0.16	8.29	0.25	0.35	Eef1g	eukaryotic translation elongation factor 1 gamma [Source:MGI Symbol;Acc:MGI:1914410]
ENSMUSG00000034994	0.21	10.76	0.01	0.03	Eef2	eukaryotic translation elongation factor 2 [Source:MGI Symbol;Acc:MGI:95288]
ENSMUSG00000035064	0.19	6.25	0.03	0.05	Eef2k	eukaryotic elongation factor-2 kinase [Source:MGI Symbol;Acc:MGI:1195261]
ENSMUSG00000033216	0.01	3.93	0.93	0.95	Eefsec	eukaryotic elongation factor, selenocysteine-tRNA-specific [Source:MGI Symbol;Acc:MGI:2137092]

continue…

Locus	log2FC	logCPM	P-value	FDR	Gene Name	Description
ENSMUSG00000022283	0.35	8.38	0.00	0.00	Pabpc1	poly(A) binding protein, cytoplasmic 1 [Source:MGI Symbol;Acc:MGI:1349722]
ENSMUSG00000011257	0.40	5.99	0.00	0.00	Pabpc4	poly(A) binding protein, cytoplasmic 4 [Source:MGI Symbol;Acc:MGI:2385206]
ENSMUSG00000034732	0.87	1.94	0.28	0.38	Pabpc5	poly(A) binding protein, cytoplasmic 5 [Source:MGI Symbol;Acc:MGI:2136401]
ENSMUSG00000022194	0.00	4.95	0.98	0.99	Pabpn1	poly(A) binding protein, nuclear 1 [Source:MGI Symbol;Acc:MGI:1859158]
ENSMUSG00000031960	-0.55	8.62	0.00	0.00	Aars	alanyl-tRNA synthetase [Source:MGI Symbol;Acc:MGI:2384560]
ENSMUSG00000023938	0.06	4.16	0.72	0.80	Aars2	alanyl-tRNA synthetase 2, mitochondrial [Source:MGI Symbol;Acc:MGI:2681839]
ENSMUSG00000010755	-0.79	7.36	0.00	0.00	Cars	cysteinyl-tRNA synthetase [Source:MGI Symbol;Acc:MGI:1351477]
ENSMUSG00000056228	-0.22	4.72	0.02	0.04	Cars2	cysteinyl-tRNA synthetase 2 (mitochondrial)(putative) [Source:MGI Symbol;Acc:MGI:1919191]
ENSMUSG00000026356	0.20	6.16	0.01	0.03	Dars	aspartyl-tRNA synthetase [Source:MGI Symbol;Acc:MGI:2442544]
ENSMUSG00000026709	-0.22	4.59	0.01	0.02	Dars2	aspartyl-tRNA synthetase 2 (mitochondrial) [Source:MGI Symbol;Acc:MGI:2442510]
ENSMUSG00000021420	0.04	3.38	0.76	0.83	Fars2	phenylalanine-tRNA synthetase 2 (mitochondrial) [Source:MGI Symbol;Acc:MGI:1917205]
ENSMUSG00000003808	-0.24	6.12	0.05	0.09	Farsa	phenylalanyl-tRNA synthetase, alpha subunit [Source:MGI Symbol;Acc:MGI:1913840]
ENSMUSG00000026245	-0.19	6.60	0.03	0.07	Farsb	phenylalanyl-tRNA synthetase, beta subunit [Source:MGI Symbol;Acc:MGI:1346035]
ENSMUSG00000029777	-0.62	8.29	0.00	0.00	Gars	glycyl-tRNA synthetase [Source:MGI Symbol;Acc:MGI:2449057]
ENSMUSG00000001380	-0.36	7.07	0.00	0.00	Hars	histidyl-tRNA synthetase [Source:MGI Symbol;Acc:MGI:108087]
ENSMUSG00000019143	-0.17	5.21	0.19	0.28	Hars2	histidyl-tRNA synthetase 2 [Source:MGI Symbol;Acc:MGI:1918041]
ENSMUSG00000037851	-0.67	7.37	0.00	0.00	Iars	isoleucine-tRNA synthetase [Source:MGI Symbol;Acc:MGI:2145219]
ENSMUSG00000026618	-0.37	5.80	0.00	0.00	Iars2	isoleucine-tRNA synthetase 2, mitochondrial [Source:MGI Symbol;Acc:MGI:1919586]
ENSMUSG00000031948	-0.03	6.69	0.82	0.88	Kars	lysyl-tRNA synthetase [Source:MGI Symbol;Acc:MGI:1934754]
ENSMUSG00000024493	-0.71	7.52	0.00	0.00	Lars	leucyl-tRNA synthetase [Source:MGI Symbol;Acc:MGI:1913808]
ENSMUSG00000035202	0.57	9.09	0.03	0.06	Lars2	leucyl-tRNA synthetase, mitochondrial [Source:MGI Symbol;Acc:MGI:2142973]
ENSMUSG00000007029	-0.29	6.24	0.00	0.00	Vars	valyl-tRNA synthetase [Source:MGI Symbol;Acc:MGI:90675]
ENSMUSG00000038838	-0.06	4.64	0.51	0.62	Vars2	valyl-tRNA synthetase 2, mitochondrial [Source:MGI Symbol;Acc:MGI:1916165]
ENSMUSG00000028029	-0.17	5.45	0.30	0.40	Aimp1	aminoacyl tRNA synthetase complex-interacting multifunctional protein 1 [Source:MGI Symbol;Acc:MGI:102774]
ENSMUSG00000029610	-0.25	5.22	0.06	0.11	Aimp2	aminoacyl tRNA synthetase complex-interacting multifunctional protein 2 [Source:MGI Symbol;Acc:MGI:2385237]
ENSMUSG00000028580	0.01	6.96	0.94	0.96	Pum1	pumilio RNA-binding family member 1 [Source:MGI Symbol;Acc:MGI:1931749]
ENSMUSG00000020594	0.27	7.75	0.08	0.14	Pum2	pumilio RNA-binding family member 2 [Source:MGI Symbol;Acc:MGI:1931751]
ENSMUSG00000041360	-0.34	6.55	0.00	0.00	Pum3	pumilio RNA-binding family member 3 [Source:MGI Symbol;Acc:MGI:106253]
ENSMUSG00000037331	0.01	7.35	0.94	0.96	Larp1	La ribonucleoprotein domain family, member 1 [Source:MGI Symbol;Acc:MGI:1890165]
ENSMUSG00000025762	-0.87	4.13	0.00	0.00	Larp1b	La ribonucleoprotein domain family, member 1B [Source:MGI Symbol;Acc:MGI:1914604]
ENSMUSG00000023025	0.37	5.96	0.05	0.09	Larp4	La ribonucleoprotein domain family, member 4 [Source:MGI Symbol;Acc:MGI:2443114]
ENSMUSG00000033499	-0.04	6.80	0.71	0.79	Larp4b	La ribonucleoprotein domain family, member 4B [Source:MGI Symbol;Acc:MGI:106330]
ENSMUSG00000034839	0.63	4.97	0.00	0.00	Larp6	La ribonucleoprotein domain family, member 6 [Source:MGI Symbol;Acc:MGI:1914807]
ENSMUSG00000027968	0.05	4.36	0.68	0.76	Larp7	La ribonucleoprotein domain family, member 7 [Source:MGI Symbol;Acc:MGI:107634]
ENSMUSG00000042426	-0.02	5.42	0.81	0.87	Dhx29	DEAH (Asp-Glu-Ala-His) box polypeptide 29 [Source:MGI Symbol;Acc:MGI:2145374]

Table S2

Gene Ontology analysis by http://geneontology.org

logFC(trapRNAseq)-logFC(totRNAseq) > 0.5

GO biological process complete	expected	Fold Enric	raw P valu	FDR
modulation of chemical synaptic transmission	42.6	1.76	2.79E-06	1.24E-02
regulation of trans-synaptic signaling	42.71	1.76	3.07E-06	1.02E-02
regulation of plasma membrane bounded cell projection organization	58.75	1.58	1.29E-05	2.15E-02
regulation of cell projection organization	59.68	1.58	1.41E-05	1.87E-02
regulation of transport	120.42	1.39	1.13E-05	2.14E-02
response to organic substance	140.08	1.32	5.69E-05	4.73E-02
regulation of localization	183.02	1.3	1.07E-05	2.37E-02
signaling	217.66	1.3	1.56E-06	2.08E-02
response to chemical	190.04	1.29	1.39E-05	2.05E-02
cell communication	226.2	1.29	1.79E-06	1.19E-02
cellular response to stimulus	310.81	1.19	4.69E-05	4.16E-02
response to stimulus	377.51	1.19	3.82E-06	1.02E-02
multicellular organismal process	353.64	1.18	2.72E-05	2.78E-02
regulation of cellular process	644.33	1.11	2.56E-05	2.84E-02
regulation of biological process	668.67	1.1	1.41E-05	1.70E-02
biological regulation	700.03	1.09	3.50E-05	3.33E-02

GO molecular function complete	expected	Fold Enric	raw P valu	FDR
gated channel activity	18.96	2.22	2.69E-06	9.98E-03

GO cellular component complete	expected	Fold Enric	raw P valu	FDR
parallel fiber to Purkinje cell synapse	2.81	3.56	6.62E-04	2.87E-02
terminal bouton	6.32	3.01	3.27E-05	3.06E-03
excitatory synapse	7.26	2.76	6.69E-05	5.41E-03
potassium channel complex	6.67	2.4	1.45E-03	4.69E-02
intrinsic component of presynaptic membrane	10.65	2.35	1.12E-04	8.34E-03
axon terminus	14.51	2.34	7.58E-06	1.13E-03
clathrin-coated vesicle	7.72	2.33	1.04E-03	3.79E-02
neuron projection terminus	16.27	2.27	5.87E-06	1.05E-03
integral component of presynaptic membrane	9.24	2.27	5.79E-04	2.65E-02
intrinsic component of synaptic membrane	21.53	2.04	1.14E-05	1.45E-03
leading edge membrane	11.82	2.03	1.13E-03	3.96E-02
integral component of synaptic membrane	19.31	2.02	4.49E-05	4.00E-03
transport vesicle membrane	13.93	1.94	1.13E-03	4.01E-02
presynaptic membrane	16.73	1.91	5.23E-04	2.59E-02
ion channel complex	20.24	1.88	2.37E-04	1.51E-02
exocytic vesicle	23.05	1.87	1.09E-04	8.47E-03
cation channel complex	15.56	1.86	1.36E-03	4.58E-02
transmembrane transporter complex	21.18	1.84	2.87E-04	1.55E-02
presynapse	50.44	1.82	4.33E-08	7.71E-05
distal axon	31.83	1.76	5.15E-05	4.37E-03
cytoplasmic vesicle membrane	25.63	1.76	2.83E-04	1.62E-02
synaptic vesicle	21.77	1.75	8.97E-04	3.55E-02
transporter complex	22.35	1.74	7.81E-04	3.16E-02
vesicle membrane	27.15	1.73	2.85E-04	1.58E-02
transport vesicle	29.37	1.7	2.71E-04	1.66E-02
glutamatergic synapse	49.27	1.66	7.57E-06	1.23E-03
synaptic membrane	40.26	1.61	1.53E-04	1.09E-02
secretory vesicle	37.21	1.61	2.82E-04	1.67E-02
postsynaptic membrane	28.55	1.61	1.40E-03	4.62E-02
plasma membrane protein complex	30.43	1.61	1.00E-03	3.81E-02
neuronal cell body	55.7	1.6	1.42E-05	1.59E-03
cell surface	36.04	1.55	1.03E-03	3.82E-02
cell body	62.84	1.54	2.21E-05	2.32E-03
plasma membrane region	81.45	1.51	4.66E-06	9.22E-04
intrinsic component of plasma membrane	74.19	1.48	3.25E-05	3.22E-03
somatodendritic compartment	84.96	1.47	1.29E-05	1.53E-03
axon	58.04	1.46	3.80E-04	1.99E-02
neuron projection	118.08	1.45	6.92E-07	3.08E-04
dendrite	63.08	1.43	5.79E-04	2.71E-02
dendritic tree	63.31	1.42	6.47E-04	2.88E-02
synapse	126.15	1.4	2.96E-06	7.53E-04
integral component of plasma membrane	69.63	1.39	7.67E-04	3.18E-02
cell junction	159.85	1.38	5.54E-07	3.29E-04
extracellular region	72.67	1.36	1.36E-03	4.66E-02
plasma membrane bounded cell projection	162.9	1.34	3.05E-06	6.79E-04
cell projection	179.63	1.34	1.39E-06	4.13E-04
bounding membrane of organelle	90.46	1.32	1.54E-03	4.90E-02
intracellular vesicle	134.81	1.28	5.59E-04	2.69E-02
cell periphery	286.94	1.28	8.51E-08	7.58E-05
cytoplasmic vesicle	134.46	1.27	6.72E-04	2.85E-02
plasma membrane	266.93	1.27	7.47E-07	2.66E-04
vesicle	141.01	1.26	9.66E-04	3.74E-02
endomembrane system	284.01	1.19	2.04E-04	1.40E-02
intrinsic component of membrane	272.43	1.18	5.10E-04	2.59E-02
membrane	500.04	1.15	7.90E-06	1.08E-03
mitochondrial protein-containing complex	26.33	0.38	2.24E-04	1.48E-02

logFC(trapRNAseq)-logFC(totRNAseq) < -0.5

GO biological process complete

No statistically significant results

GO molecular function complete

No statistically significant results

GO cellular component complete	expected	Fold Enric	raw P valu	FDR
postsynaptic membrane	37.21	1.67	1.01E-04	1.80E-02
synaptic membrane	52.46	1.53	1.85E-04	2.35E-02
postsynaptic specialization	53.98	1.5	2.75E-04	3.27E-02
asymmetric synapse	50.78	1.5	4.51E-04	4.73E-02
integral component of plasma membrane	90.73	1.44	2.31E-05	1.03E-02
postsynapse	88.29	1.43	5.46E-05	1.62E-02
dendritic tree	82.5	1.42	1.29E-04	1.91E-02
intrinsic component of plasma membrane	96.68	1.42	3.53E-05	1.26E-02
dendrite	82.19	1.41	1.65E-04	2.27E-02
somatodendritic compartment	110.71	1.41	1.31E-05	7.80E-03
neuron projection	153.86	1.3	8.96E-05	1.77E-02
synapse	164.38	1.27	2.76E-04	3.07E-02
plasma membrane	347.83	1.25	1.09E-07	9.71E-05
cell periphery	373.91	1.24	5.91E-08	1.05E-04
intrinsic component of membrane	355	1.18	7.26E-05	1.62E-02
integral component of membrane	342.49	1.18	1.10E-04	1.79E-02
membrane	651.59	1.11	7.01E-05	1.79E-02

Table S3

Details about sequences cloned in lentiviral vectors.

- "SrfI_Foxg1(cds-3'term)-EGFP_ApaI" fragment

> SrfI_mmuFoxg1-cds (nt1282-to-endSTOP-less)

GGGCCGCGTCCTCCTCTACGTCGCCGCAGGCCCCCTCGACCCTGCCCTGTGAGTCTTTAAGAC
CCTCTTTGCCAAGTTTTACGACAGGACTGTCCGGGGGACTGTCTGATTATTTCACACATCAAA
ATCAGGGGTCTTCTTCCAACCCTTTAATACAT

>5xGS-repeats

CTCGAGGGCTCCGGAAGCGGGTCTGGAAGCGGCTCCCTCGAG

> EGFP-2xSTOP_ApaI

ATGGTGAGCAAGGGCGAGGAGCTGTTCACCGGGGTGGTGCCCATCCTGGTCGAGCTGGACGGC
GACGTAAACGGCCACAAGTTCAGCGTGTCCGGCGAGGGCGAGGGCGATGCCACCTACGGCAAG
CTGACCCTGAAGTTCATCTGCACCACCGGCAAGCTGCCCGTGCCCTGGCCCACCCTCGTGACC
ACCCTGACCTACGGCGTGCAGTGCTTCAGCCGCTACCCCGACCACATGAAGCAGCACGACTTC
TTCAAGTCCGCCATGCCCGAAGGCTACGTCCAGGAGCGCACCATCTTCTTCAAGGACGACGGC
AACTACAAGACCCGCGCCGAGGTGAAGTTCGAGGGCGACACCCTGGTGAACCGCATCGAGCTG
AAGGGCATCGACTTCAAGGAGGACGGCAACATCCTGGGGCACAAGCTGGAGTACAACTACAAC
AGCCACAACGTCTATATCATGGCCGACAAGCAGAAGAACGGCATCAAGGTGAACTTCAAGATC
CGCCACAACATCGAGGACGGCAGCGTGCAGCTCGCCGACCACTACCAGCAGAACACCCCCATC
GGCGACGGCCCCGTGCTGCTGCCCGACAACCACTACCTGAGCACCCAGTCCGCCCTGAGCAAA
GACCCCAACGAGAAGCGCGATCACATGGTCCTGCTGGAGTTCGTGACCGCCGCCGGGATCACT
CTCGGCATGGACGAGCTGTACAAGTAAGTCGACGGATCCTAAGGGCC

- "Flag-rnoGrin1-203-HA" fragment

>SalI(XhoI-comp)_ rnoGrin1-203-5'utr

TCGACCGCGCACTCGACTCAGCGTCAGGAAGCGGGGGCGGTGGGAGGGGTAGAACGCGTAGGT
CCCGCTCATGACTCCGCAGCTGCTGCAGTCGCCGCAGCATCGGGACCAGTCGCGCAGTCCGCG
CTGCTGTCCTTTCCGCCTTTTCCGCGCGGGTGTTCGAGCAGCGCCAAACACGCTTCAGCACCT
CGGACAGCATCCGCCGCGCTCGCCCGGGGCTCCTAGAGAACCCGGGGGCGCTTGACCGCGCGC
GGGCGGCCCGCGGGTCGTACATCGCGAGGTCGTCGCACTCGCGCAACCCAGAGCCAGGCCCGC
TGTGCCCGGAGCTC

> rnoGrin1-203-cds(signal-peptide)

ATGAGCACCATGCACCTGCTGACATTCGCCCTGCTTTTTTCCTGCTCCTTCGCCCGC

>3xFlag

GATTACAAGGACCACGACGGAGACTACAAAGATCATGATATCGATTATAAGGACGATGACGAT
AAG

> rnoGrin1-203-cds(aa20-end)

GCCGCCTGCGACCCCAAGATCGTCAACATCGGCGCGGTGCTGAGCACGCGCAAGCATGAACAG
ATGTTCCGCGAGGCAGTAAACCAGGCCAATAAGCGACACGGCTCTTGGAAGATACAGCTCAAC
GCCACTTCTGTCACCCACAAGCCCAACGCCATACAGATGGCCCTGTCAGTGTGTGAGGACCTC
ATCTCTAGCCAGGTCTACGCTATCCTAGTTAGCCACCCGCCTACTCCCAACGACCACTTCACT
CCCACCCCTGTCTCCTACACAGCTGGCTTCTACAGAATCCCTGTCCTGGGACTGACTACCCGA
ATGTCCATCTACTCTGACAAGAGTATCCACCTGAGTTTCCTTCGCACGGTGCCGCCCTACTCC
CACCAGTCCAGCGTCTGGTTTGAGATGATGCGAGTCTACAACTGGAACCACATCATCCTGCTG
GTCAGCGACGACCACGAGGGACGGGCAGCGCAGAAGCGCTTGGAGACGTTGCTGGAGGAACGG
GAGTCCAAGGCAGAGAAGGTGCTGCAGTTTGACCCAGGAACCAAGAATGTGACGGCTCTGCTG
ATGGAGGCCCGGGAACTGGAGGCCCGGGTCATCATCCTTTCTGCAAGCGAGGACGACGCTGCC
ACAGTGTACCGCGCAGCCGCAATGCTGAACATGACGGGCTCTGGGTACGTGTGGCTGGTCGGG
GAACGCGAGATCTCTGGGAACGCCCTGCGCTACGCTCCTGATGGCATCATCGGACTTCAGCTC
ATCAATGGCAAGAATGAGTCAGCCCACATCAGTGACGCCGTGGGCGTGGTGGCACAGGCAGTT
CACGAACTCCTAGAGAAGGAGAATATCACTGACCCACCGCGGGGTTGCGTGGGCAACACCAAC
ATCTGGAAGACAGGACCATTGTTCAAGAGGGTGCTGATGTCTTCTAAGTATGCGGACGGAGTG
ACTGGCCGTGTGGAATTCAATGAGGATGGGGACCGGAAGTTTGCCAACTATAGTATCATGAAC
CTGCAGAACCGCAAGCTGGTGCAAGTGGGCATCTACAATGGTACCCATGTCATCCCAAATGAC
AGGAAGATCATCTGGCCAGGAGGAGAGACAGAGAAACCTCGAGGATACCAGATGTCCACCAGA
CTAAAGATAGTGACAATCCACCAAGAGCCCTTCGTGTACGTCAAGCCCACAATGAGTGATGGG
ACATGCAAAGAGGAGTTCACAGTCAATGGTGACCCAGTGAAGAAGGTGATCTGTACGGGGCCT
AATGACACGTCCCCAGGCAGCCCACGCCACACAGTGCCCCAGTGCTGCTATGGCTTCTGCATA
GACCTGCTCATCAAGCTGGCGCGGACCATGAATTTTACCTATGAGGTGCACCTGGTGGCAGAT
GGCAAGTTTGGCACACAGGAGCGGGTAAACAACAGCAACAAAAAGGAGTGGAACGGAATGATG
GGCGAGCTACTCAGTGGCCAAGCGGACATGATTGTGGCACCACTGACCATCAACAATGAGCGT
GCGCAGTACATAGAGTTCTCCAAGCCCTTCAAGTACCAGGGCCTGACCATTTTGGTCAAGAAG
GAGATTCCCAGGAGCACACTGGACTCATTTATGCAGCCTTTTCAGAGCACACTGTGGTTGCTA
GTAGGACTGTCAGTTCATGTGGTGGCTGTGATGCTGTACCTGCTGGACCGCTTCAGTCCCTTT
GGCCGATTCAAGGTGAACAGTGAGGAGGAGGAGGAAGATGCACTGACCCTGTCCTCTGCCATG
TGGTTTTCCTGGGGCGTCCTGCTCAACTCCGGCATTGGGGAAGGTGCCCCCCGGAGTTTCTCT
GCACGTATCCTAGGCATGGTGTGGGCTGGTTTCGCCATGATCATAGTGGCTTCCTACACTGCC
AACTTGGCAGCTTTCCTGGTGCTGGATCGGCCTGAGGAGCGCATCACGGGCATCAATGACCCC
AGGCTCAGAAACCCCTCAGACAAGTTCATCTACGCAACTGTAAAGCAGAGCTCCGTGGACATC
TACTTCCGGAGGCAGGTGGAGTTGAGTACCATGTACCGGCACATGGAAAAACACAATTACGAG
AGCGCAGCTGAGGCCATCCAGGCTGTGCGGGACAACAAGCTGCACGCCTTTATCTGGGACTCG
GCCGTGCTGGAGTTTGAGGCTTCACAGAAGTGCGATCTGGTGACCACGGGTGAGCTGTTCTTC
CGCTCAGGCTTTGGCATCGGCATGCGCAAGGACAGCCCCTGGAAGCAGAACGTTTCCCTGTCC
ATACTCAAGTCCCATGAGAATGGCTTCATGGAAGATCTGGATAAGACATGGGTTCGGTATCAG
GAATGCGACTCCCGCAGCAATGCTCCTGCAACCCTCACTTTTGAGAACATGGCAGGGGTCTTC
ATGCTGGTGGCTGGAGGCATCGTAGCTGGGATTTTCCTCATTTTCATTGAGATCGCCTACAAG
CGACACAAGGATGCCCGTAGGAAGCAGATGCAGCTGGCTTTTGCAGCCGTGAACGTGTGGAGG
AAGAACCTGCAGGATAGAAAGAGTGGTAGAGCAGAGCCCGACCCTAAAAAGAAAGCCACATTT

AGGGCTATCACCTCCACCCTGGCCTCCAGCTTCAAGAGACGTAGGTCCTCCAAAGACACGAGC
ACCGGGGGGTGGACGCGGCGCTTTGCAAAACCAAAAAGACACAGTGCTGCCGCGACGCGCTATT
GAGAGGGAGGAGGGCCAGCTGCAGCTGTGTTCCCGTCATAGGGAGAGC

>3xHA-STOP

TACCCGTACGATGTTCCAGATTACGCTGGCTATCCCTATGACGTCCCTGACTACGCAGGATCC
TATCCTTACGACGTGCCGGACTATGCTTGA

> rnoGrin1-203-3'utr(3'D4nt)

GACGCCCCGCCCGCCCTCCTCTGCCCCTCCCCCGCAGACAGACGCACGGGACAGCGGCCTGGC
CCACGCAGAGCCCCGGAGCACGACGGGGTCGGGGGAGGAGCACTCCCAGCCTCCCCCAGGCCG
TGCCCGCCTGCCCACCGGTCGGCCGGCTGGCCGGTCCACCCTGTCCCGGCCCCGCGCGTGCCC
CCGACGTCGGAGCTAACGGGCCGCCTTGTCTGTGTATTTCTATTTTACAGCAGTACCATCCCA
CTGATATCACGGGCCCGCTCAACCTCTCAGATCCCTCGGTCAGCACCGTGGTGTGAGGCCCCC
CGGAGGCGCCCACCTGCCCAGTTAGCCCGGCCAAGGACACTGATGAGTCCTGCTGCTCGGGAA
GGCCTGAGGGAAGCCCACCCGCCCCAGAGACTGCCCACCCTGGGCCTCCCGTCCGCCTGCTCT
GCTGCCTGGCGGGCAGCCCCTGCAGGACCAAGGTGCGGACCAGAGCGGCTGAGGATGGGCCAG
AGCTGAGCCGGCTGGGCAGGGCCACAGGGCGCTCCGGCAGAGGCAGGGCCCTGAGGTCTCTGA
GCAGTGGGGTGAGGGGCCTAAGTGGCCCCGGTCGGAGGAGTCTGGAGCAGAAATGGCAGCCCC
ATCCTTCCTCCAGCCACTACCCCAAGCTACAGTGGGGGCCTATGGCCCCAGCTTGCTAGGTCA
CCCCCGACCCTTCCTCCAGCGCCTGCTCTCTGCAACTTGATTTCCACCTCTCTCCTGCTGCAC
CACCCTCCCACGACATTTCCCCACCCCATTCACTGGGTTGTCTCTGACCTTTCCCAGGGCTAG
CCTTCACTGCCCTAGTGGCAGTGCTTCAGGGGTGCTTTCTGGCTCCCAGACATCTAGGGCTCC
AGACTCCAAGAGGGCTGAGCCTTCTCTTCTGTCCGCAGCCACAATAGGCTTCCTCAGACGCTG
GCTCGTGATGAGTCCCGCACCTTGGGCACCAGGGAGCGCCATCTGCCTCCCAGTCCGGTGTCA
CTCACCCCACTACCTTGTACATGACCAGCTCTCCCAGTGTCCCAGTGTCTGCCCCAGGGACAC
CGGGCGCGCACAGCCACCCCTAATCCCGGTATTCAGTGGTGATGCCTAAAGGAATGTCAGAAA
A

>polyA-synth_XbaI

AAAAAAAAAAAGCGGCCGCAATAAAAGATCTTTATTTTCATTAGATCTGTGTGTTGGTTTTTT
GTGTGT

- "rnoGrin1-203*.full" fragment

> SalI(XhoI-comp)_ polylinker(sx)-rnoGrin1-203-5'utr

TCGACTTCGAACGCGCACTCGACTCAGCGTCAGGAAGCGGGGGCGGTGGGAGGGGTAGAACGC
GTAGGTCCCGCTCATGACTCCGCAGCTGCTGCAGTCGCCGCAGCATCGGGACCAGTCGCGCAG
TCCGCGCTGCTGTCCTTTCCGCCTTTTCCGCGCGGGTGTTCGAGCAGCGCCAAACACGCTTCA
GCACCTCGGACAGCATCCGCCGCGCTCGCCCGGGGCTCCTAGAGAACCCGGGGGCGCTTGACC
GCGCGCGGGCGGCCCGCGGGTCGTACATCGCGAGGTCGTCGCACTCGCGCAACCCAGAGCCAG
GCCCGCTGTGCCCGGAGCTC

> rnoGrin1-203-cds(aa1-30)-STOP

ATGAGCACCATGCACCTGCTGACATTCGCCCTGCTTTTTTCCTGCTCCTTCGCCCGCGCCGCC
TGCGACCCCAAGATCGTCAACATCGGCTGA

>polylinker-rnoGrin1-203-cds(aa31-end)

GTTTAAACTCCGGACTCGAGGCGGTGCTGAGCACGCGCAAGCATGAACAGATGTTCCGCGAGG
CAGTAAACCAGGCCAATAAGCGACACGGCTCTTGGAAGATACAGCTCAACGCCACTTCTGTCA
CCCACAAGCCCAACGCCATACAGATGGCCCTGTCAGTGTGTGAGGACCTCATCTCTAGCCAGG
TCTACGCTATCCTAGTTAGCCACCCGCCTACTCCCAACGACCACTTCACTCCCACCCCTGTCT
CCTACACAGCTGGCTTCTACAGAATCCCTGTCCTGGGACTGACTACCCGAATGTCCATCTACT
CTGACAAGAGTATCCACCTGAGTTTCCTTCGCACGGTGCCGCCCTACTCCCACCAGTCCAGCG
TCTGGTTTGAGATGATGCGAGTCTACAACTGGAACCACATCATCCTGCTGGTCAGCGACGACC
ACGAGGGACGGGCAGCGCAGAAGCGCTTGGAGACGTTGCTGGAGGAACGGGAGTCCAAGGCAG
AGAAGGTGCTGCAGTTTGACCCAGGAACCAAGAATGTGACGGCTCTGCTGATGGAGGCCCGGG
AACTGGAGGCCCGGGTCATCATCCTTTCTGCAAGCGAGGACGACGCTGCCACAGTGTACCGCG
CAGCCGCAATGCTGAACATGACGGGCTCTGGGTACGTGTGGCTGGTCGGGGAACGCGAGATCT
CTGGGAACGCCCTGCGCTACGCTCCTGATGGCATCATCGGACTTCAGCTCATCAATGGCAAGA
ATGAGTCAGCCCACATCAGTGACGCCGTGGGCGTGGTGGCACAGGCAGTTCACGAACTCCTAG
AGAAGGAGAATATCACTGACCCACCGCGGGGTTGCGTGGGCAACACCAACATCTGGAAGACAG
GACCATTGTTCAAGAGGGTGCTGATGTCTTCTAAGTATGCGGACGGAGTGACTGGCCGTGTGG
AATTCAATGAGGATGGGGACCGGAAGTTTGCCAACTATAGTATCATGAACCTGCAGAACCGCA
AGCTGGTGCAAGTGGGCATCTACAATGGTACCCATGTCATCCCAAATGACAGGAAGATCATCT
GGCCAGGAGGAGAGACAGAGAAACCTCGAGGATACCAGATGTCCACCAGACTAAAGATAGTGA
CAATCCACCAAGAGCCCTTCGTGTACGTCAAGCCCACAATGAGTGATGGGACATGCAAAGAGG
AGTTCACAGTCAATGGTGACCCAGTGAAGAAGGTGATCTGTACGGGGCCTAATGACACGTCCC
CAGGCAGCCCACGCCACACAGTGCCCCAGTGCTGCTATGGCTTCTGCATAGACCTGCTCATCA
AGCTGGCGCGGACCATGAATTTTACCTATGAGGTGCACCTGGTGGCAGATGGCAAGTTTGGCA
CACAGGAGCGGGTAAACAACAGCAACAAAAAGGAGTGGAACGGAATGATGGGCGAGCTACTCA
GTGGCCAAGCGGACATGATTGTGGCACCACTGACCATCAACAATGAGCGTGCGCAGTACATAG
AGTTCTCCAAGCCCTTCAAGTACCAGGGCCTGACCATTTTGGTCAAGAAGGAGATTCCCAGGA
GCACACTGGACTCATTTATGCAGCCTTTTCAGAGCACACTGTGGTTGCTAGTAGGACTGTCAG
TTCATGTGGTGGCTGTGATGCTGTACCTGCTGGACCGCTTCAGTCCCTTTGGCCGATTCAAGG
TGAACAGTGAGGAGGAGGAGGAAGATGCACTGACCCTGTCCTCTGCCATGTGGTTTTCCTGGG
GCGTCCTGCTCAACTCCGGCATTGGGGAAGGTGCCCCCCGGAGTTTCTCTGCACGTATCCTAG
GCATGGTGTGGGCTGGTTTCGCCATGATCATAGTGGCTTCCTACACTGCCAACTTGGCAGCTT
TCCTGGTGCTGGATCGGCCTGAGGAGCGCATCACGGGCATCAATGACCCCAGGCTCAGAAACC
CCTCAGACAAGTTCATCTACGCAACTGTAAAGCAGAGCTCCGTGGACATCTACTTCCGGAGGC
AGGTGGAGTTGAGTACCATGTACCGGCACATGGAAAAACACAATTACGAGAGCGCAGCTGAGG
CCATCCAGGCTGTGCGGGACAACAAGCTGCACGCCTTTATCTGGGACTCGGCCGTGCTGGAGT
TTGAGGCTTCACAGAAGTGCGATCTGGTGACCACGGGTGAGCTGTTCTTCCGCTCAGGCTTTG
GCATCGGCATGCGCAAGGACAGCCCCTGGAAGCAGAACGTTTCCCTGTCCATACTCAAGTCCC
ATGAGAATGGCTTCATGGAAGATCTGGATAAGACATGGGTTCGGTATCAGGAATGCGACTCCC
GCAGCAATGCTCCTGCAACCCTCACTTTTGAGAACATGGCAGGGGTCTTCATGCTGGTGGCTG
GAGGCATCGTAGCTGGGATTTTCCTCATTTTCATTGAGATCGCCTACAAGCGACACAAGGATG
CCCGTAGGAAGCAGATGCAGCTGGCTTTTGCAGCCGTGAACGTGTGGAGGAAGAACCTGCAGG
ATAGAAAGAGTGGTAGAGCAGAGCCCGACCCTAAAAAGAAAGCCACATTTAGGGCTATCACCT

CCACCCTGGCCTCCAGCTTCAAGAGACGTAGGTCCTCCAAAGACACGAGCACCGGGGGTGGAC
GCGGCGCTTTGCAAAACCAAAAAGACACAGTGCTGCCGCGACGCGCTATTGAGAGGGAGGAGG
GCCAGCTGCAGCTGTGTTCCCGTCATAGGGAGAGCTGA

> rnoGrin1-203-3'utr(3'D4nt)

GACGCCCCGCCCGCCCTCCTCTGCCCCTCCCCCGCAGACAGACGCACGGGACAGCGGCCTGGC
CCACGCAGAGCCCCGGAGCACGACGGGGTCGGGGGAGGAGCACTCCCAGCCTCCCCCAGGCCG
TGCCCGCCTGCCCACCGGTCGGCCGGCTGGCCGGTCCACCCTGTCCCGGCCCCGCGCGTGCCC
CCGACGTCGGAGCTAACGGGCCGCCTTGTCTGTGTATTTCTATTTTACAGCAGTACCATCCCA
CTGATATCACGGGCCCGCTCAACCTCTCAGATCCCTCGGTCAGCACCGTGGTGTGAGGCCCCC
CGGAGGCGCCCACCTGCCCAGTTAGCCCGGCCAAGGACACTGATGAGTCCTGCTGCTCGGGAA
GGCCTGAGGGAAGCCCACCCGCCCCAGAGACTGCCCACCCTGGGCCTCCCGTCCGCCTGCTCT
GCTGCCTGGCGGGCAGCCCCTGCAGGACCAAGGTGCGGACCAGAGCGGCTGAGGATGGGCCAG
AGCTGAGCCGGCTGGGCAGGGCCACAGGGCGCTCCGGCAGAGGCAGGGCCCTGAGGTCTCTGA
GCAGTGGGGTGAGGGGCCTAAGTGGCCCCGGTCGGAGGAGTCTGGAGCAGAAATGGCAGCCCC
ATCCTTCCTCCAGCCACTACCCCAAGCTACAGTGGGGGCCTATGGCCCCAGCTTGCTAGGTCA
CCCCCGACCCTTCCTCCAGCGCCTGCTCTCTGCAACTTGATTTCCACCTCTCTCCTGCTGCAC
CACCCTCCCACGACATTTCCCCACCCCATTCACTGGGTTGTCTCTGACCTTTCCCAGGGCTAG
CCTTCACTGCCCTAGTGGCAGTGCTTCAGGGGTGCTTTCTGGCTCCCAGACATCTAGGGCTCC
AGACTCCAAGAGGGCTGAGCCTTCTCTTCTGTCCGCAGCCACAATAGGCTTCCTCAGACGCTG
GCTCGTGATGAGTCCCGCACCTTGGGCACCAGGGAGCGCCATCTGCCTCCCAGTCCGGTGTCA
CTCACCCCACTACCTTGTACATGACCAGCTCTCCCAGTGTCCCAGTGTCTGCCCCAGGGACAC
CGGGCGCGCACAGCCACCCCTAATCCCGGTATTCAGTGGTGATGCCTAAAGGAATGTCAGAAA
A

>synthetic-DNA-contruct_XbaI

AAAAAAAAAAAGCGGCCGCGGATCCCCTT

7. BIBLIOGRAPHY

Ahlgren S, Vogt P and Bronner-Fraser M (2003). *Excess FoxG1 causes overgrowth of the neural tube*. J Neurobiol 57, 337-349.

Ainsley JA, Drane L, Jacobs J, Kittelberger KA, and Reijmers LG (2014). *Functionally diverse dendritic mRNAs rapidly associate with ribosomes following a novel experience*. Nat Commun 5, 4510.

Arava Y, Wang Y, Storey JD, Liu CL, Brown PO, and Herschlag D (2003). *Genome-wide analysis of mRNA translation profiles in Saccharomyces cerevisiae*. Proc Natl Acad Sci USA 100, 3889–3894.

Artimagnella O, and Mallamaci A (2020). *RNASeq profiling of Foxg1-GOF neocortical neurons*. (Version v2) Zenodo [Data set].

Aviner R, Geiger T, and Elroy-Stein O (2014). *Genome-wide identification and quantification of protein synthesis in cultured cells and whole tissues by puromycin-associated nascent chain proteomics (PUNCH-P)*. Nat Protoc 9, 751–760.

Baez MV, Cercato MC, and Jerusalinsky DA (2018). *NMDA Receptor Subunits Change after Synaptic Plasticity Induction and Learning and Memory Acquisition*. Neural Plast 2018, 5093048.

Bielle F, Griveau A, Narboux-Nême N, Vigneau S, Sigrist M, Arber S, Wassef M, and Pierani A (2005). *Multiple origins of Cajal-Retzius cells at the borders of the developing pallium*. Nat Neurosci 8, 1002–1012.

Bohn JA, Van Etten JL, Schagat TL, Bowman BM, McEachin RC, Freddolino PL, and Goldstrohm AC (2018). *Identification of diverse target RNAs that are functionally regulated by human Pumilio proteins*. Nucleic Acids Res 46, 362-386

Bourguignon C, Li J, and Papalopulu N (1998). *XBF-1, a winged helix transcription factor with dual activity, has a role in positioning neurogenesis in Xenopus competent ectoderm*. Dev Camb Engl 125, 4889–4900.

Brancaccio M, Pivetta C, Granzotto M, Filippis C, and Mallamaci A (2010). *Emx2 and Foxg1 inhibit gliogenesis and promote neuronogenesis*. Stem Cells 28, 1206–1218.

Bredenkamp N, Seoighe C, and Illing N (2007). *Comparative evolutionary analysis of the FoxG1 transcription factor from diverse vertebrates identifies conserved recognition sites for microRNA regulation*. Dev Genes Evol 217, 227–233.

Brunet I, Di Nardo AA, Sonnier L, Beurdeley M, and Prochiantz A (2007). *The topological role of homeoproteins in the developing central nervous system*. Trends Neurosci 30, 260-267.

Brunet I, Weinl C, Piper M, Trembleau A, Volovitch M, Harris W, Prochiantz, A, and Holt C (2005). *The transcription factor Engrailed-2 guides retinal axons*. Nature 438, 94–98.

Bulstrode H, Johnstone E, Marques-Torrejon MA, Ferguson KM, Bressan RB, Blin C, et al. (2017). *Elevated FOXG1 and SOX2 in glioblastoma enforces neural stem cell identity through transcriptional control of cell cycle and epigenetic regulators*. Genes Dev 31, 757-773.

Cargnin F, Kwon JS, Katzman S, Chen B, Lee JW, and Lee SK (2018). *FOXG1 Orchestrates Neocortical Organization and Cortico-Cortical Connections*. Neuron 100, 1083-1096.

Cercato MC, Vázquez CA, Kornisiuk E, Aguirre AI, Colettis N, Snitcofsky M, Jerusalinsky DA, and Baez MV (2017). *GluN1 and GluN2A NMDA Receptor Subunits Increase in the Hippocampus during Memory Consolidation in the Rat*. Front Behav Neurosci 10, 242.

Chiola S, Do MD, Centrone L, and Mallamaci A (2019). *Foxg1 Overexpression in Neocortical Pyramids Stimulates Dendrite Elongation Via Hes1 and pCreb1 Upregulation*. Cereb Cortex 29, 1006–1019.

Chung HK, Jacobs CL, Huo Y, Yang J, Krumm SA, Plemper RK, et al. (2015). *Tunable and reversible drug control of protein production via a self-excising degron*. Nat Chem Biol 11, 713–720.

Coffer PJ, and Burgering BM (2004). *Forkhead-box transcription factors and their role in the immune system.* Nat Rev Immunol 4, 889-899.

Dali R, Verginelli F, Pramatarova A, Sladek R, and Stifani S (2018). *Characterization of a FOXG1:TLE1 transcriptional network in glioblastoma-initiating cells*. Mol Oncol 12, 775-787.

Danesin C, and Houart C (2012). *A Fox stops the Wnt: implications for forebrain development and diseases*. Curr Opin Genet Dev 22, 323-330.

Dastidar SG, Landrieu PM, and D'Mello SR (2011). *FoxG1 promotes the survival of postmitotic neurons*. J Neurosci 31, 402–413.

Dermit M, Dodel M, and Mardakheh FK (2017). *Methods for monitoring and measurement of protein translation in time and space*. Mol Biosyst 13, 2477-2488.

Diebold B, Delepine C, Nectoux J, Bahi-Buisson N, Parent P, and Bienvenu T (2014). *Somatic mosaicism for a FOXG1 mutation: Diagnostic implication*. Clin Genet 85, 589–591.

Dieterich DC, Hodas JJ, Gouzer G, Shadrin IY, Ngo JT, Triller A, Tirrell DA and Schuman EM (2010). *In situ visualization and dynamics of newly synthesized proteins in rat hippocampal neurons*. Nat Neurosci 13, 897–905.

Dieterich DC, Lee JJ, Link AJ, Graumann J, Tirrell DA, and Schuman EM (2007). *Labelling, detection and identification of newly synthesized proteomes with bioorthogonal non-canonical amino-acid tagging*. Nat Protoc 2, 532–540.

Dörrbaum AR, Alvarez-Castelao B, Nassim-Assir B, Langer JD, and Erin M Schuman (2020). *Proteome dynamics during homeostatic scaling in cultured neurons*. Elife 9, e52939.

Dou C, Lee J, Liu B, Liu F, Massague J, Xuan S, and Lai E (2000). *BF-1 interferes with transforming growth factor beta signaling by associating with Smad partners*. Mol Cell Biol 20, 6201-6211.

Ehlers MD (2003). *Activity level controls postsynaptic composition and signaling via the ubiquitin proteasome system*. Nature Neurosci 6, 231–242.

Falcone C, Santo M, Liuzzi G, Cannizzaro N, Grudina C, Valencic E, Peruzzotti-Jametti L, Pluchino S, and Mallamaci A (2019). *Foxg1 Antagonizes Neocortical Stem Cell Progression to Astrogenesis*. Cereb Cortex 29, 4903-4918.

Florian C, Bahi-Buisson N, and Bienvenu T (2012). *FOXG1-Related Disorders: From Clinical Description to Molecular Genetics*. Mol Syndromol 2, 153-163.

Gioran A, Nicotera P, and Bano D (2014). *Impaired mitochondrial respiration promotes dendritic branching via the AMPK signaling pathway*. Cell Death Dis 5, e1175.

Gorski JA, Talley T, Qiu M, Puelles L, Rubenstein JLR, and Jones KR (2002). *Cortical excitatory neurons and glia, but not GABAergic neurons, are produced in the Emx1-expressing lineage*. J Neurosci 22, 6309–6314.

Grosshans DR, Clayton DA, Coultrap SJ and Browning MD (2002). *LTP leads to rapid surface expression of NMDA but not AMPA receptors in adult rat CA1*. Nature Neurosci 5, 27–33.

Halstead JM, Lionnet T, Wilbertz JH, Wippich F, Ephrussi A, Singer RH, and Chao JA (2015). *Translation. An RNA biosensor for imaging the first round of translation from single cells to living animals*. Science 347, 1367-671.

Hanashima C, Li SC, Shen L, Lai E, and Fishell G (2004). *Foxg1 suppresses early cortical cell fate*. Science 303, 56-59.

Hanashima C, Shen L, Li SC, and Lai E (2002). *Brain factor-1 controls the proliferation and differentiation of neocortical progenitor cells through independent mechanisms*. J Neurosci 22, 6526–6536.

Hardcastle Z, and Papalopulu N (2000). *Distinct effects of XBF-1 in regulating the cell cycle inhibitor p27(XIC1) and imparting a neural fate*. Development 127, 1303-1314.

Hardy RJ, and Friedrich Jr VL (1996). *Oligodendrocyte progenitors are generated throughout the embryonic mouse brain, but differentiate in restricted foci*. Development 122, 2059-69.

Heiman M, Kulicke R, Fenster RJ, Greengard P, and Heintz N (2014). *Cell type-specific mRNA purification by translating ribosome affinity purification (TRAP)*. Nat Protoc 9, 1282-1291.

Hinz FI, Dieterich DC, Tirrell DA, and Schuman EM (2012). *Non-canonical amino acid labeling in vivo to visualize and affinity purify newly synthesized proteins in larval zebrafish*. ACS Chem Neurosci 3, 40-49.

Hou P, Ó hAilín D, Tanja Vogel T, and Hanashima C (2020). *Transcription and Beyond: Delineating FOXG1 Function in Cortical Development and Disorders*. Front Cell Neurosci 14:35.

Ingolia NT, Ghaemmaghami S, Newman JR, and Weissman JS (2009). *Genome-wide analysis in vivo of translation with nucleotide resolution using ribosome profiling*. Science 324, 218–223.

Iwasaki S, and Ingolia NT (2017). *The Growing Toolbox for Protein Synthesis Studies*. Trends Biochem Sci 42, 612-624.

Jackson RJ, Hellen CUT, and Pestova TV (2010). *The mechanism of eukaryotic translation initiation and principles of its regulation*. Nat Rev Mol Cell Biol 11, 113-27.

Karakas E, and Furukawa H (2014). *Crystal structure of a heterotetrameric NMDA receptor ion channel*. Science 344, 992-7.

Kessaris N, Fogarty M, Iannarelli P, Grist M, Wegner M, and Richardson WD (2006). *Competing waves of oligodendrocytes in the forebrain and postnatal elimination of an embryonic lineage*. Nat Neurosci 9, 173–179.

Kriegstein A, and Alvarez-Buylla A (2009). *The glial nature of embryonic and adult neural stem cells*. Annu Rev Neurosci 32, 149-84.

Kubelka J, Hofrichter J, and Eaton WA (2004). *The protein folding 'speed limit'*. Curr Opin Struct Biol 14, 76-88.

Kumamoto T, and Hanashima C (2017). *Evolutionary conservation and conversion of Foxg1 function in brain development*. Dev Growth Differ 59, 258-269.

Lau CG, and Zukin RS (2007). *NMDA receptor trafficking in synaptic plasticity and neuropsychiatric disorders*. Nat Rev Neurosci 8, 413-26.

Letinic K, Zoncu R, and Rakic P (2002). *Origin of GABAegic neurons in the human neocortex*. Nature 417, 645–649.

Li W, Cogswell C, and LoTurco J (1998). *Neuronal differentiation of precursors in the neocortical ventricular zone is triggered by BMP*. J Neurosci 18, 8853–8862.

Li X, Wang W, Wang J, Malovannaya A, Xi Y, Li W, Guerra R, Hawke DH, Qin J, and Chen J (2015). *Proteomic analyses reveal distinct chromatin-associated and soluble transcription factor complexes*. Mol Syst Biol 11:775.

Mabie P, Mehler M, and Kessler J (1999). *Multiple roles of bone morphogenetic protein signaling in the regulation of cortical cell number and phenotype*. J Neurosci 19, 7077–7088.

Mariani J, Coppola G, Zhang P, Abyzov A, Provini L, Tomasini L, Amenduni M, Szekely A, Palejev D, Wilson M, Gerstein M, Grigorenko EL, Chawarska K, Pelphrey KA, Howe JR, and Vaccarino FM (2015). *FOXG1-Dependent Dysregulation of GABA/Glutamate Neuron Differentiation in Autism Spectrum Disorders*. Cell 162, 375–390.

Martynoga B, Morrison H, Price DJ, and Mason JO (2005). *Foxg1 is required for specification of ventral telencephalon and region-specific regulation of dorsal telencephalic precursor proliferation and apoptosis*. Dev Biol 283, 113–127.

Mattson MP, Gleichmann M, and Cheng A (2008). *Mitochondria in neuroplasticity and neurological disorders*. Neuron 60, 748–766.

Mitter D, Pringsheim M, Kaulisch M, Plumacher KS, Schroder S, Warthemann R, Abou Jamra R, Baethmann M, Bast T, Buttel HM, et al. (2017). *FOXG1 syndrome: Genotype-phenotype association in 83 patients with FOXG1 variants*. Genet Med 20, 98-108.

Miyoshi G, and Fishell G (2012). *Dynamic FoxG1 expression coordinates the integration of multipolar pyramidal neuron precursors into the cortical plate*. Neuron 74, 1045–1058.

Molyneaux BJ, Arlotta P, Menezes JRL, and Macklis JD (2007). *Neuronal subtype specification in the cerebral cortex*. Nat Rev Neurosci 8, 427–437.

Morishita W, Marie H, and Malenka RC (2005). *Distinct triggering and expression mechanisms underlie LTD of AMPA and NMDA synaptic responses*. Nature Neurosci 8, 1043–1050.

Mu Y, Otsuka T, Horton AC, Scott DB, and Ehlers MD (2003). *Activity-dependent mRNA splicing controls ER export and synaptic delivery of NMDA receptors*. Neuron 40, 581–594.

Muzio L, and Mallamaci A (2005). *Foxg1 confines Cajal-Retzius neuronogenesis and hippocampal morphogenesis to the dorsomedial pallium*. J Neurosci 25, 4435–4441.

Nédélec S, Foucher I, Brunet I, Bouillot C, Prochiantz A, and Trembleau A (2004). *Emx2 homeodomain transcription factor interacts with eukaryotic translation initiation factor 4E (eIF4E) in the axons of olfactory sensory neurons*. Proc Natl Acad Sci USA 101, 10815-10820.

Niessing D, Blanke S, and Jäckle H (2002). *Bicoid associates with the 5'-cap-bound complex of caudal mRNA and represses translation*. Genes Dev 16, 2576-82.

Ong S, Blagoev B, Kratchmarova I, Kristensen DB, Steen H, Pandey A, and Mann M (2002). *Stable isotope labeling by amino acids in cell culture, SILAC, as a simple and accurate approach to expression proteomics*. Mol Cell Proteomics 1, 376-86.

Pancrazi L, Di Benedetto G, Colombaioni L, Della Sala G, Testa G, Olimpico F, Reyes A, Zeviani M, Pozzan T, and Costa M (2015). *Foxg1 localizes to mitochondria and coordinates cell differentiation and bioenergetics*. Proc Natl Acad Sci USA 112, 13910-13915.

Paoletti P, Bellone C, and Zhou Q (2013). *NMDA receptor subunit diversity: impact on receptor properties, synaptic plasticity and disease*. Nat Rev Neurosci 14, 383-400.

Patriarchi T, Amabile S, Frullanti E, Landucci E, Lo Rizzo C, Ariani F, Costa M, Olimpico F, W Hell J, M Vaccarino F, Renieri A, and Meloni I (2016). *Imbalance of excitatory/inhibitory synaptic protein expression in iPSC-derived neurons from FOXG1(+/-) patients and in foxg1(+/-) mice*. Eur J Hum Genet 24, 871–880.

Pelletier J, and Sonenberg N (2019). *The Organizing Principles of Eukaryotic Ribosome Recruitment*. Annu Rev Biochem 88, 307-335.

Prybylowski KL, Grossman SD, Wrathall JR, and Wolfe BB (2001). *Expression of splice variants of the NR1 subunit of the N-methyl-D-aspartate receptor in the normal and injured rat spinal cord*. J Neurochem 76, 797-805

Raciti M, Granzotto M, Duc MD, Fimiani C, Cellot G, Cherubini E, and Mallamaci A (2013). *Reprogramming fibroblasts to neural-precursor-like cells by structured overexpression of pallial patterning genes*. Mol Cell Neurosci 57, 42–53.

Rakic P (2006). *A century of progress in corticoneurogenesis: from silver impregnation to genetic engineering*. Cereb Cortex Suppl 1, i3-17.

Rakic P (2009). *Evolution of the neocortex: a perspective from developmental biology*. Nat Rev Neurosci 10, 724-35.

Regad T, Roth M, Bredenkamp N, Illing N, and Papalopulu N (2007). *The neural progenitor-specifying activity of FoxG1 is antagonistically regulated by CKI and FGF*. Nat Cell Biol 9, 531-540.

Rodrigues DC, Mufteev M, Weatheritt RJ, Djuric U, Ha KCH, Ross PJ et al. (2020). *Shifts in Ribosome Engagement Impact Key Gene Sets in Neurodevelopment and Ubiquitination in Rett Syndrome*. Cell Rep 30, 4179-4196.

Schmidt EK, Clavarino G, Ceppi M, and Pierre P (2009). *SUnSET, a nonradioactive method to monitor protein synthesis*. Nat Methods 6, 275-7.

Schwanhausser B, Busse D, Li N, Dittmar G, Schuchhardt J, Wolf J, Chen W, and Selbach M (2011). *Global quantification of mammalian gene expression control*. Nature 473, 337–342.

Selbach M, Schwanhäusser B, Thierfelder N, Fang Z, Khanin R, and Rajewsky N (2008). *Widespread changes in protein synthesis induced by microRNAs*. Nature 455, 58-63.

Shen Q, Wang Y, Dimos JT, Fasano CA, Phoenix TN, Lemischka IR, Ivanova NB, Stifani S, Morrisey EE, and Temple S (2006). *The timing of cortical neurogenesis is encoded within lineages of individual progenitor cells*. Nat Neurosci 9, 743-751.

Shen W, Ba R, Su Y, Ni Y, Chen D, Xie W, Pleasure SJ, and Zhao C (2019). *Foxg1 Regulates the Postnatal Development of Cortical Interneurons*. Cereb Cortex 29, 1547-1560.

Shoichet SA, Kunde SA, Viertel P, Schell-Apacik C, von Voss H, Tommerup N, Ropers HH, and Kalscheuer VM (2005). *Haploinsufficiency of novel FOXG1B variants in a patient with severe mental retardation, brain malformations and microcephaly*. Hum Genet 2005, 117, 536–544.

Snyder EM, Philpot BD, Huber KM, Dong X, Fallon JR, and Bear MF (2001). *Internalization of ionotropic glutamate receptors in response to mGluR activation*. Nat Neurosci 4, 1079-85.

Söderberg O, Gullberg M, Jarvius M, Ridderstråle K, Leuchowius K, Jarvius J, et al. (2006). *Direct observation of individual endogenous protein complexes in situ by proximity ligation*. Nat Methods 3(12):995-1000.

Spigoni G, Gedressi C, and Mallamaci A. (2010). *Regulation of Emx2 expression by antisense transcripts in murine cortico-cerebral precursors*. PloS One 5, e8658.

Stelzl U, Worm U, Lalowski M, Haenig C, Brembeck FH, Goehler H, Stroedicke M, Zenkner M, Schoenherr A, Koeppen S, Timm J, Mintzlaff S, Abraham C, Bock N, Kietzmann S, Goedde A, Toksöz E, Droege A, Krobitsch S, Korn B, Birchmeier W, Lehrach H, and Wanker EE (2005). *A human protein-protein interaction network: a resource for annotating the proteome*. Cell 122, 957-968.

Sur M, and Rubenstein JLR (2005). *Patterning and plasticity of the cerebral cortex*. Science 310, 805-10.

Takahashi T, Nowakowski RS, and Caviness Jr VS (1995). *The cell cycle of the pseudostratified ventricular epithelium of the embryonic murine cerebral wall*. J Neurosci 15, 6046-57.

Tigani W, Rossi MP, Artimagnella O, Santo M, Rauti R, Sorbo T, Ulloa Severino FP, Provenzano G, Allegra M, Caleo M, Ballerini L, Bozzi Y, and Mallamaci A (2020). *Foxg1 Upregulation Enhances Neocortical Activity*. Cereb Cortex 30, 5147-5165.

Toma K, Kumamoto T, and Hanashima C (2014). *The timing of upper-layer neurogenesis is conferred by sequential derepression and negative feedback from deep-layer neurons*. J Neurosci 34, 13259–13276.

tom Dieck S, Kochen L, Hanus C, Heumüller M, Bartnik I, Nassim-Assir B, Merk K, et al. (2015). *Direct visualization of newly synthesized target proteins in situ*. Nat Methods 12, 411-4.

Udagawa T, Swanger SA, Takeuchi K, Kim JH, Nalavadi V, Shin J, Lorenz LJ, Zukin RS, Bassell GJ, and Richter JD (2012). *Bidirectional control of mRNA translation and synaptic plasticity by the cytoplasmic polyadenylation complex*. Mol Cell 47, 253-66.

Vegas N, et al. (2018). *Delineating FOXG1 syndrome: From congenital microcephaly to hyperkinetic encephalopathy*. Neurol Genet 4, e281.

Vrajová M, Stastný F, Horácek J, Lochman J, Serý O, Peková S, Klaschka J, and Höschl C (2010). *Expression of the hippocampal NMDA receptor GluN1 subunit and its splicing isoforms in schizophrenia: postmortem study*. Neurochem Res 35, 994-1002.

Weise SC, Arumugam G, Villarreal A, Videm P, Heidrich S, Nebel N, et al. (2019). *FOXG1 regulates PRKAR2B transcriptionally and posttranscriptionally via miR200 in the adult hippocampus*. Mol Neurobiol 56, 5188–5201.

Wethmar K, Barbosa-Silva A, Andrade-Navarro MA, and Leutz A (2014). *uORFdb--a comprehensive literature database on eukaryotic uORF biology*. Nucleic Acids Res 42, D60–67.

Wilson SW, and Houart C (2004). *Early steps in the development of the forebrain*. Dev Cell 6, 167–181.

Wonders CP, and Anderson SA (2006). *The origin and specification of cortical interneurons*. Nat Rev Neurosci 7, 687–696.

Wong LC, Singh S, Wang HP, Hsu CJ, Hu SC, and Lee WT (2019). *FOXG1-Related Syndrome: From Clinical to Molecular Genetics and Pathogenic Mechanisms*. Int J Mol Sci 20, 4176.

Wu B, Eliscovich C, Yoon YJ, and Singer RH (2016). *Translation dynamics of single mRNAs in live cells and neurons*. Science 352, 1430-5.

Wu GY, Deisseroth K, and Tsien RW (2001). *Spaced stimuli stabilize MAPK pathway activation and its effects on dendritic morphology*. Nat Neurosci 4, 151-8.

Xuan S, Baptista CA, Balas G, Tao W, Soares VC, and Lai E (1995). *Winged helix transcription factor BF-1 is essential for the development of the cerebral hemispheres*. Neuron 14, 1141–1152.

Yang Y, Shen W, Ni Y, Su Y, Yang Z, and Zhao C (2017). *Impaired Interneuron Development after Foxg1 Disruption.* Cereb Cortex 27, 793-808.

Yu B, Liu J, Su M, Wang C, Chen H, and Zhao C (2019). *Disruption of Foxg1 impairs neural plasticity leading to social and cognitive behavioral defects*. Mol Brain 12, 63.

Zecevic N, Hu F, and Jakovcevski I (2011). *Interneurons in the developing human neocortex*. Dev Neurobiol 71:18-33.

Zeng F, Xue M, Xiao T, Li Y, Xiao S, Jiang B, et al. (2016). *MiR-200b promotes the cell proliferation and metastasis of cervical cancer by inhibiting FOXG1*. Biomed Pharmacother 79, 294–301.

Zhang M, et al. (2012). *Rational design of true monomeric and bright photoactivatable fluorescent proteins*. Nat Methods 9(7):727-9.

Zhao J, Qin B, Nikolay R, Spahn CMT, and Zhang G (2019). *Translatomics: The Global View of Translation*. Int J Mol Sci 20, 212.

Zhou L, Lim QE, Wan G, and Too HP (2010). *Normalization with genes encoding ribosomal proteins but not GAPDH provides an accurate quantification of gene expressions in neuronal differentiation of PC12 cells*. BMC Genomics 29, 11-75.

Zhou P, Zhang Y, Ma Q, Gu F, Day DS, He A, Zhou B, Li J, Stevens SM, Romo D, and Pu WT (2013). *Interrogating translational efficiency and lineage-specific transcriptomes using ribosome affinity purification*. Proc Natl Acad Sci USA 110, 15395-15400.

Zhu W, Zhang B, Li M, Mo F, Mi T, Wu Y, Teng Z, Zhou Q, Li W, and Hu B (2019). *Precisely controlling endogenous protein dosage in hPSCs and derivatives to model FOXG1 syndrome*. Nature Commun 10, 928.

Zukin RS, and Bennett MV (1995). *Alternatively spliced isoforms of the NMDARI receptor subunit*. Trends Neurosci 18, 306-13.

Acknowledgments

We thank Simone Mortal for helping us with hippocampal cell culture and live-imaging experiments (Fig. 1G,H).
We thank to Cristina Fimiani for cloning “LVrc_TREt-pl-BGHpA”, employed as the backbone of some lentiviruses used in this study.